

NOVEL INSIGHTS INTO TACE REGULATION OF AUTOCRINE AND PARACRINE  
SIGNALING IN EPITHELIAL CELLS

By

Eric Newman Bunker

B.S. The Evergreen State College 2011

A thesis submitted to the

Faculty of the Graduate School of the

University of Colorado in partial fulfillment

of the requirement for the degree of

Doctor of Philosophy

Department of Chemistry and Biochemistry

2017

This thesis entitled:  
Novel Insights into TACE Regulation of Autocrine and Paracrine Signaling in Epithelial  
Cells

written by Eric Newman Bunker  
has been approved for the Department of Chemistry and Biochemistry

---

Xuedong Liu

---

Amy Palmer

Date\_\_\_\_\_

The final copy of this thesis has been examined by the signatories, and we find that both the content and the form meet acceptable presentation standards of scholarly work in the above mentioned discipline.

## Abstract

Bunker, Eric Newman (Ph.D., Biochemistry)

TACE Regulation and Role in an Epithelial Cell Model

Thesis Directed by Professor Xuedong Liu

A multitude of cellular functions are controlled by the activity of the membrane-bound protease TACE, including immune response and development. Through cleavage of its membrane anchored substrates, TACE can activate a myriad of signaling pathways in an auto- or paracrine manner, transferring signals across a tissues and systems.

Despite its importance, it is highly debated how TACE is regulated. I helped generate TSen, a fluorescence-based sensor of TACE activity, a critical tool that proved necessary to interrogate the underlying signaling that leads to TACE activation. TSen enabled us to uncover a wide variation between cell lines and their underlying signaling in regards to TACE which may account for much of the confusion about its regulation.

Furthermore, we used this sensor to find that TACE is intimately tied actin cytoskeletal dynamics, which appears to be a novel mechanism of TACE activation. I then used TSen to monitor TACE activity in single cells in conjunction with an ERK reporter to measure both activities simultaneously for the first time. I was able to confirm past results showing the propagation of ERK pulses from cell to cell, as well as identify a new type of activity pulse: spikes in ligand shedding. These pulses of TACE activity occur in neighbor cells prior to an ERK pulse, which is followed by another spike in ligand shedding, validating the model that ERK pulses propagate between cells through ligand shedding. I then probed cell junctions for their role in TACE signaling. Because

the aggressiveness of an epithelial-derived cancer is highly correlated with loss of cell junctions, I generated an  $\alpha$ -catenin knockdown in HaCaT cells, recreating a phenotype of mesenchymal morphology and hyper proliferation. I found that silencing  $\alpha$ -catenin in this system generates a large increase in ligand shedding and subsequent proliferation and that the hyper proliferative phenotype does not occur in the absence of TACE. My findings contribute to the overall understanding of TACE regulation, as well as the downstream effects of this signaling molecule in ERK pulses and proliferation.

## Contents

### CHAPTER

I.	Background	
	Epithelial Junctions and EMT	2
	ERK Signaling and Activity Pulses	10
	TACE	14
II.	A biosensor for the activity of the "sheddase" TACE (ADAM17) reveals novel and cell type-specific mechanisms of TACE activation.	
	Introduction	20
	Results	22
	Discussion	44
	Methods and Materials	45
III.	Automated Image Processing and Analysis and Dual Sensor Reporting of ERK and TACE in Single Cells	
	Introduction	51
	Results	53
	Discussion	77
	Methods and Materials	79
IV.	Loss of Junctions by $\alpha$ -catenin Silencing Enhances Proliferation and MAPK through Enhanced Ligand Shedding	
	Introduction	111
	Results	113
	Discussion	128
	Methods and Materials	133

V.	Discussion	
	Significance	138
	A biosensor for TACE Activity	139
	Autocrine and Paracrine Signaling	141
	Ligand shedding is increase up $\alpha$ -catenin knockdown	144
	Citations	147

## List of Tables

### Tables

Table 1.1 A list of TACE substrates from multiple cell lines and protein families. 15

Table 2.1 A complete list of chemicals used to screen for TACE regulation 41

## List of Figures

### Figures

1.1	Overview of a cadherens junction	3
1.2	Cadherin-cadherin interactions form an adherens junction	5
2.1	TSen measures the catalytic activity of TACE in live cells	23
2.2	The kinetics of TSen activation in response to PMA.	26
2.3	Epidermal Growth Factor is an Activator of TACE.	30
2.4	Actin Depolymerization Activates TACE	33
2.5	The kinetics of TSen activation in response to EGF	34
2.6	EGF and CytoD, but not PMA, Dependent TACE Activation Requires ER Exit of Nascent Proteins	36
2.7	Validation of CytoD dependent activation of TACE	39
3.1	Example of Automated Image Processing for Analysis	55
3.2	Automated single cell segmentation techniques	59
3.3	Epithelial cell segmentation at cell junctions	62
3.4	Heat map display of reported ERK and TACE activity in single cells	64
3.5	Example of data traces obtained from ERKTR used to identify ERK activity pulses	66
3.6	Identified ERK pulses are compared to neighbor cell ERK pulses	67
3.7	Processing of TSen reported signal to gauge TACE activity	69
3.8	Comparison of ERKTR reported ERK activity and processed TSen reported TACE activity	71
3.9	Validation of TACE pulses with the non-cleavable sensor (NCS).	73

3.10	Identified ERK pulses are compared to processed TSen in same cells and neighbor cells.	74
3.11	Identified ERK pulses are compared to processed TSen in neighbor cells identified for an ERK pulse in the timeframe	76
4.1	$\alpha$ -Catenin knockdown causes scattering in HaCaT cells	114
4.2	Phenotype of HaCaT cells with $\alpha$ -catenin knockdown.	116
4.3	HaCaT cells require TACE activity for TGF $\alpha$ shedding	118
4.4	ERK pulses require EGFR activity and ligand shedding	120
4.5	CRISPR-Cas knockout of TACE in HaCaT cells does not prevent TSen cleavage under all conditions	121
4.6	ERK activity is lost upon TACE knockout in HaCaT cells	123
4.7	ERK pulses are almost completely lost in HaCaT cells with a TACE knockout	124
4.8	HaCaT cells cease almost all proliferation in the absence of TACE	126
4.9	$\alpha$ -catenin knockdown increases ligand shedding in HaCaT cells	127
4.10	Silencing $\alpha$ -catenin in a TACE null background	129
4.11	Knocking down $\alpha$ -catenin increases proliferation in wild-type cells but retains a negligible fraction of dividing cells in a TACE null background	130
4.12	Representation of increased ligand shedding upon loss of cell junctions	134

## Chapter 1

### Background

This chapter aims to tie together several characteristics of epithelial cells and their growth, both in healthy cells and disease. Mammalian organisms rely on epithelial cells to maintain a barrier that protects the body from the environment and pathogens. The epidermis performs this function by providing a constantly proliferating barrier of cells connected by a multitude of cell-cell junctions. These junctions provide structural integrity to the epidermis, grant osmotic control of solutes and water, and modulate signaling in these cells<sup>1-3</sup>. Some of the most common types of cancer are formed from epithelial cells, which obtain invasive capabilities and increased proliferation from the loss of these junctions. To understand how this process works we tie in a core signaling pathway, the extracellular signal-regulated kinase (ERK) cascade. ERK has been shown to be fundamental to a cell's decisions to proliferate and recent work has indicated that activity pulses are important for this process. While ERK signaling is a well-studied subject, the regulation that leads to ERK activity pulses is less understood. What is clear is that ERK activity pulses appear to propagate from cell to cell and that this process seems to be regulated by ligand shedding. The membrane bound protease TNF $\alpha$  converting enzyme (TACE) is an essential signaling protein for autocrine and paracrine activation of epidermal growth factor receptor (EGFR), as well as cleavage of a wealth of other substrates. The mechanism of TACE regulation is widely debated and generating a better understanding of this protein is paramount to understanding its downstream effects. This dissertation aims to contribute understanding to the

regulation of ERK pulses and the signaling tied to cell-cell junctions in the context of TACE as well as how TACE activity is regulated at a cellular level.

## **Epithelial Junctions and EMT**

Epithelial cells form a constantly dividing barrier to the external environment. The epidermis is composed of four layers of keratinocytes: the stratum basale (basal layer), stratum spinosum, stratum granulosum, and stratum corneum<sup>4</sup>. The basal layer is adjacent to the basal lamina, which separates the epidermis from the dermis and contains epidermal stem cells, which proliferate and provide cells for upper differentiated layers. Intercellular junctions between epithelial cells are fundamental to the cells' role in both forming and maintaining the epithelium. These junctions are made up of adherens junctions (AJ), tight junctions (TJ), and desmosomes. Tight junctions provide a semi-permeable barrier within the epithelium to control transport of solutes across their osmotic gradients as well as confining apical and basal membrane components of epithelial cells to their region to maintain polarity<sup>1</sup>. AJs are made up of nectin-afadin complexes and cadherins. Nectins are important for establishing adherens and tight junction formation and inactivation of this complex is lethal during embryogenesis<sup>5</sup>. Cadherins are  $\text{Ca}^{2+}$ -dependent adhesion molecules that bind cadherin molecules of the same type on adjacent cells (Fig.1.1)<sup>6</sup>. A calcium gradient mediates epithelial cell differentiation throughout the epithelial layers; as the calcium increases outward a large number of changes in keratins and desmosomes occur, as well as loss of P-cadherin, replaced with E-cadherin<sup>4,7</sup>.

Cadherins bind AJs to actin through the cadherin-catenin complex. The cytosolic region of cadherins forms a complex with  $\alpha$ -catenin,  $\beta$ -catenin, and p120-catenin, where

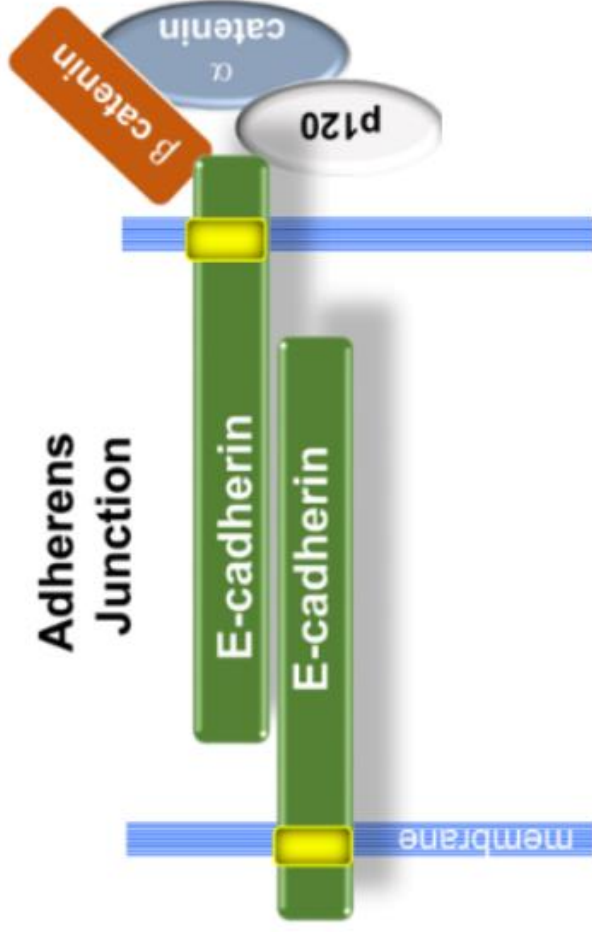


**Figure 1.1 Overview of a cadherens junction** adapted from Yu, Y., & Elble, R. C. (2016). A representation of an adherens junction made up of E-cadherin and the catenin complex. The extracellular domain of E-cadherin binds to a like cadherin and the intracellular domain forms a complex with the catenins  $\alpha$ -,  $\beta$ -, and p120 catenin.

$\beta$ - and p120-catenin bind directly, but  $\alpha$ -catenin binds through  $\beta$ -catenin<sup>1</sup>. While it had long been thought that  $\alpha$ -catenin linked this complex to the actin cytoskeleton because of its actin-binding domain and  $\beta$ -catenin binding domain,  $\alpha$ -catenin does not bind both actin and  $\beta$ -catenin simultaneously.  $\alpha$ -catenin resides in three states: monomeric  $\alpha$ -catenin can either bind to  $\beta$ -catenin as a heterodimer and then to E-cadherin or it can bind another molecule of  $\alpha$ -catenin to form a homodimer capable of binding actin filaments<sup>8,9</sup> (Fig.1.2). This finding of dimer specificity effectively decoupled the cadherin-catenin complex from the actin cytoskeleton, but a wealth of data had already established some sort of connection between the two. In an effort to resolve this inconsistency, it was found that while  $\alpha$ -catenin does not bind both the cadherin complex and actin simultaneously in solution<sup>8,9</sup>, tensional force across the complex causes a significant increase in F-actin binding affinity<sup>10</sup>. This tensional force has furthermore been shown to unfurl  $\alpha$ -catenin, allowing it to bind vinculin, which stabilizes the elongated conformation<sup>11-13</sup>, and forms an indirect bridge to actin.

The formation of junctions in epithelial cells is fundamental to their physiological role but is a reversible process. Epithelial to mesenchymal transition (EMT) is the process of epithelial cells losing epithelial cell apical-basal and planar polarity, losing cell-cell junctions, reorganizing the cytoskeleton, redistributing organelles, and morphological changes allowing for an invasive phenotype<sup>14,15</sup>. EMT is an essential process conserved across a wide array of multicellular organisms to alter epithelial cell morphology into one appropriate for migrating through the extracellular space. This process is fundamental for the formation of several organs and structures in

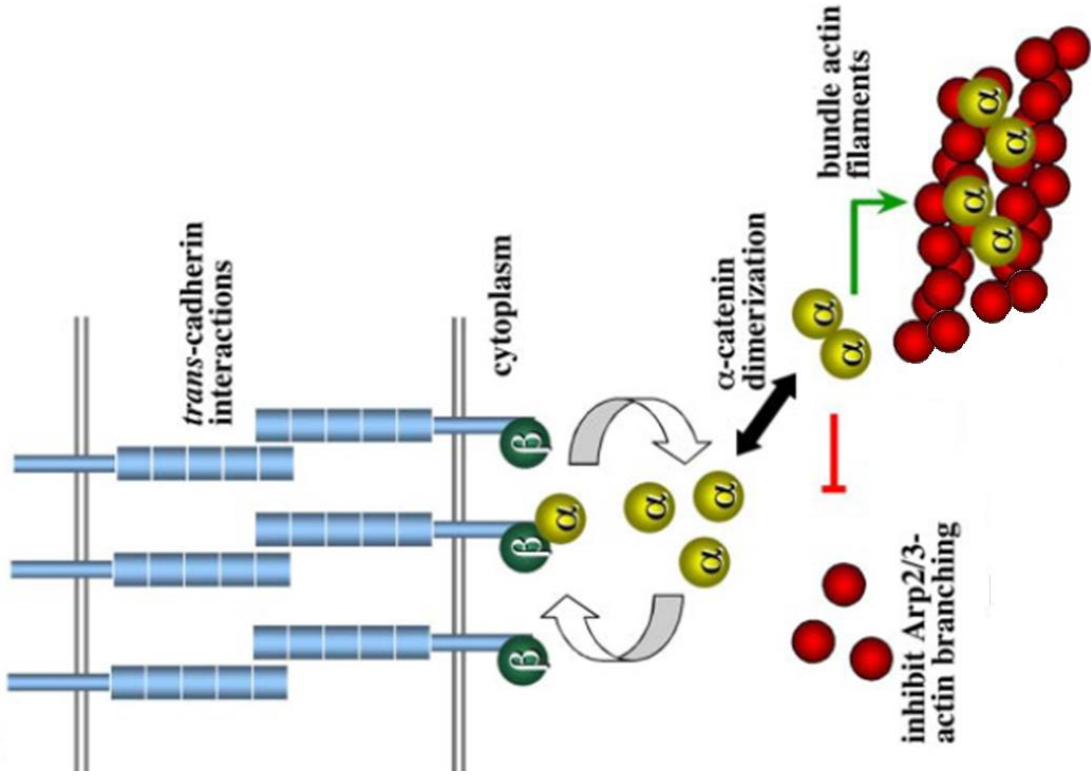


**Figure 1.2** Adapted from Weis, W. I., & Nelson, W. J. (2006). Cadherin-cadherin interactions form an adherens junction.  $\beta$ -catenin binds the cytoplasmic domain of the cadherin and  $\alpha$ -catenin can bind this complex as a heterodimer or to itself as a homodimer.  $\alpha$ -catenin homodimers can bind actin and inhibit Arp2/3-mediated actin branching.

development such as the heart, musculoskeletal system, and peripheral nervous system<sup>15</sup>.

EMT is commonly studied because of its role in cancer progression. When a normal epithelium begins to proliferate beyond routine maintenance and healing, cells can begin to form an adenoma. Further changes in these cells can alter this to a carcinoma which is still attached to the basement membrane like the original epithelial cells. When EMT occurs, single cells can split off from this carcinoma to form an invasive phenotype that penetrates the basement membrane and can migrate through the body in a process called metastasis. These migratory cells can then form micrometastases or undergo mesenchymal to epithelial transition (MET) and colonize another site in the body as a macrometastasis<sup>15</sup>. When a cancer is able to metastasize in this manner, it makes treatment much more difficult and this type of transition is commonly associated with aggressive cancers.

EMT was first discovered from what was called the scatter factor, a component of fibroblast-conditioned media, which was capable of making Madin-Darby canine kidney (MDCK) switch from epithelial-cell colonies to migratory fibroblast cells<sup>16</sup>. This factor was later found to be hepatocyte growth factor, (HGF) a ligand of c-met receptor<sup>17</sup>. HGF stimulates Ras activity which further activates Rac and the mitogen-activated protein kinase (MAPK) pathway, the mechanism used to induce EMT in a bladder carcinoma cell line<sup>18</sup>. Another model system found that Ras activation of PI3K was important for scattering and survival whereas MAPK signaling induced EMT<sup>19</sup>. One of the consequences of HGF stimulation is the activation of SH2-domain-containing inositol 5'phosphatase (SHIP)-1. SHIP-1 has been associated with actin cytoskeleton

rearrangement and its overexpression is associated with a branching morphology in response to HGF<sup>20</sup>. Furthermore, SHIP-1 phosphatase activity leads to an EMT-like phenotype with loss of cortical actin, stress fiber formation, and loss of adherens-junctions<sup>21</sup>. Furthermore, it was shown that HGF no longer caused a scattering phenotype in MDCK cells with a phosphatase-dead mutation indicating that SHIP-1 is fundamental to this process<sup>21</sup>. Overall, MAPK signaling and cytoskeletal changes appear fundamental to the changes occurring during EMT.

In conjunction with MAPK pathway activation, a very potent inducer of EMT is the ligand transforming growth factor beta (TGF $\beta$ ). Because TGF $\beta$  is also involved in growth arrest and apoptosis, it can prevent tumor function under most conditions but when combined with active MAPK signaling can cause EMT. The canonical TGF $\beta$  pathway activates Smad2 which was shown to induce tumor cell migration on its own and, in conjunction with increased H-Ras levels, accumulates in the nucleus and causes EMT<sup>22</sup>. To differentiate the targets of Ras from each other under TGF $\beta$  treatment, inhibitors were used to determine that hyperactive Raf with TGF $\beta$  was important for EMT, whereas PI3K activity was important for surviving TGF $\beta$ -induced apoptosis<sup>19</sup>. TGF $\beta$  is one of the most well-known activators of EMT, though it has paradoxical roles in suppression and activation of cancerous phenotypes.

One of the most important changes in EMT is the loss of E-cadherin; this loss is necessary for a cell to detach from its neighbors and invade the basement membrane, and has long been correlated with aggressive tumors and metastases<sup>23-25</sup>. Reduced E-cadherin levels have been seen in cases of atypical DNA methylation of the CDH1 promoter, as well as in cases where it has been repressed by transcription factors<sup>26,27</sup>,

including Snail, Slug, and Zeb2 responding to extracellular cues such as TGF- $\beta$ , WNT, or IL6 signaling<sup>28</sup>. Silencing E-cadherin in a breast epithelial model was sufficient to generate an EMT phenotype with increases in vimentin, N-cadherin, and Twist, as well as generating a more invasive tumor in nude mice<sup>29</sup>. This only occurred when the entire E-cadherin protein was silenced; a dominant-negative truncated construct lacking the ectodomain caused a loss of cell junctions but no distinct mesenchymal morphology. The functional nature of the cytoplasmic tail was predicted to act by binding  $\beta$ -catenin, and so loss of the entire protein instead of simply its ectodomain would release  $\beta$ -catenin and cause EMT-related transcription. To determine if the cytoplasmic tail acts through  $\beta$ -catenin, it was silenced in E-cadherin knockdown cells. Mesenchymal markers N-cadherin, vimentin, and fibronectin were lowered but epithelial marker cytokeratin-8 remained low. Constitutively active  $\beta$ -catenin was overexpressed in the presence of E-cadherin revealing that it is required but not sufficient for mesenchymal marker expression. Seventeen transcription factors including Twist and Zeb-1 changed in E-cadherin knockdown cells. Silencing of Twist prevented the induction of N-cadherin, but not vimentin, and hindered the invasive phenotype seen in E-cadherin knockdown cells<sup>29</sup>. This provides key insight into the role of E-cadherin; its cytosolic region is apparently a crucial regulator of EMT, and this control is through more than stimulation of  $\beta$ -catenin activity, but it is not clear how this control is conveyed.

Loss of E-cadherin is not always sufficient to cause EMT, however. MDCK cells are another epithelial model where loss of E-cadherin generates a more invasive phenotype with a fibroblast morphology in sub-confluent cells<sup>30</sup>, though at higher cell densities it was found that loss of E-cadherin was unable to remove apical-basal cell

polarity or disrupt formation of TJs<sup>31</sup>. This incongruity was partially explained by a redundant cadherin, cadherin-6, where silencing of both genes, but neither individually, was capable of displacing  $\beta$ -catenin from the membrane but still not able to remove ZO-1 from cell junctions. It was then found that loss of  $\alpha$ -catenin was capable of disrupting cell junctions and that these cells appeared to have a mesenchymal phenotype, with loss of both AJs and TJs and apical-basal polarity, but with no effect on  $\beta$ -catenin levels<sup>31</sup>. This implicates  $\alpha$ -catenin as an important regulator of how E-cadherin signaling occurs and it has this effect in the presence of redundant cadherins as well.

Vasioukhin et al. have shown that  $\alpha$ -catenin null mice had major skin and hair follicle defects. They found that despite little change in the level of AJ proteins and that  $\beta$ -catenin was conserved and associated with E-cadherin at cell junctions, large segments of the epidermis were missing with visible peeling at other sites. Diminished hair follicle morphogenesis accompanied a lack of whiskers. The normally clear layers of the epidermis were thick and disorganized and, while several signs of differentiation persisted between the layers, mitosis appeared throughout the epidermis instead of being restricted to the basal layer. The  $\alpha$ -catenin null cells showed a morphology of being unusually large, hyperproliferative, defective in cell polarity, and multinucleated, overall resembling a precancerous squamous cell carcinoma<sup>32</sup>. Loss of the cytoplasmic domain of E-cadherin (and redundant cadherins) causes a large effect that is only partially explained by  $\beta$ -catenin signaling. These results show that removal  $\alpha$ -catenin can cause drastic changes *in vivo* and may explain another side of cadherin-catenin signaling.

Because  $\alpha$ -catenin loss does not affect  $\beta$ -catenin protein levels or localization<sup>31</sup>, it is unclear how it regulates cell signaling to such a high degree. What is known is that the homodimer of  $\alpha$ -catenin directly inhibits actin dynamics when bound to filamentous actin by inhibiting Arp2/3-mediated polymerization<sup>9</sup>. Arp2/3 activity was completely suppressed at nearly ten-fold the estimated concentration in the cytosol, indicating that a relatively high local concentration of  $\alpha$ -catenin must exist if this inhibition is to be biologically relevant. Because  $\alpha$ -catenin forms a complex with  $\beta$ -catenin and E-cadherin, and this complex forms at cell junctions, it is plausible that the local concentration of  $\alpha$ -catenin bound at cell junctions would be increased. When dissociating from these complexes,  $\alpha$ -catenin would then be able to form homodimers, inhibit Arp2/3 activity, and prevent actin branching and lamellipodia formation near the site of cell-cell junctions<sup>33</sup>. While it is unclear how cytoskeletal changes affect proliferation and EMT, they are clearly important for aggressive cancer phenotypes<sup>14,15,20</sup>.

### **ERK Signaling and Activity Pulses**

The epidermis is constantly renewing itself to maintain a barrier against the external environment. Cells within the basal layer of the epidermis rapidly divide to replace differentiated cells on the exterior, which undergo programmed cell death and eventually slough off into the environment. The turnover of this process is remarkably high, with the outer layers being replenished every two weeks<sup>34</sup>. Epithelial cells not only have to proliferate long after the adult organism is grown, but they have to be able to up-regulate proliferation even further upon injury as well as becoming migratory to seal

the wound. With these mechanisms in place, it is not surprising that basal-cell and squamous-cell carcinomas are some of the most common cancers<sup>35</sup>.

Epithelial cells must maintain a balance of proliferation – excessive growth leads to neoplasia and even cancerous states whereas too little results in fragile skin and epidermal atrophy<sup>36</sup>. To maintain this balance the keratinocytes that make up the epidermis regulate growth through a number of signaling pathways and core amongst them is the ERK cascade. MAPK cascades are capable of controlling a large number of cellular processes such as proliferation, motility, and survival both by altering gene expression and direct activation of existing proteins<sup>37</sup>. The ERK1/2 pathway has been shown to be particularly important for cell proliferation, as it is a key regulator in cell-cycle progression from G1 to S phase<sup>38</sup>.

The phenotype of ERK activation can be drastically altered by changing the duration of activation. PC12 pheochromocytoma cells stimulated with nerve growth factor (NGF) exhibit sustained ERK activation and nuclear translocation of ERK protein, resulting in the differentiation of these cells to a sympathetic neuron phenotype, whereas EGF induces a transient activity, reduced nuclear translocation, and no differentiation<sup>39</sup>. The fibronectin-induced progression to S phase via transient ERK activation was found to be proportional to the integral of ERK activation rather than either magnitude or lifetime alone<sup>40</sup>. These results show that the kinetics of ERK signaling are vital to its function in controlling cell behavior.

Signaling can be modulated by the frequency of transition between on-off states by its signaling molecules rather than the magnitude, or number, of molecules generating the signal. In yeast, calcium spikes have been shown to activate the

transcription factor Crz1 by controlling the frequency of its nuclear localization rather than the magnitude, allowing for proportional expression of target genes regardless of expression<sup>41</sup>. The stress response transcription factor Msn2 can respond similarly by modulating its amplitude, frequency, and duration of nuclear localization to transmit diverse external stresses; this was found to generate differential gene expression through varied transcription factor binding properties and the kinetics of promoter transition to an off state<sup>42</sup>. Following DNA damage, the tumor suppressor p53 is expressed in a series of discrete pulses, where the number of pulses depends on the amount of damage but the width and amplitude seem fixed<sup>43</sup>. Treatment with tumor necrosis factor (TNF)- $\alpha$  was seen to generate pulsing activity in nuclear factor (NF)- $\kappa$ B, where it responded in a digital manner creating a heterogeneous population with analogue information such as timing, intensity, and number of pulses<sup>44</sup>.

Tracking ERK activity in single cells revealed that its activity is comprised of discrete activity pulses<sup>45-49</sup>. Upon titrating EGF, these pulses appear to increase in frequency and duration instead of a continuous increase in population activity<sup>45,47</sup>. Pulse frequency and proliferation also both increased with serum concentration and correlated with each other to show a bell-shaped response to changing cell density<sup>46</sup>. The downstream effectors of ERK Fra-1 and c-Myc have expression levels proportional to the frequency of ERK pulses and Rb phosphorylation or geminin activity indicated that entry into S phase has a nonlinear dependence on ERK<sup>45</sup>. Aoki et al. used a light-activated c-Raf system to show that intermittent light at a similar frequency to naturally occurring ERK pulses stimulates proliferation compared to continuous light or dark conditions. Simulated ERK activity pulses but not continuous activation led to the

induction of serum response factor (SRF)-regulated genes<sup>46</sup>. Overall, these findings indicate that ERK pulses have different downstream effects than continuous activity and appear to be tied directly to proliferation.

Modulation of ERK pulses by pathway inhibitors has helped shed some light on their regulation. EGFR inhibition lowers the frequency of pulses, whereas MEK inhibition reduces amplitude<sup>45</sup> and low doses of a Raf inhibitor lead to an increased pulse width<sup>46</sup>. The propagation of ERK activity pulses to neighboring cells appears to be modulated by ligand shedding as it was abolished by inhibitors of MMPs or EGFR<sup>46</sup>. To further probe ERK pulse regulation, Sparta et al. overexpressed TrkA in MCF10A cells. TrkA is a receptor tyrosine kinase (RTK) that responds to NGF by receptor dimerization, much like EGFR to its ligands<sup>50</sup> and shares the Raf-MEK-ERK cascade but differs in kinetics and in how it recruits adaptor proteins to activate the GTPases Ras and Gap<sup>51</sup>. Titrating NGF showed a steady increase in ERK levels as oppose to treatment with EGF which caused erratic pulsing activities; this shows that the pulsing activity is likely due to the different mechanisms of GTPase recruitment by adaptor proteins at the receptor level. The importance of EGFR was also shown by treatment with the EGFR inhibitor gefitinib, which indicated that not only does it remove the pulsing activity but also prevents pulses that are still rising in activity from fully reaching their peak<sup>47</sup>.

ERK activity pulses appear to be a fundamental mechanism of regulating downstream effects in a manner than depends on the ligand stimulating the pathway. The pulses themselves appear highly correlated with entry into S phase and subsequent proliferation. There is still a great deal of ambiguity in our understanding of

ERK pulses and where they originate as both the stochastic activation of Raf<sup>46</sup> and the receptor<sup>47</sup> have been implicated. Furthermore, ERK pulses appear to propagate from cell to cell and this dissemination appears to require ligand shedding - another field riddled with uncertainty.

## **TACE**

The ADAM (A Disintegrin And Metalloproteinase) family of transmembrane proteases is closely related to matrix metalloproteinases (MMPs) as well as ADAM-TSs (ADAMS with thrombospondin domains) and snake venom metalloproteinases (SVMPs)<sup>52</sup>. The ADAM family shares diverse functions in cell adhesion and signaling from growth to modulating inflammatory response. ADAM17, also referred to as TACE, is one of the most studied proteins in the family as it maintains a large array of substrates and appears fundamental to development and disease<sup>53</sup>. When TACE-activity null mice were generated by removing the zinc-binding site, the few mice that survived had abnormalities in their skin, eyes, organs, and hair reminiscent of mice lacking TGF $\alpha$  and cells from these mice were unable to release TGF $\alpha$ ; a discovery that TACE cleaves more than TNF $\alpha$  but is also responsible for release of the EGFR ligand transforming growth factor alpha (TGF $\alpha$ );<sup>54</sup>. TACE is therefore able to the release of TGF $\alpha$  to activate EGFR on nearby cells as well as the cell releasing it; this is an example of a process called ligand shedding.

Over the years it has been discovered that TACE cleaves a large array of substrates from many categories of ectodomain containing proteins (Table 1.1)<sup>55</sup>, both to cut a pro-form into an active structure, like with EGFR ligands, or to deactivate the

Receptors		Cytokines		Adhesions	Other	
TNF-a RI	ACE2	ErbB4	TNF	SEMA4D	ICAM-1	APP
TNF-a RII	Notch1	TrkA	TGF $\alpha$	LAG-3	VCAM-1	GP
TNFRSF8	SDC1	NGFR	AREG	DLL1	NCAM	CA9
TNFRSF5	SDC4	VEGFR2	EREG	KL-1	ALCAM	PRNP
IL-6Ra	SORT1	PTPRF	EPGN	KL-2	L1-CAM	KL
IL-1R2	SORL1	PTPRZ	NRG1	MICA	EpCAM	MUC-1
IGF2-R	SORCS1	GP1ba	HB-EGF	MICB	DSG2	LYPD3
IGF2R	SORCS3	GPV	Pref1	Jagged	CD62L	VASN
FCAR	LOX-1	GPVI	Fractalkine	LTA	Collagen XVII	CD163
CSF1R	APOER	EPCR	TRANCE	TMEFF2	PVRL4	PMEL17
GHR	NPR		CSF-1	FLT-3L	CD44	
					F11R	

**Table 1.1 A list of TACE substrates from multiple cell lines and protein families**

protein such as a RTK. Substrate specificity is at least in part due to the non-catalytic domains of TACE despite these domains not binding the substrate. This likely due to steric hindrance preventing non-substrates from reaching the catalytic site and appears to be a common feature among the ADAM family<sup>56</sup>. Though substrate specificity is controlled by proximity and adjacent domains, the cleavage site of its preferred ligands has a well-defined motif comprised of alanine and valine residues<sup>57</sup>.

TACE transport from the endoplasmic reticulum (ER) to the Golgi apparatus and outward to the membrane is a key form of regulation. Macrophages express the non-catalytic intramembrane protein iRhom2 and its knockout led to a complete loss of TACE activity<sup>58</sup>. It was found that TACE is retained in the ER until trafficked out by iRhom2, then its prodomain is cleaved in the Golgi where it is glycosylated, and then it can proceed to the membrane as an active protease<sup>58,59</sup>. How signaling affects this process is unclear but it does seem that in this system iRhom2 is essential for TACE activity by means of transport.

The cytoplasmic domain of TACE has several phosphorylation sites. Niu et al. reported a phosphorylation of TACE on tyrosine residue 702 by Src in C2C12 myoblasts as a response to mechanical stretch<sup>60</sup>. Reactive oxygen species activated PKC-epsilon in a lung carcinoma line which resulted in serine and threonine phosphorylation on the cytoplasmic tail of TACE and promoted shedding of EGFR ligands<sup>61</sup>. ERK has been found to directly phosphorylate the cytoplasmic tail of TACE at threonine 735 with possible roles in trafficking from the ER<sup>62</sup>. Phosphosite mutants T735A and T735E were generated to be an unphosphorylatable form of TACE and a phosphomimetic, respectively. It was found that without phosphorylation TACE was retained in the ER

but the phosphomimetic appeared to progress through the secretory pathway<sup>62</sup>. T735 was also found to be phosphorylated by p38, causing a TACE-mediated release of EGFR ligands and proliferation in response to cell stresses commonly used to activate p38<sup>63</sup>. Because TACE is both activated by stressors through p38 and by pro-growth and survival signals through ERK, this protein can integrate these signals into a circuit capable of activating EGFR from multiple contexts, as well as propagate this signal to nearby cells<sup>64</sup>.

Once at the membrane it is unclear if phosphorylation retains a regulatory role on TACE; there are, however, several potential regulators still in play. One finding is that TACE appears to be quickly activated at the membrane and that this activity is apparently independent of inhibitory domains or endogenous protein inhibitors. An inhibitor that binds the active site of TACE is able to quickly bind active cells but not quiescent ones and that TACE activity appears to be rapidly reversible upon washout of stimulus<sup>65</sup>. Consistent with this concept is the result that TACE activity at the membrane is modulated by the redox environment at the plasma membrane. This can be altered by thiol isomerases, and it was found that inhibiting or silencing protein disulfide isomerase was sufficient to enhance TACE-mediated ligand shedding in a rapid and reversible manner<sup>66</sup>. A separate finding is that the small pool of TACE at the plasma membrane is capable of forming dimers and that these dimers are more susceptible to inhibition by the tissue-inhibitor of metalloproteinase-3 (TIMP3) as seen by increased binding by TIMP3 when coupled by a cysteine trap<sup>67</sup>, which is inconsistent with the result from Le Gall's group<sup>65</sup>. Moreover, the equilibrium of TACE monomers and dimers appears to change rapidly in response to ERK or p38 stimulation<sup>67</sup>. TACE

activity at the membrane was also found to be enhanced by the presence of phosphatidylserine at the outer leaflet, both during apoptosis and as a transient event potentially common to all TACE-activating stimuli<sup>68</sup>. There is a great deal of inconsistency the mechanism of TACE activation, several lines of evidence are disjointed such as the primary regulation being transport<sup>58</sup> or transient exposure to phosphatidylserine<sup>68</sup>, and others completely contradictory to each other<sup>65,67</sup> making TACE regulation a murky subject to understand.

Because TACE is capable of tying multiple signaling pathways together to generate an EGFR response<sup>64</sup>, it transfers signals like stress into a proliferation phenotype<sup>63</sup>. More than just activating proliferation, TACE is able to act through EGFR to up-regulate several MMPs to promote cell invasion phenotypes<sup>69</sup>. It was found that TGF $\beta$  acted through TACE and ErbB3 for PI3K and AKT activation<sup>70</sup> as well as through TACE to generate a migratory and invasive phenotype<sup>71</sup>. TACE has the paradoxical role of both cleaving EGFR ligands and RTKs which means that its inhibition both causes a decrease in the EGFR pathway and an increase in a related RTK pathway which is referred to as bypass signaling, a common mechanism cancers use for developing kinase inhibitor resistance<sup>72</sup>. The dual role of TACE in ligand and receptor cleavage generates both positive and negative feedback capable of integrating multiple pathways together to direct cell motility and growth and proliferation<sup>64,73</sup>. This places TACE as a direct modulator of disease state in multiple types of cancer. This protein is of crucial importance for development, immune response, wound healing, and disease but its regulation is still widely debated.

Because the mechanism of TACE regulation remains disputed, there is a need for more tools in the field to assess its activity. As TACE regulation becomes more understood, it is imperative to understand how its regulation and role are tied in cells. For example, ERK pulse propagation appears to depend on ligand shedding but several reports on TACE regulation show that extracellular mechanisms control TACE activity. Also, the pathways tied to EMT and metastasis are intricately connected to TACE signaling through MAPK pathways and motility but its role and regulation in this process are not understood. In this dissertation I describe a novel biosensor for TACE activity which I then use to validate signaling regulation of TACE, discover a novel regulator of TACE, compare TACE activity in single cells to their ERK pulsing behavior, and address how cell-cell junctions affect TACE activity with the removal of  $\alpha$ -catenin.

## Chapter 2

### **A biosensor for the activity of the "sheddase" TACE (ADAM17) reveals novel and cell type-specific mechanisms of TACE activation.**

*Published with permission from Science Signaling*

#### **Introduction**

The Tumor Necrosis Factor- $\alpha$  Converting Enzyme (TACE/ADAM17) is a transmembrane protease that has been implicated in numerous physiological processes, including inflammation<sup>74,75</sup>, wound healing<sup>76</sup>, development<sup>77</sup> and cancer progression<sup>78,79</sup>. In these diverse processes, TACE plays a common role as an extracellular sheddase that cleaves the pro-/transmembrane form of a wide variety of ligands and receptors<sup>79</sup>. For example, TACE activity mediates auto/paracrine release of TNF $\alpha$  during immune response through the cleavage of pro-TNF $\alpha$  and release of soluble TNF $\alpha$ , which binds to and activates the TNF receptor<sup>74</sup>. Similarly, TACE activity mediates auto/paracrine release of TGF $\alpha$  and amphiregulin<sup>80</sup>, both of which are Epidermal Growth Factor Receptor (EGFR1) ligands that regulate cellular motility during development, wound healing, and metastasis<sup>81,82</sup>. Although ligand shedding has gained increased attention as a major posttranslational modification mechanism and significant research has been conducted in an effort to understand the consequences of auto/paracrine release of TACE substrates, relatively less is known about how TACE activity is itself regulated. Several lines of evidence suggest that TACE activity is spatially and temporally regulated within a cell or a tissue<sup>58,65,83</sup>. TACE activation has been proposed to require the proteolytic cleavage of the auto inhibited pro-TACE form<sup>84</sup>,

via the protease activity of Furin<sup>79</sup>, however, Furin deficient cells have displayed a clear ability to mature and activate TACE<sup>85</sup>. Thus, the mechanism of proteolytic activation of TACE still remains unclear. It has been suggested that the trafficking of TACE to the plasma membrane is the primary means of TACE regulation in cells. Direct phosphorylation of TACE at Thr735 by either p38 or Erk has been proposed to facilitate trafficking of TACE to the plasma membrane, and subsequent extracellular activity<sup>62,63,86–88</sup>. Other studies point to the importance of ER exit due to the action of iRhom2 in the activation of TACE<sup>58</sup>. Additionally, pathophysiological mutants of Src have been shown to regulate plasma membrane display of TACE, and there is some evidence that wild type Src may also mediate this process<sup>89,90</sup>. Clearly, there are many outstanding questions in the field that aim to answer how the TACE protease is able to be regulated in such a manner as to have 76 substrates<sup>79</sup> and various roles in diverse physiological and pathophysiological processes. The current mechanistic understanding of TACE regulation is hampered by a lack of effective tools to measure the spatiotemporal regulation of TACE activity in live cells. In this study, we demonstrate the use of a novel FRET biosensor for TACE activity and how its use in live cells reveals that there are at least three distinct mechanisms, including a novel actin-cytoskeleton dependent pathway, by which TACE is activated in a cell type specific context. We find that in some cells TACE activation depends solely upon the kinase activities of p38 and Erk, while in other cells TACE activity depends upon either vesicle trafficking alone or a combination of kinase activation and vesicle trafficking. Our data clearly shows that there are multiple distinguishable mechanisms for TACE activation that can be either cell type specific, or TACE activator specific (i.e. PMA or EGF specific). Such insight

into the complexity of TACE regulation can help explain how TACE activity may be targeted to specific cellular substrates in order to mediate the diverse cellular responses.

## **Results**

### **The TSen FRET biosensor was designed using a mixture of domains from TGF $\alpha$ and TNF $\alpha$**

Using a chimeric protein design approach, we developed a novel, genetically encoded FRET biosensor, which we call TSen, to measure TACE activity in live cells by fluorescence microscopy. As displayed schematically in Fig. 2.1a, TSen has an N-terminal leader sequence derived from TGF $\alpha$ , a TACE cleavage site from TNF $\alpha$  flanked by linker regions, a PDGFR (platelet-derived growth factor receptor) transmembrane domain, an eCFP (enhanced cyan fluorescent protein) FRET donor, and a YPET [a yellow fluorescent protein (YFP) variant] FRET acceptor in a similar manner as to what has been used for the MMP14 (matrix metalloproteinase 14) FRET biosensor<sup>91</sup>. A key difference between TSen and other protease cleavage biosensor designs is that two tandem valines make up the immediate C-terminal end of the sensor, which mimic the C-terminal valines that are required for TGF $\alpha$  maturation in live cells<sup>92</sup>. The use of a TACE cleavage site derived from TNF $\alpha$  in TSen is the result of extensive research that identified a small peptide region within TNF $\alpha$  as an efficient and specific substrate of TACE over other metalloproteinases<sup>93,94</sup>. Although a TACE-specific cleavage site derived from TNF $\alpha$  is incorporated into TSen, TSen differs from the TNF $\alpha$  and TGF $\alpha$  proteins in the distance between the cleavage site and the transmembrane domain

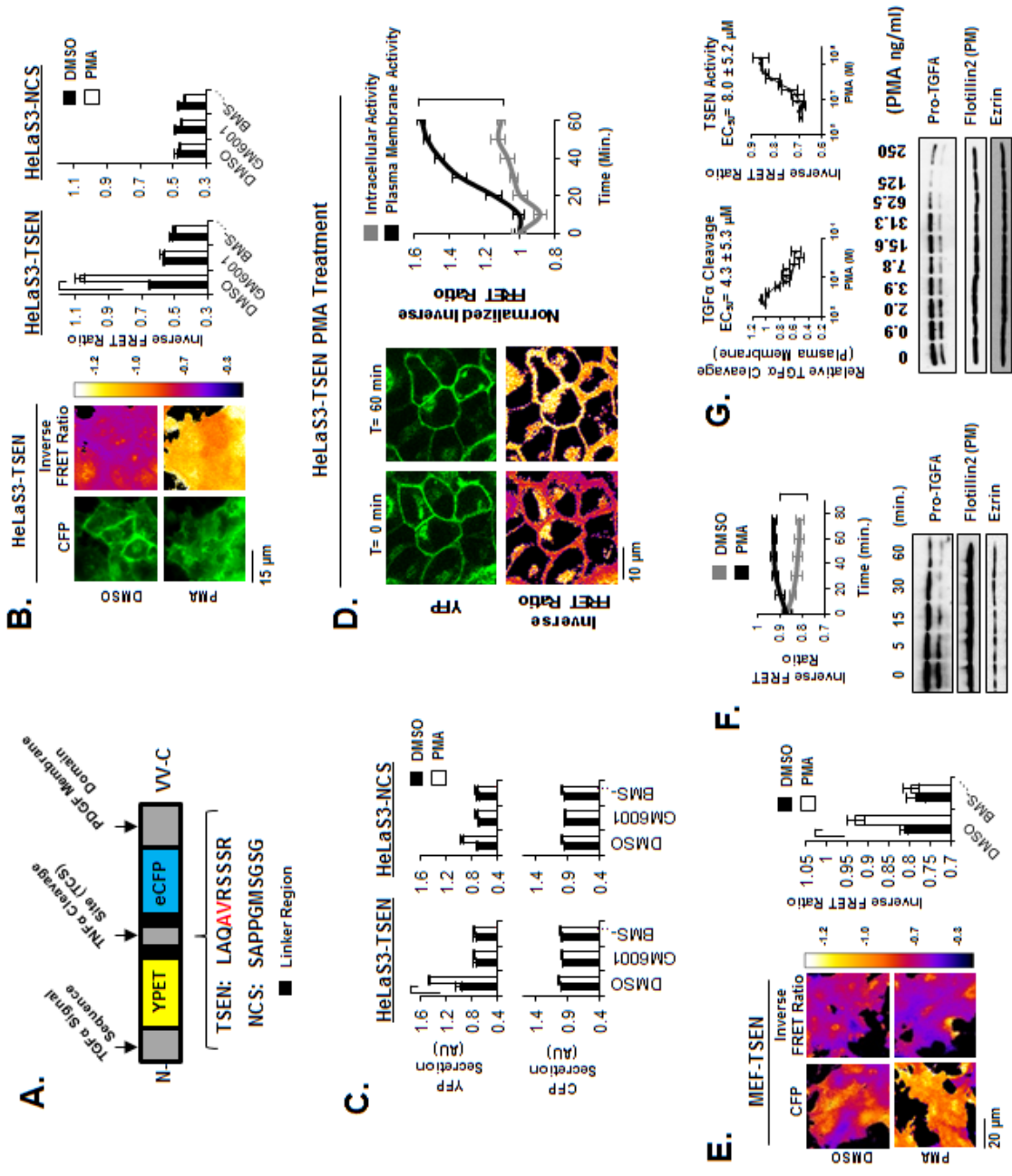


**Figure 2.1. TSen measures the catalytic activity of TACE in live cells.** (A) Schematic of the TSen FRET biosensor and the noncleavable control sensor (NCS). (B) Activity of TACE assessed by the cleavage of the sensor (inverse FRET ratio) in HeLa S3 cells stably expressing TSen and cultured with either PMA or vehicle for 1 hour. (C) Abundance of YPET in the medium from HeLa S3 cells stably expressing TSen and cultured with PMA or vehicle for 3 hours in the presence of TACE inhibitors. AU, arbitrary units. (D) Confocal microscopy of TACE activity assessed by FRET analysis of TSen in HeLa S3-TSen cells cultured with PMA. Images are of the same cells at both time points. (E) Activity of TACE by FRET analysis in MEF-TSen cells cultured with PMA and TACE inhibitor for 1 hour. (F) Timecourse of TACE activity by FRET analysis (top) in live cells or Western blotting for pro-TGF $\alpha$  (bottom) in plasma membrane (PM) fractions of MEF-TSen cells treated with PMA. (G) Relative abundance of pro-TGF $\alpha$  at the plasma membrane (left) and the inverse FRET ratio of TSen (right) in MEF-TSen cells cultured with PMA for 1 hour. Microscopy data are means  $\pm$  SEM from three trials, >500 cells each. Brackets: P < 0.01 by t test. All data are representative

along the polypeptide chain (about 245, 18, and 7 amino acids, respectively). However, in TSen, the TACE cleavage site is separated from the PDGFR transmembrane domain with an eCFP domain, whose N and C termini are positioned within  $22 \pm 1.8 \text{ \AA}$  (corresponding to a distance of about six amino acids) of each other, according to the eCFP structure in Protein Data Bank (identifier 2WSN)<sup>95</sup>. Thus, although the TACE cleavage site in TSen is fairly distant from the transmembrane domain in the primary structure, these two domains are likely positioned near each other in the tertiary structure. Additionally, TSen differs from TNF $\alpha$  in that TSen is a type I transmembrane protein, whereas TNF $\alpha$  is a type II. Because TGF $\alpha$ , another TACE substrate, is a type I transmembrane protein, it appears that TACE does not take into account the type of transmembrane protein as a parameter for selectivity. Despite the highly chimeric structure of TSen relative to the structures of endogenous TACE substrates, we found that this chimeric nature did not interfere with TSen being a highly suitable substrate for TACE.

### **TSen measures TACE activity in live cells**

TSen measures TACE activity as a function of inverse FRET ratio (CFP/FRET), meaning that the FRET signal decreases relative to CFP when TSen is cleaved, presumably by TACE, and the CFP and YPET fluorophores are separated, where YPET is then released as a soluble protein into the surrounding medium. In HeLa S3 cells stably expressing TSen, the inverse FRET ratio rapidly increased when PMA (phorbol 12-myristate 13-acetate), a previously reported activator of TACE<sup>63</sup>, was added to the culture medium (Fig. 2.1b and 2.2a). This PMA-induced change in the FRET signal was blocked by the addition of TACE inhibitors BMS-561392 (DPC-333) or GM6001. BMS-

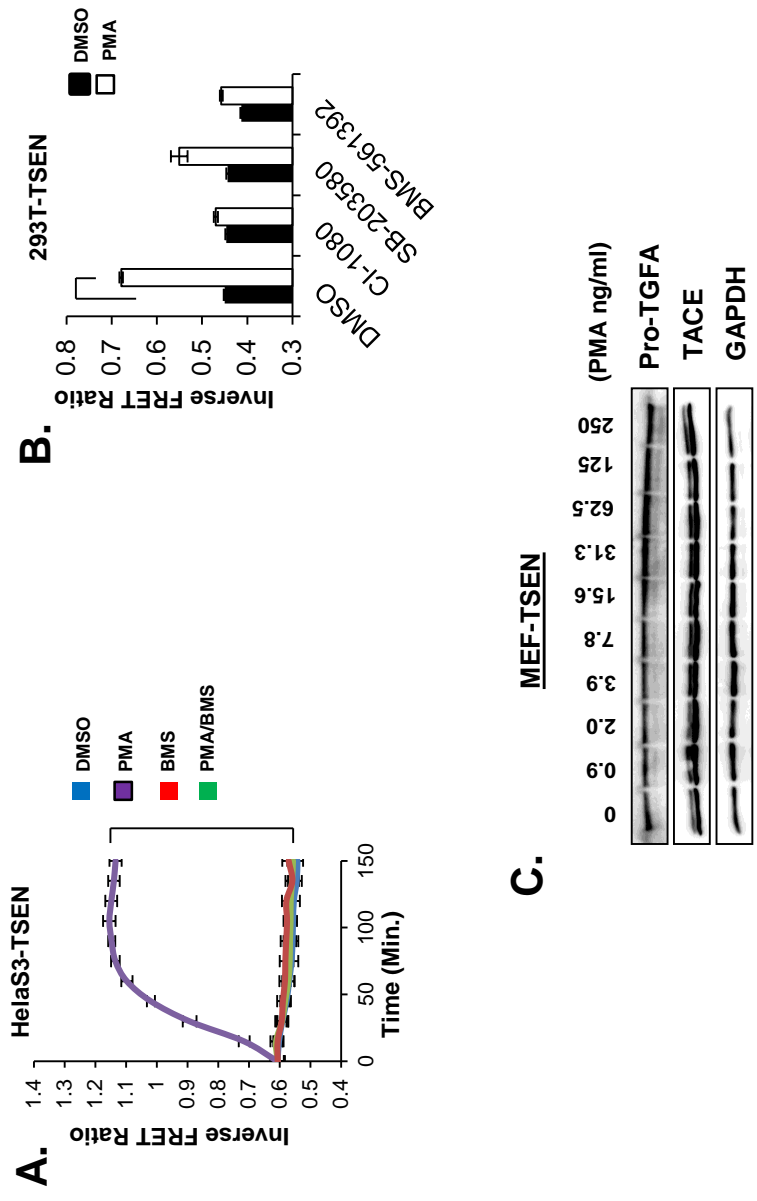


**Figure 2.2. The kinetics of TSen activation in response to PMA.** (a) A timecourse of inverse FRET ratio reveals that PMA induces a rapid activation of TACE, which can be blocked by co-treatment of BMS-561392. (b) TACE activity reported using TSen in 293T-TSen cells depends upon Erk, p38, and TACE activity.

561392 is a partially selective TACE inhibitor ( $K_i = 180$  pM) and has 100-fold selectivity over several other MMPs and ADAM family members [MMP12:  $IC_{50}$  (half maximal inhibitory concentration) = 2 nM; MMP13:  $IC_{50} = 12$  nM; ADAMTS4:  $IC_{50} = 10$  nM), whereas GM6001 is a nonselective MMP/TACE inhibitor<sup>96</sup>. Similar results were found in human embryonic kidney 293T cells transfected with TSen (herein called 293T-TSen cells) (Fig. 2.2b). To determine whether PMA-dependent TACE activity, as measured by our sensor, is contingent on the specific sequence of the TNF $\alpha$  cleavage site, we constructed a noncleavable sensor, in which the TACE cleavage site no longer resembled an ideal TACE substrate (Fig. 2.1a). The noncleavable sensor sequence was predicted to be a poor TACE substrate, according to a previous study<sup>57</sup>. PMA-dependent activation was not observed in HeLa S3 cells stably expressing the noncleavable sensor compared to those stably expressing TSen (HeLa S3-TSen cells) (Fig. 2.1b), validating that the TACE cleavage site is the primary and required feature of TSen to show PMA-dependent TACE activity.

Because TSen was designed to display reduced FRET efficiency through proteolytic cleavage, we validated that cleavage was indeed occurring. To this end, we additionally measured the release of YPET and CFP from HeLa S3-TSen cells after a 3-hour period of PMA stimulation in the presence or absence of either BMS-561392 or GM6001. PMA enhanced YPET, but not CFP, release into the medium, and YPET release was inhibited by either pharmacological TACE inhibitor (Fig. 2.1c). When the same experiment was conducted in HeLa S3 cells transfected with the noncleavable sensor, PMA-stimulated YPET release was greatly reduced but was not completely absent (Fig. 2.1c). This residual PMA-dependent cleavage of the “noncleavable” sensor is likely still

dependent on TACE because both GM6001 and BMS-561392 inhibited its activation. The remaining small portion of TACE activity detected through YPET release is likely to be attributed to cleavage at a cryptic site located between CFP and YPET in the noncleavable sensor that is independent of the TNF $\alpha$  cleavage site. These YPET secretion experiments, in conjunction with the microscopy experiments, demonstrate the versatility of TSen. Thus, TSen can be used in either a secretion-based fluorescent spectroscopy assay, in a similar manner to the available TACE bioassays<sup>97</sup>, or in a FRET-based live cell microscopy assay.

The use of TSen in live cells also enabled the determination of the intracellular location at which TACE is active. Using confocal microscopy, we repeated our experiments with HeLa S3-TSen cells in the presence of PMA to determine whether cleaved TSen localizes to intracellular vesicles or to the plasma membrane. We found that TSen cleavage localizes to a large degree to the plasma membrane and to a far lesser degree to intracellular vesicles under these conditions (Fig. 2.1d). This may be the result of selectively localized TACE activity, or more likely, it is a reflection of the selective localization of TSen. Therefore, TSen is not expected to show all possible subcellular locations where TACE may be active, nor does it elucidate where TACE itself is activated within a cell. Rather, the observations suggest that TSen is primarily a sensor of TACE activity at the plasma membrane.

**TSen reports TACE activity with similar dose and kinetic profiles to that of pro-TGF $\alpha$  cleavage at the plasma membrane**

Mouse embryonic fibroblasts (MEFs) have been used previously to study TACE-dependent cellular responses, wherein TACE mediates the cleavage of EGFR ligands<sup>77</sup>. MEFs stably expressing TSen (MEF-TSen) responded to PMA stimulation with TACE activation, assessed by an increase in inverse FRET ratio (Fig. 2.1e), similar to that observed for both HeLa S3-TSen and 293T-TSen cells (Fig. 2.1b and 2.2b). We aimed to determine whether the time and dose profiles of TACE activity in response to PMA were similar between TSen-measured activation of TACE and endogenous TGF $\alpha$  cleavage assessed by Western blot analysis. Although we could not detect cleavage of endogenous pro-TGF $\alpha$  in whole-cell lysates (Fig. 2.2c), we could detect the time-dependent disappearance of pro-TGF $\alpha$  in subcellular fractions enriched for plasma membrane (Fig. 2.1f). The time- and dose-dependent amount of pro-TGF $\alpha$  at the plasma membrane closely resembled the TACE activity as reported by TSen in fluorescence microscopy experiments (Fig. 2.1, f and g). These similarities between the PMA-induced dose- and time-response profiles for TSen and TGF $\alpha$  cleavage suggest that TSen may be a faithful reporter of TACE activity in general at the plasma membrane.

### **TSen reports TACE activity with high specificity**

To determine the specificity of TSen for measuring TACE activity, we stably expressed short hairpin RNA (shRNA) against *ADAM17* (the mRNA encoding TACE) in HeLa S3-TSen cells. Knocking down TACE (Fig. 2.3a) showed that the PMA-induced change in FRET ratio reported by TSen was dependent on TACE (Fig. 2.3b). Similarly, *Adam17*<sup>-/-</sup> MEFs transfected with TSen had no measurable changes in the TSen-reported inverse FRET ratio in response to PMA, in contrast to wild-type MEF-

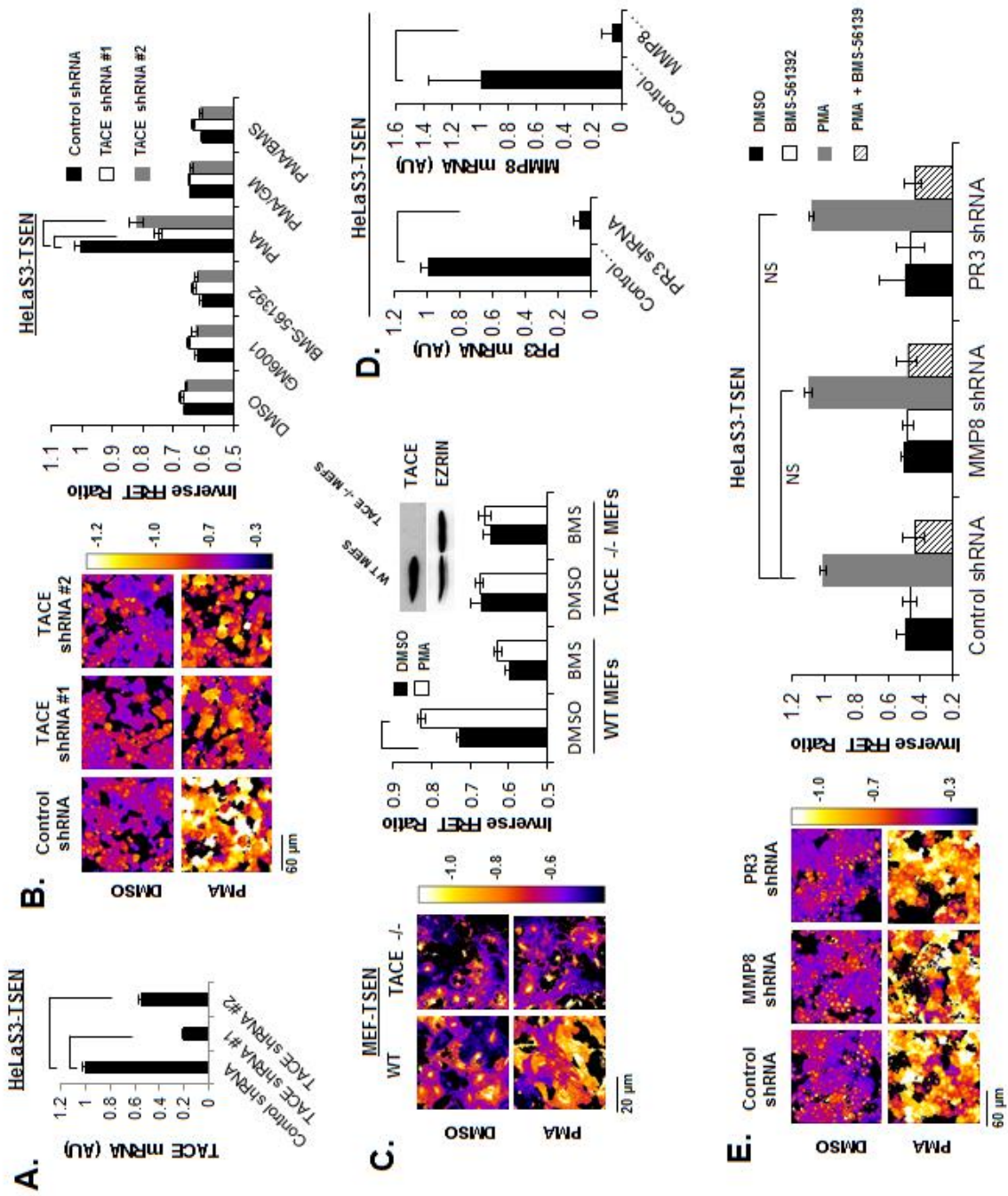


**Figure 2.3 Epidermal Growth Factor is an Activator of TACE.**

(a) HaCaT-TSen cells were used to determine the degree of TACE activation by EGF, and its dependence on TACE, EGFR, MEK1, and p38 activities. The same was done for SCC13-TSen cells (b) and VMCUB1-TSen cells (c). All data represents data at 3 hours after EGF stimulation. Cross symbols within plots signify statistical significance ( $p < 0.01$ ) of relevant conditions compared to all other conditions.

TSen cells, which display a significant increase in inverse FRET ratio in response to PMA (Fig. 2.3c). Previous studies show that TNF $\alpha$  can be cleaved not only by TACE but also by the protease PR3 (proteinase 3, encoded by *PRTN3*)<sup>98</sup>. Additionally, the peptidomimetic gelatinase B inhibitor Regasepin-1 is capable of inhibiting not only gelatinase B but also MMP8 and TACE to the same degree, suggesting that these proteases may share overlapping substrate specificity<sup>99</sup>. However, knocking down either MMP8 or the protease PR3 in HeLa S3-TSen cells (Fig. 2.3d) was insufficient to alter either the basal or PMA-stimulated inverse FRET ratio of TSen (Fig. 2.3e). Together, these series of experiments show that TSen is a biosensor that faithfully reports TACE activity with specificity for TACE over other similar proteases

### **TACE activation by stimulating EGFR is p38- and ERK-dependent**

TACE has been reported to mediate the proteolytic activation of several EGFR ligands<sup>74,80</sup>. We determined that PMA-dependent TACE activation measured through TSen depends partially on the kinases p38 and ERK (Fig 2.4a), which is consistent with the findings in other studies<sup>62,63</sup>. Because p38 and ERK are both activated upon stimulation of EGFR, and there is uncertainty whether this can enhance TACE activation<sup>65</sup>, we aimed to determine the breadth of the phenomenon of EGFR-mediated activation of TACE in several established cell lines. To this end, we created three additional stable epithelial cell lines expressing TSen (HaCaT keratinocytes, SCC13 squamous carcinoma cells, and VMCUB1 bladder cancer cells) and tested their responses to EGF. Although TACE was not activated by exogenous EGF in HeLa S3-TSen cells (Fig 2.5a), EGF efficiently activated TACE in HaCaT, SCC13, and VMCUB1 cells (Fig 2.4, b-d). The kinetics of activation of TACE was faster in PMA-stimulated

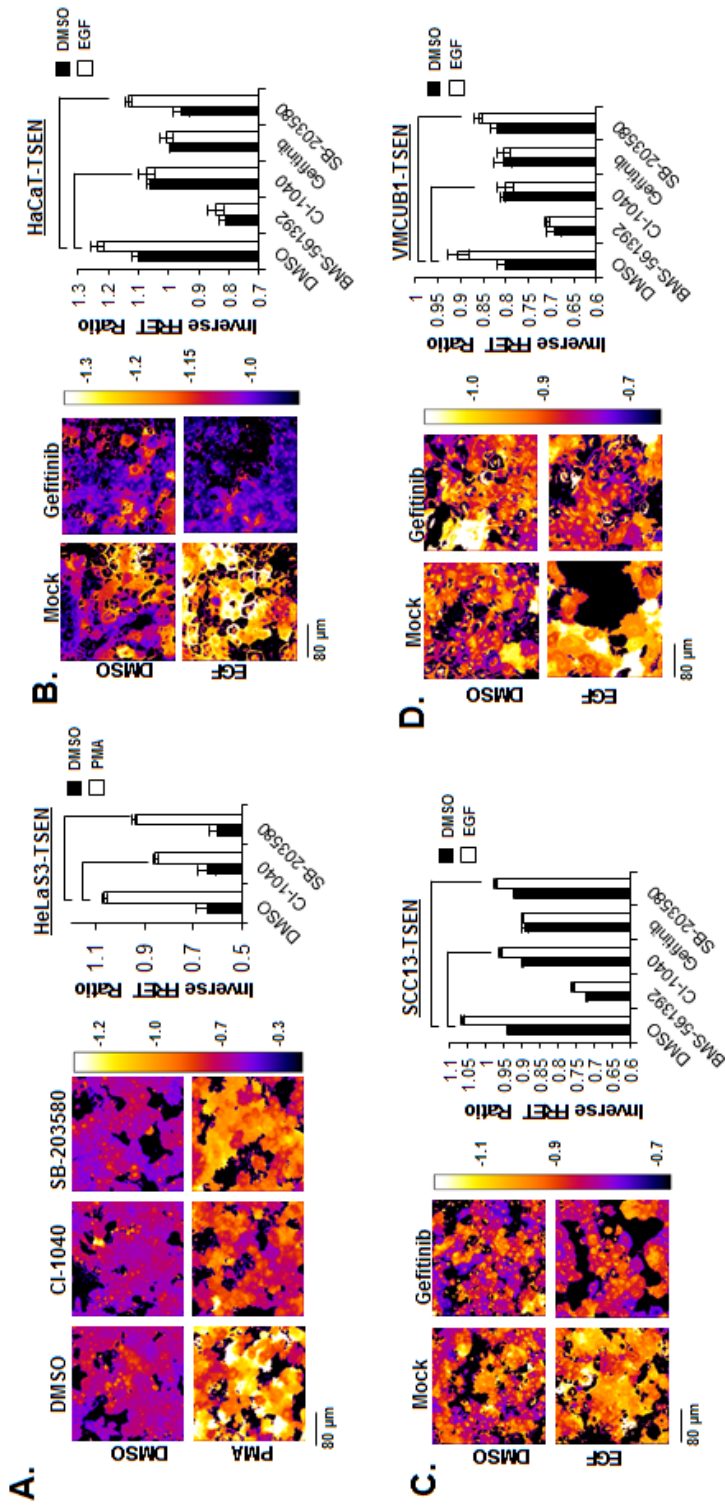


**Figure 2.4 Actin Depolymerization Activates TACE.**

(a) An unbiased chemical library screen in HaCaT-TSen cells reveal four candidate activators/repressors of TACE. All drugs in the screen were used at 10  $\mu$ M and measurements were made after 1 hour. (b) Cytochalasin D (CytoD) efficiently activates TACE in a dose dependent manner after 1 hour treatment. (c) CytoD dependent activation of TACE does not depend upon MEK or p38 activites. (d) Similar results to (c) were observed for SCC13-TSen cells. (e) A FRET reporter for Erk (EKAR) was used to determine that CytoD can cause EGFR1 activation through TACE proteolytic activity. Inhibitors in co-treatment experiments were introduced as 30 min pre-treatments. Cross symbols within plots signify statistical significance ( $p < 0.01$ ) of relevant conditions compared to DMSO controls.

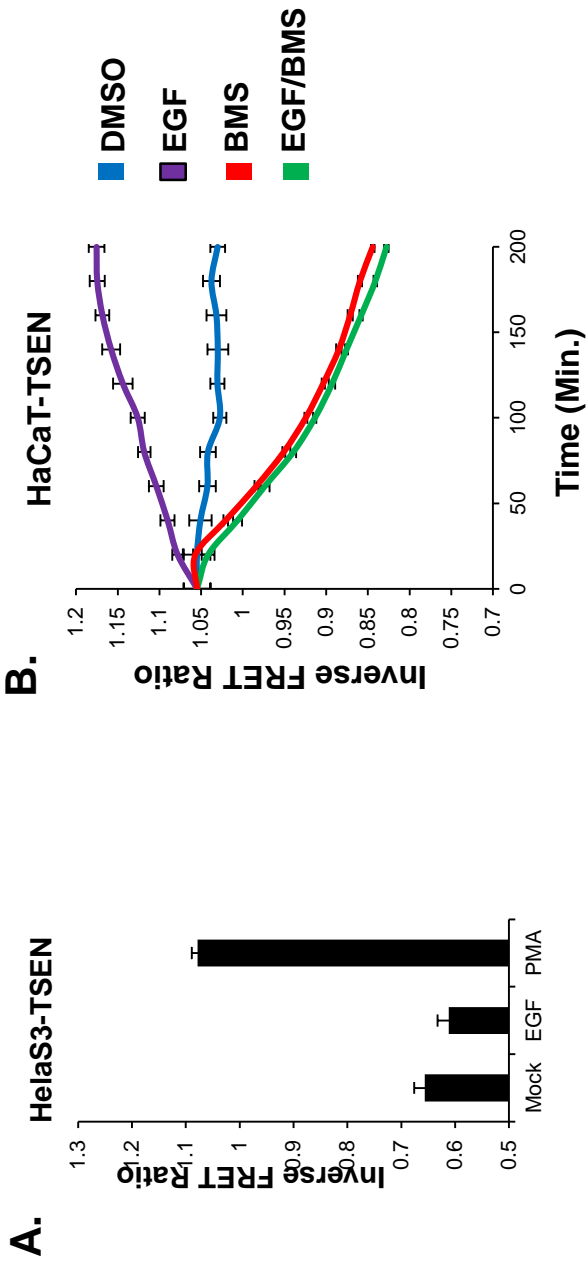


**Figure 2.5 The kinetics of TSen activation in response to EGF.**  
 (a) HeLaS3-TSen cells do not display activation of TACE in response to EGF. (b) In contrast, HaCaT-TSen cells display EGF dependent activation of TACE with slower kinetics to that of PMA in HeLaS3-TSen cells.

cells (1 hour to saturation, Fig. 2.2a), compared to EGF-stimulated cells (3 hours to saturation, Fig. 2.5b). EGF-dependent TACE activation was blocked in all cell lines by pharmacological EGFR inhibition using gefitinib, which is consistent with the theory that the activation of TACE by EGF occurs through EGFR. As expected, the TACE inhibitor BMS-561392 diminished both basal and EGF-dependent TACE activation, revealing that only a portion of the total TACE activity in all three of these cell types was dependent on EGFR. Additionally, the effects of the inhibitors SB-203580 and CI-1040, which target p38 and MEK1 (MAPK kinase 1, which phosphorylates ERK), respectively, consistently showed the importance of both of these kinases in EGF-dependent TACE activation. Thus, EGF-dependent activation of TACE in these three cell lines was similar to that of PMA-dependent activation of TACE in both HeLa S3 and 293T cells (Fig. 2.1e and 2.2b), in which both chemical and biochemical activation of TACE were p38- and ERK-dependent.

### **Chemical compound screening reveals novel activators and inhibitors of TACE**

To further understand the cellular regulation of TACE, we conducted an unbiased screen of small-molecule compounds in HaCaT-TSen cells to find those that are capable of modifying TACE activity. We screened 81 compounds that affect diverse cellular functions (table 1.1), from a library of small molecules that either have been widely used research tools or are approved by the Food and Drug Administration for clinical applications. Thus, each compound has a known mechanism of action. Our screen revealed two candidate compounds that activate TACE [cytochalasin D (CytoD) and quinacrine] and two candidate compounds that repress TACE (doxorubicin and sunitinib) (Fig 2.6a). All four candidates were validated in independent titration

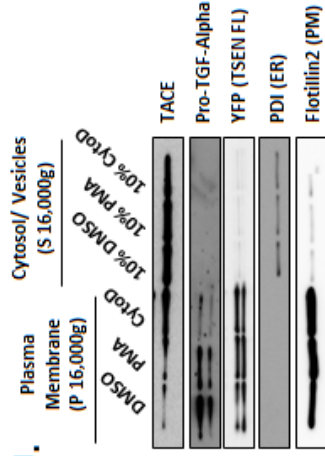
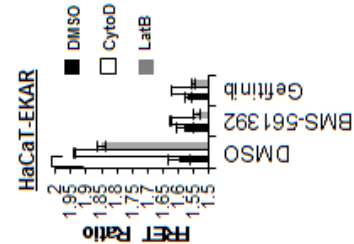
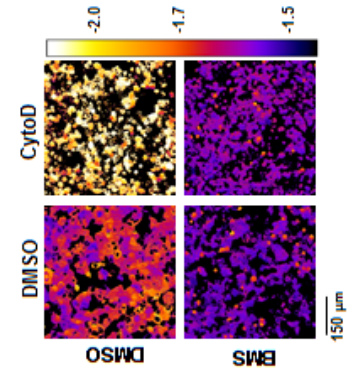
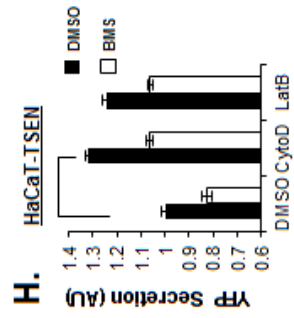
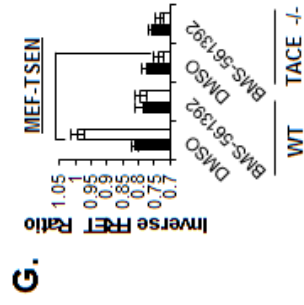
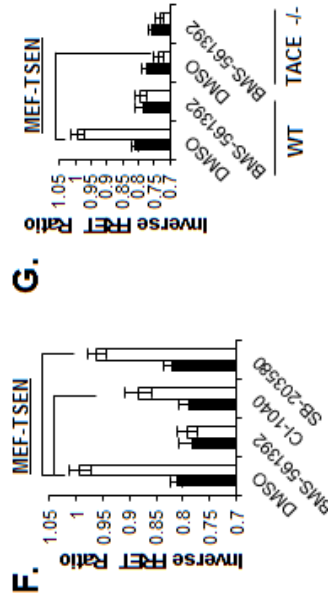
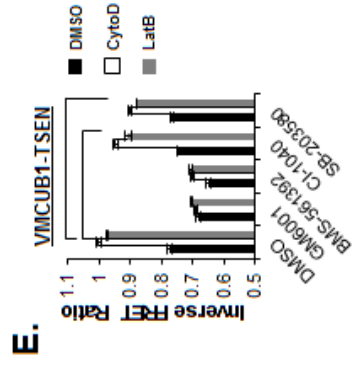
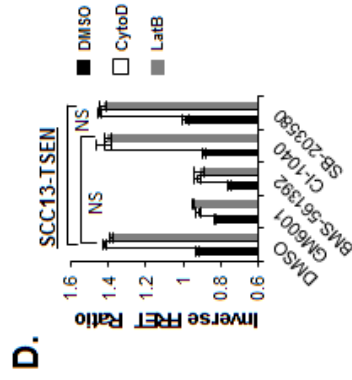
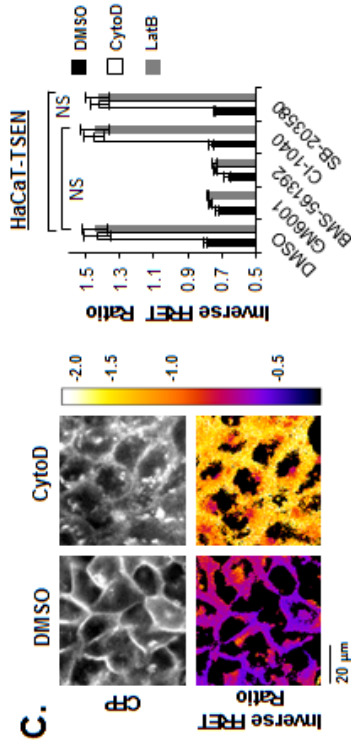
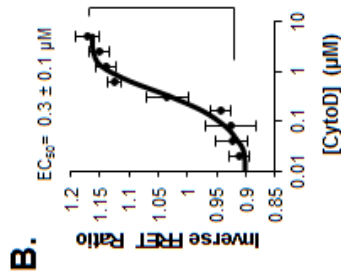
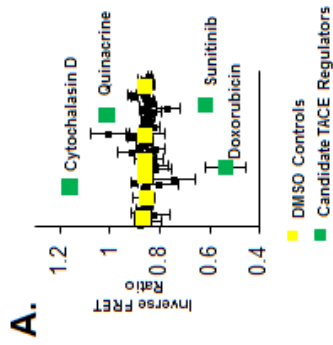


**Figure 2.6 EGF and CytoD, but not PMA, Dependent TACE Activation Requires ER Exit of Nascent Proteins.**  
(a) In HeLaS3-TSen cells, PMA stimulation of TACE cannot be inhibited by 30 min Brefeldin A (BFA) pre-treatment.  
(b) Similar results were obtained for 293T-TSen cells. (c) In contrast, EGF and CytoD pre-treatment in HaCaT-TSen cells can almost completely block TACE activation. (d) VMCUB1-TSen cells, which respond to PMA, EGF and CytoD treatments, depend upon ER exit for all three means of TACE activation. All measurements depict data after 3 hours of TACE activation. Cross symbols within plots signify statistical significance ( $p < 0.01$ ) of relevant conditions compared to the appropriate DMSO control.

experiments (Fig 2.6b and 2.7a-c). Doxorubicin is a DNA-damaging agent that can activate an apoptosis response in cells through the activation of caspase-8, a protease capable of activating TACE<sup>100</sup>. Although we observed doxorubicin to be an inhibitor of TACE activity, we investigated whether this suppression was an indirect effect as a result of its activation of apoptosis. We found that doxorubicin did not activate apoptosis as assessed by caspase-3 cleavage under the experimental conditions we used, but it can cause the accumulation of pro-TGF $\alpha$  in whole-cell lysates, supporting the claim that doxorubicin inhibits TACE (Fig. 2.7d). Presumably, this inability of doxorubicin to activate apoptosis in these cells may be attributed to the high density (1200 cells/mm<sup>2</sup>) at which cells were screened, which leads to density-dependent inhibition of cellular proliferation (Fig. 2.7e) and hence to decreased DNA replication and a decreased amount of doxorubicin-associated DNA intercalating damage.

### **Actin cytoskeleton–dependent activation of TACE relies on the accumulation of TACE at the plasma membrane**

Because CytoD, an inhibitor of actin polymerization, emerged as the strongest potential activator of TACE, we investigated the possible regulatory connection between the actin cytoskeleton and TACE activity. We conducted a dose-response experiment in HaCaT-TSen cells using latrunculin B (LatB), which is another actin-depolymerizing agent with a mechanism of action that is different from that of CytoD. We found that LatB had a similar ability to increase the inverse FRET ratio (Fig. 2.7f and 2.6 c-e) with faster kinetics than that of EGF (half maximum at ~30 min compared with ~120 min, respectively) (Fig. 2.5b and 2.7h). We confirmed that these actin-targeting drugs were capable of modulating the actin cytoskeletal structure at their respective EC<sub>50</sub> (half

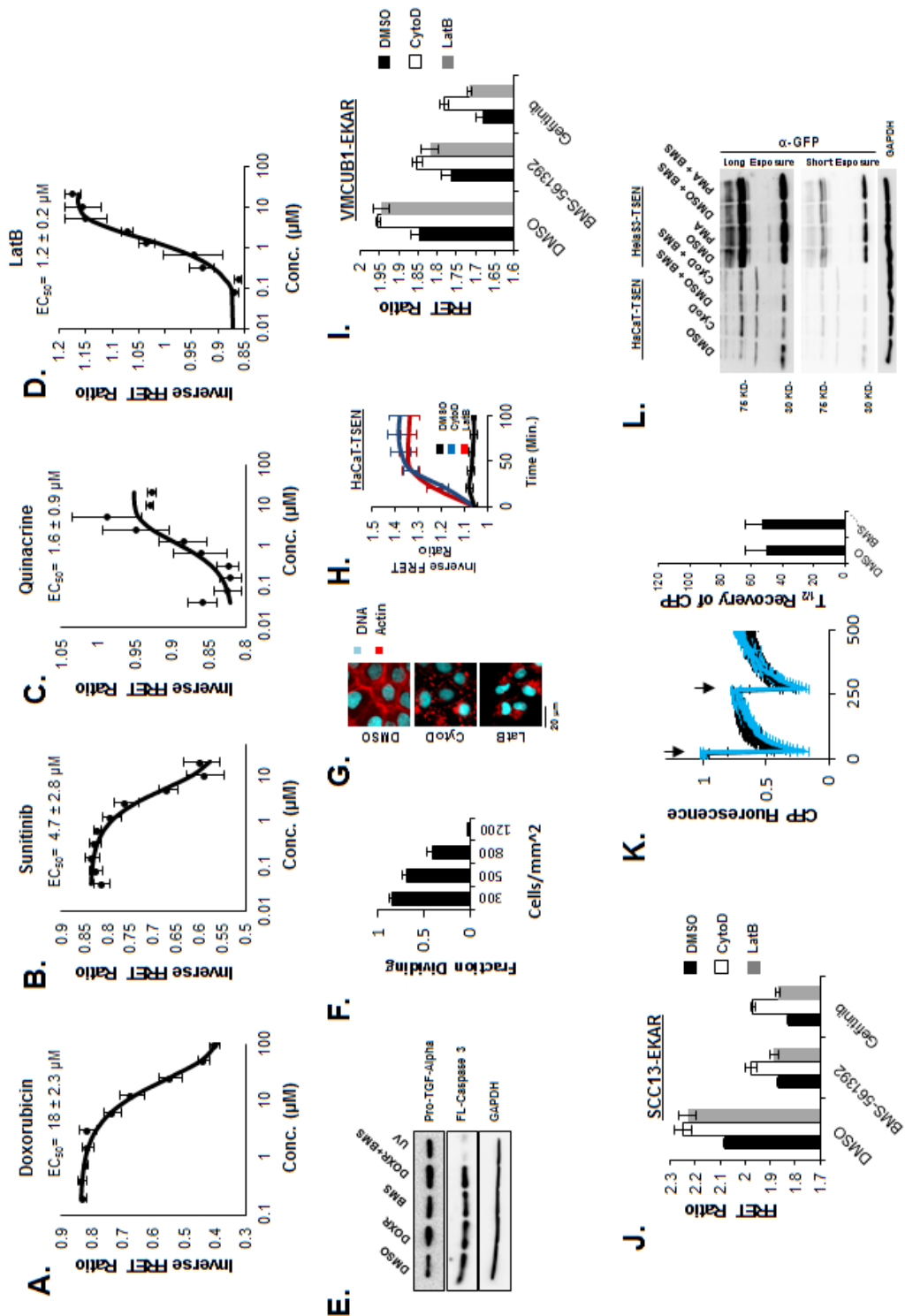


**Fig. 2.7. Validation of CytoD dependent activation of TACE.**

(a) Dose response curve of Doxorubicin after 1 hour in HaCaT-TSen cells. (b) Dose response curve of Sunitinib after 1 hour in HaCaT-TSen cells. (c) Dose response curve of Quinacrine after 1 hour in HaCaT-TSen cells. (d) Dose response curve of Latrunculin B after 1 hour in HaCaT-TSen cells. (e) Phalloidin and DAPI staining of fixed HaCaT cells reveals effective depolymerization of actin in response to CytoD and LatB (f) YFP secretion over 3 hours from HaCaT-TSen cells into the surrounding media was measured in the presence and absence of either CytoD or LatB. (g) Kinetic profile of TACE activation by CytoD and LatB in HaCaT-TSen cells. (h) CytoD and LatB both activate TACE in VMCUB1-TSen cells, which does not depend greatly on Erk or P38 activities. (i) VMCUB1-EKAR cells display EGFR1 activation in response to CytoD and LatB. (j) The same is true for SCC13-EKAR cells. Cross symbols within plots signify statistical significance ( $p < 0.01$ ) of relevant conditions compared to all other conditions.

Allopurinol	Dacarbazine	Ixabepilone	Romidepsin
Altretamine	Dactinomycin	Lapatinib Ditosylate	Sirolimus (Rapamycin)
Aminolevulinic Acid	Dasatinib	Lenalidomide	sorafenib
Anastrozole	Daunorubicin HCl	Letrozole	Streptozocin
Arsenic Trioxide	Decitabine	Lomustine; CCNU	Sunitinib Malate
Axitinib	Dexrazoxane HCl	Mechlorethamine HCl	Tamoxifen Citrate
Azacitidine	Docetaxel	Mercaptopurine	Temozolomide
Bortezomib	Doxorubicin HCl	Methotrexate	Teniposide
Busulfan	Etoposide	Methoxsalen	Thalidomide
Cabazitaxel	Everolimus	Mitomycin C	Thioguanine
Capecitabine	Exemestane	Mitoxantrone HCl	Thiotepa
Carmustine	Floxuridine	Nelarabine	Topotecan HCl
Celecoxib	Fluorouracil (5-FU)	Paclitaxel	Tretinoin
Chlorambucil	Fulvestrant	Pazopanib HCl	Uracil mustard
Cisplatin	Gefitinib	Pemetrexed Disodium	valrubicin
Cladribine	Gemcitabine HCl	Pentostatin	vandetanib
Crizotinib	Hydroxyurea	Pralatrexate	Vemurafenib
Cyclophosphamide	Ifosfamide	Procarbazine HCl	Vinblastine Sulfate
Cytarabine; Ara-C	Imatinib Mesylate	Quinacrine	Vincristine Sulfate
Cytochalasin D	Irinotecan HCl	Raloxifene HCl	Vismodegib
			Vorinostat

Table 2.1. A complete list of chemicals used to screen for TACE regulators.

maximal effective concentration) concentrations by fixing HaCaT cells in the presence or absence of either CytoD or LatB and staining for F-actin using phalloidin–rhodamine B (Fig. 2.7g). Furthermore, the actin depolymerization–induced increase of the inverse FRET ratio in TSen-expressing cells did not require the kinase activity of ERK or p38 in HaCaT and SCC13 cells (Fig 2.6c and d), but it did in VMCUB1 cells and MEFs (Fig 2.6e and f). Although this ERK and p38 dependence was cell type–specific, the fact that actin disruption can occur independently of these kinase activities suggests that actin disruption is capable of regulating TACE activity through a mechanism that is distinct from TACE phosphorylation.

Three observations suggested that actin cytoskeletal disruption does indeed cause endogenous activation of TACE. First, CytoD-dependent induction of an inverse FRET ratio in MEF-TSen cells was completely blocked upon deletion of the *Adam17* gene (Fig 2.6g). Second, actin-depolymerizing drugs efficiently induced the release of YPET into the surrounding medium, which was blocked by pharmacological inhibition of TACE with BMS-561392 (Fig 2.6f). Third, actin-depolymerizing agents induced EGFR-dependent ERK activation in HaCaT, SCC13, and VMCUB1 cells stably expressing a well-known ERK FRET biosensor, EKAR<sup>101</sup>, which was blocked by pretreating cells with either BMS-561392 or gefitinib (Fig 2.6i and 2.7i and j). These experiments provide additional support that TSen enabled the detection of a previously unknown mechanism of TACE activation: perturbation of the actin cytoskeleton.

Because cytoskeletal disruption is variably mediated by p38 and ERK activities across the many cell lines investigated, we sought to explain how actin-depolymerizing drugs were capable of activating TACE independently of p38 and ERK. The actin cytoskeleton

is important for a myriad of cellular processes, including endocytosis through clathrin-coated pits<sup>102</sup>. Thus, we performed subcellular fractionation of MEFs by differential centrifugation to separate the plasma membrane in cell lysates from the vesicle and soluble components of the cytosol. TACE accumulated at the plasma membrane in cells exposed to CytoD but not PMA (Fig 2.6j). However, pro-TGF $\alpha$  abundance was decreased in cells exposed to either PMA or CytoD, the latter eliciting a greater magnitude change (Fig 2.6j), which was consistent with our fluorescence microscopy experiments (Fig 2.4b and 2.6i). Upon either PMA or CytoD treatments, the abundance of the TACE sensor TSen at the plasma membrane remained unchanged. The accumulation of TACE at the plasma membrane is likely to be independent of the kinase activity of p38 or ERK, because PMA-dependent activation of TACE consistently relies on the activity of these kinases, but it did not lead to an accumulation of TACE at the plasma membrane. Although cleavage of the full-length sensor was expected to mirror the cleavage of pro-TGF $\alpha$ , we were unable to detect a substantial decrease of the uncleaved TSen by Western blot, although the cleaved product (YPET) accumulated in the medium (Fig 2.6h). To explain this observation, we performed fluorescence recovery after photobleaching (FRAP) in HaCaT-TSen cells, which revealed that TSen turnover at the plasma membrane occurred with a half-life of 1 min, independently of TACE activity (Fig. 2.7k). In contrast, the activation of TSen measured by fluorescence microscopy occurred about 30 times more slowly (Fig. 2.7h). These data suggest that the combination of a relatively small portion of plasma membrane-localized TSen being cleaved by TACE and the high turnover of TSen at the plasma membrane may preclude the ability to detect TSen cleavage by Western blotting.

Nevertheless, our subcellular fractionation data suggest that only actin cytoskeleton disruption, not PMA stimulation, alters the subcellular trafficking of TACE to and from the plasma membrane.

## **DISCUSSION**

Our study illustrates not only a novel technique for measuring plasma membrane-localized TACE activity with high specificity in live cells but also how the TSen sensor can successfully be used to shed light on the complexity of TACE activation in cells. The development and use of TSen enabled us to discover a previously unknown actin cytoskeleton-dependent mechanism of TACE activation by regulating its accumulation at the plasma membrane. We propose that this mechanism for TACE activation highlights a role for the actin cytoskeleton as a sensory structure, whose integrity is functionally linked to TACE activation, EGFR ligand shedding, and subsequent ERK activation. ERK regulates cytoskeletal remodeling through cortactin activation<sup>103–106</sup>, suggesting that cells may use TACE-mediated shedding of EGFR ligands as a means to induce ERK-mediated actin remodeling and repair in response to actin damage.

In addition, TSen enabled us to determine that EGF-dependent activation of TACE was driven by a combination of p38- and ERK-dependent mechanisms ubiquitously, but to varying degrees, across the many cell lines investigated. This observation suggests that cells may engage a positive feedback system for TACE-dependent shedding of EGFR ligands, where TACE activity can promote subsequent increases in TACE activity through EGFR and p38 and/or ERK activation. Such positive feedback has been proposed in previous studies<sup>73</sup>. One physiologically relevant occurrence of such a

feedback loop may be in the skin to promote wound healing. In wound healing model systems for the skin, epithelial sheets of keratinocytes undergo sustained motility upon wounding, which depends on sustained EGFR activity<sup>107</sup>. Initiation of epithelial sheet migration may rely on a wide range of possible initial stimuli, such as reactive oxygen species<sup>108</sup>, that activate p38 and/or ERK in response to direct wounding. Our study suggests that TACE-mediated EGFR ligand shedding likely continues after the initial activation of p38 or ERK subsides, even when the initial stimulus has been removed. Using TSen may provide insight into not only how individual cells respond to environmental stimuli, as shown here, but also how groups of cells respond during a physiological process like wound healing. This TACE biosensor should facilitate the investigation of mechanisms regulating TACE activation and the development of new pharmacological agents to control its activity.

## **MATERIALS AND METHODS**

### **Cell culture and pharmacological inhibitors**

All cells were cultured using Dulbecco's modified Eagle's medium as previously described<sup>107</sup>. Wild-type and *Adam17* null MEFs were gifts from C. Blobel. Unless explicitly stated in the figures, the following doses were used for cell treatments: EGF, 100 nM; BMS-561392, 2.5  $\mu$ M; GM6001, 10  $\mu$ M; CytoD, 1  $\mu$ M; LatB, 2.5  $\mu$ M; PMA, 200 nM; gefitinib, 1  $\mu$ M; CI-1040, 500 nM; SB-203580, 10  $\mu$ M; doxorubicin, 5  $\mu$ M.

### **Construction of the TACE sensor**

The parental vector for TSen, EKAREV, is described by Komatsu *et al.*<sup>109</sup> and provided by K. Aoki and M. Matsuda. A cassette encoding a TGF $\alpha$  signal peptide (MVPSAGQLALFALGIVLAACQALENSTSPLSDPPVAAAVVSH), hemagglutinin (HA) tag (YPYDVPDYA), PDGFR transmembrane domain, and FLAG tag VV (DYKDDDDKVV) was synthesized by GenScript (sequence is available upon request) and subcloned into the Eco RI–Sal I site of EKAREV to produce the pBBSR-TGFA-HA-PDGF-FLAG plasmid. Oligonucleotides encoding the TACE cleavage site (sense strand: 5'-TCGAGAGCGGCCTGAGATCTAGCGGCCTGGCCCAGGCCGTGAGATCCAGCTCCAGAGCGGCAGCGGATCCACCAGC-3', and antisense strand: 5'-GGCCGCTGGTGGATCCGCTGCCGCCTCTGGAGCTGGATCTCACGGCCTGGGCCAGGCCGCTAGATCTCAGGCCGCTC-3') or a noncleavable site (sense strand: 5'-TCGAGAGCGGCAGCGGCAGCAGCGGCAGCGCTCCCCGGGCATGAGCGGCAGCGCGGCAGCGGCACC-3', and antisense strand: 5'-GGCCGGTGCCGCTGCCGCCGCGCTGCCGCTCATGCCCGGGGAGCGCTGCCGCTGCTGCCGCTGCCGCTC-3') were inserted in Xho I–Not I site of the EKAREV plasmid to generate TACE-REV and NCS-REV plasmids, respectively. The fragments encoding YPET-TACE-REV-ECFP or YPET-NCS-REV-ECFP were excised by digestion with Eco RI–Xba I and inserted in between the HA and PDGFR domains (Eco RI–Avr II) of pBBSR-TGFA-HA-PDGF-FLAG. The resultant vectors were named as TSen and NCS (Fig. 2.1a).

### **FRET data analysis and fluorescence spectroscopy**

Live cell microscopy was conducted as previously described (42). Filters used for FRET measurements were the following: FRET excitation 438/24-25, dichroic 520LP, emission 542/27-25 (Semrock MOLE-0189); CFP excitation 438/24-25, dichroic 458LP, emission 483/32-25 (Semrock CFP-2432B-NTE-Zero). Time lapse microscopy images were analyzed, and FRET calculations were performed using MATLAB (data file S1). Briefly, images were background-corrected through subtraction using images acquired from samples of cell-free media. Pixels representing cells were identified as having an intensity 1000 units above background. FRET ratio or inverse FRET ratio was calculated as either FRET intensity against CFP intensity or CFP intensity against FRET intensity, respectively, and all relevant pixels were averaged. Each image was acquired at  $\times 4$  magnification for calculations, which encompasses data from at least 1000 cells per measurement. Measurements were done in triplicate. For images displayed,  $\times 40$  magnification was used. A similar method of inverse FRET ratio calculations was used in confocal microscopy experiments, where a zplane of 1- $\mu\text{m}$  height at  $\times 100$  magnification was measured, and segmentation of membrane and vesicle fractions was performed in MATLAB.

### **Fluorescent protein secretion experiments**

YPET media secretion was quantified by transfer of media supernatant to 96-well plates, followed by measurement of YPET fluorescence using a Tecan Microplate reader (excitation 500/20, emission 550/20). CFP media secretion was performed in the same manner with different parameters (excitation 438/20, emission 485/20).

### **Stable shRNA expression**

Stable shRNA expression was achieved using TRC Lentiviral shRNA (Thermo) with the following shRNA constructs: *ADAM17* (TACE), TRCN0000052172 and TRCN0000052168; *PR3*, TRCN0000418696; *MMP8*, TRCN0000373060; and SHC016 (a control construct). Stable shRNA knockdown cell lines were selected in the presence of puromycin (2 µg/ml). Lentiviral manufacturing was done in 293T cells, using pHCMV-VSVg, pMDLg, and pREV vectors.

### **Western blotting**

Whole-cell lysates were prepared in radioimmunoprecipitation assay buffer [25 mM tris-HCl (pH 7.4), 150 mM NaCl, 1% sodium deoxycholate, 1% Triton X-100, 0.1% SDS, 1 mM EDTA, 1 mM phenylmethylsulfonyl fluoride (PMSF)]. Subcellular fractionation was achieved by lysis in fractionation buffer [25 mM tris-HCl (pH 7.4), 150 mM NaCl, 1 mM PMSF, 0.1% Tween 20], with a buffer-to-cell ratio (by volume) of 10:1, for 10 min at 4°C, followed by seven volume strokes with a 1-ml syringe/25G needle. Lysate was centrifuged at 3000g to pellet nuclei. Supernatant was then centrifuged at 16,000g. The resulting pellet was used as the plasma membrane fraction, whereas the supernatant was used as the cytosol/vesicle fraction. Antibodies used for Western blots were against pro-TGFα (3715S, Cell Signaling Technology), TACE (Ab39162, Abcam), GAPDH (SC47724, Santa Cruz Biotechnology), caspase-3 (9665p, Cell Signaling Technology), flotillin-2 (3436s, Cell Signaling Technology), PDI (3501p, Cell Signaling Technology), and YPET (632376, Clontech Laboratories).

### **Reverse transcription polymerase chain reaction**

For RT-PCR, the following primers were used: *ADAM17* (TACE), 5'-GAGCCACTTTGGAGATTTGTTAATG-3' (forward) and 5'-GTTCCGATAGATGTCATCAACTCTGTC-3' (reverse); *PR3*, 5'-ATGGCCTCCCTGCAGATGCGGGGG-3' (forward) and 5'-GCCAGCCAACCTCAGTGCCTCCG-3' (reverse); and *MMP8*, 5'-AGCTGTCAGAGGCTGAGGTAGAAA-3' (forward) and 5'-CCTGAAAGCATAGTTGGGATACAT-3' (reverse).

### **Small-molecule compound library**

All drugs in the screen were used at 10  $\mu$ M, and measurements were made after 1 hour. The small-molecule compound libraries included selected compounds from the Approved Oncology Drugs Set and the Structural Diversity Set, which were provided by the National Cancer Institute Developmental Therapeutics Program ([http://dtp.nci.nih.gov/branches/dscb/repo\\_open.html](http://dtp.nci.nih.gov/branches/dscb/repo_open.html)).

### **FRAP experiments**

TSen-expressing HaCaT cells were imaged using a Nikon A1R LSM confocal microscope. Measurements for CFP were achieved using a 405 laser with a 450/50 emission filter. A 100 $\times$  oil immersion objective was used. A 2  $\mu$ m  $\times$  2  $\mu$ m square was selected over both the cellular junctions and an unoccupied extracellular space, where photobleaching was performed for 4 s at 100% laser power.  $n = 20$  cells in each of two independent experiments. Image analysis was performed in MATLAB.

### **Cell proliferation assay**

The Click-IT EdU Alexa Fluor 488 Imaging Kit (Life Technologies) was used to assay the percentage of cells dividing in populations of cells plated at different density, according to the manufacturer's instructions. Cells were exposed to EdU (5-ethynyl-2'-deoxy-uridine) for 8 hours.

### **Statistical analysis**

All comparisons indicated with brackets were the result of a two-tailed *t* test, from which *P* values were obtained, using Microsoft Excel. Two-tailed *t* tests were conducted between data collected from triplicate trial measurements in individual experiments.

## Chapter 3

### Automated Image Processing and Analysis and Dual Sensor Reporting of ERK and TACE in Single Cells

#### Introduction

Microscopy has an essential role in biological research. It is sometimes the most direct route to answering a question, especially those about large-scale structures or localization. It has the potential to track changes in real time while simultaneously registering where they are in space. Some questions cannot be answered without microscopy as a tool, for instance single cell tracking experiments have revealed behaviors within a population other types of assays could never have measured<sup>43,45</sup>. The power of this technique has led researchers to generate creative techniques for the indirect measurement of cellular activities.

Fluorescence resonance energy transfer (FRET) is the nonradiative movement of energy from an excited-state donor molecule to an acceptor. The efficiency of this transfer depends on the overlap between donor emission and acceptor excitation, the distance between the two molecules, and the orientation of the chromophore dipoles relative to each other<sup>110</sup>. By placing a FRET pair around a binding site of interest, FRET can be used to measure secondary messengers or to decipher cellular activities<sup>111,112</sup>. This technique was used to place the ERK docking domain, phosphorylation substrate peptide, and a linker separated phospho-binding domain between a FRET pair so that active ERK would cause a conformational change, subsequently increasing FRET detectable in live cells<sup>101</sup>. This sensor was later optimized with the FRET pair YPET

and eCFP as well as an extended linker region optimized to improve dynamic range by lowering FRET of unphosphorylated sensor, termed EKAR-ev<sup>109</sup>.

In an attempt to lower the number of wavelengths a sensor needs to report activity, the Covert lab developed kinase translocation reporters (KTRs) so that signaling could be monitored by the position of the sensor rather than FRET. By modifying a minimal fragment of c-Jun to include two phosphorylation sites and its nuclear export signal attached to a fluorescent protein, it was found that kinase activity could lead to altered localization between the nucleus and cytoplasm. This construct was further adapted by adding inhibitory phosphorylation sites adjacent to the nuclear localization signal to lower import so that kinase activity would both increase export and prevent re-entry to the nucleus. This construct was adapted for other kinases by changing the docking site to those of interest and the sensor was validated for ERK, p38, and JNK<sup>113</sup>.

Using both EKAR-ev and the KTR for ERK (ERKTR), ERK activity has been seen in single-cell tracking experiments as discrete activity pulses<sup>45-49</sup>. ERK activity pulses are correlated with both EGF concentration and proliferation. Stimulating ERK with the same dynamics as the pulses caused expression of SRF-regulated genes and increased proliferation compared to prolonged activation<sup>46</sup>. There are contradictory results as to the origin of ERK activity pulses; one set of experiments indicated that cellular noise leads to stochastic activation of Raf to activate ERK and propagate through ligand shedding to nearby cells<sup>46</sup>. However, another finding is that changing the system to a related tyrosine kinase receptor did not result in pulsing activity but retained Raf as an upstream component to ERK, indicating that ERK activity pulses originate at

the receptor<sup>47</sup>. These results agree in that autocrine/paracrine ligand shedding appears to aid in the appearance of ERK pulses for signal propagation but there is still a fundamental lack of information as to how these pulses are regulated.

## Results

To generate rapid and unbiased results from a high-content microscope, it is essential to generate methods for automated processing and analysis of acquired images. This chapter will cover the basic techniques used to prepare images for accurate quantification as well as some more advanced algorithms used to obtain novel results. Some of these techniques, to the knowledge of the author, are novel and could be useful for others. In general, images are first flat-field corrected if they have an artificially bright center, then background subtracted to lower an inaccurately high signal. Once pixel values are adjusted, segmentation can be performed to identify the pixels of interest for quantification; a method that changes drastically with the assay being assessed.

## General Processing

Many images acquired in this thesis were acquired on a microscope with a large (2160x2160 pixel) camera but with restricted light flow between the sample and the camera. While a large camera has the advantage of obtaining larger sample sizes, an undesired side effect is vignetting. Vignetting generates an artificially bright center to the image and dim edges and corners; this can be accounted for by a flat-field correction given in the following equation:

$$C = \frac{(R - D) * m}{F - D}$$

where C = corrected image, R= raw image, F = flat field image (an example vignette), D = dark frame (signal with no incident light), and m = average value of (F-D)<sup>114</sup>. While it is reasonable to obtain example vignette images in each experiment, many microscopes make it difficult to completely block the camera for a dark frame. If the dark frame image is considered negligible and C can be estimated:

$$C \approx \frac{R*m}{F}$$

The raw image R (Fig. 3.1b) is divided by an image of a well containing only media (Fig. 3.1a) and multiplied by the image's mean to retain its average value to generate a flat-field corrected image (Fig. 3.1c). If no background image is obtained, and no large features exist in the image, a Gaussian filter with a large standard deviation could potentially be use for flat-field correction<sup>115</sup>.

Once working with a flat image, either after correction or in a situation where flat-field correction is not necessary, it is important to subtract background signal. A common method for subtracting background in fluorescence microscopy is to select a region of interest (ROI) in which there are no cells, average the pixels within the ROI, and subtract it as a flat number across the image. For automated image analysis, this would become the rate-limiting step by a considerable amount as well as being prone to human error. Another common approach is to move a structuring element across an image and determine the average intensity within that element and subtract it. This has the advantage of removing uneven backgrounds because it subtracts regionally instead of a flat number from all pixels but has the major drawback of including non-background pixels in the calculation. If pixels of interest are included in a background subtraction

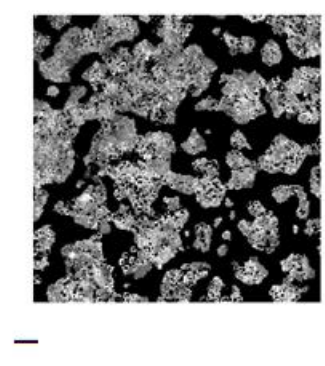
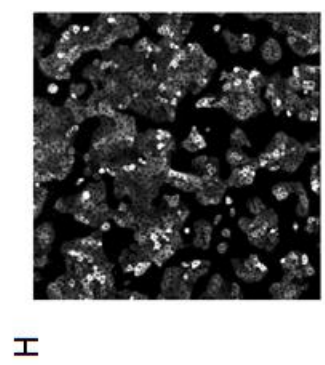
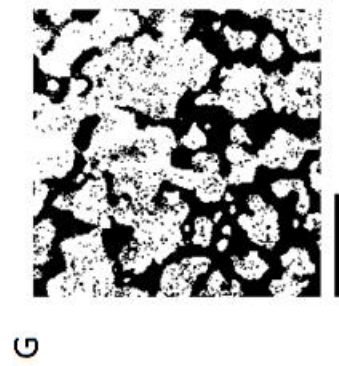
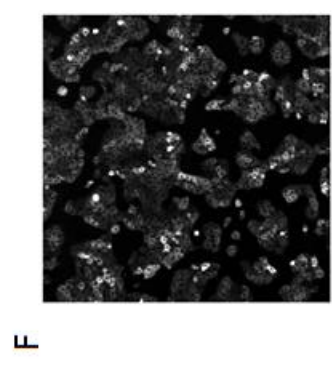
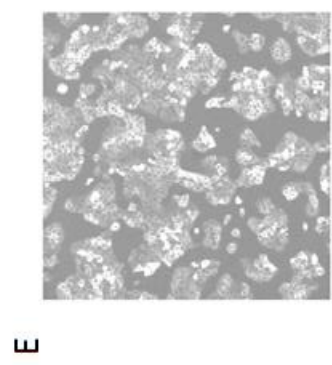
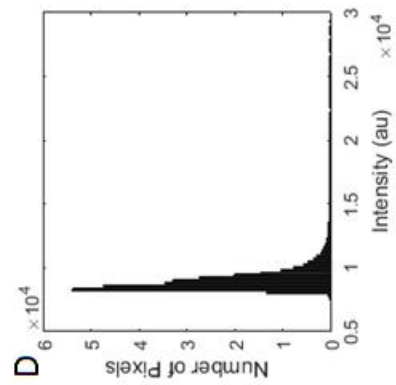
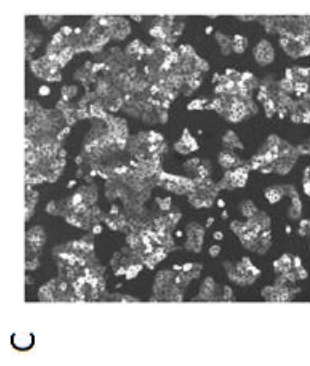
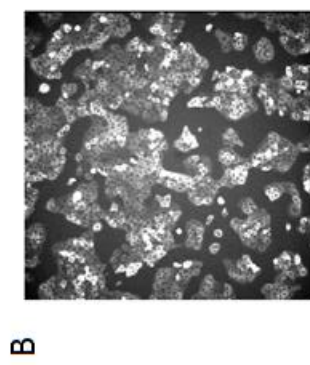
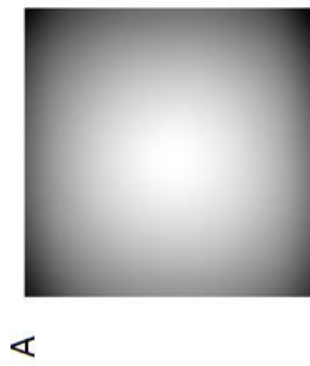


**Figure 3.1 Example of Automated Image Processing for Analysis.** (A) A typical image of media only (DMEM lacking phenol red). (B) Raw image FRET image of HaCaT cells expressing EKAR-ev NES. (C) Flatfield corrected FRET image. (D) Histogram of pixel intensities in the FRET channel. (E) Flatfield corrected FRET image. (F) Flatfield corrected and background subtracted FRET image. (G) Thresholded binary image of the FRET channel. (H) FRET channel with low intensity pixels set to zero. (I) FRET over CFP ratio. Scale bar indicates 500  $\mu\text{m}$ .

then quantification can be massively distorted, especially when comparing the FRET ratio across populations of cells. A common feature of fluorescence images is that the pixels of interest are brighter than background pixels, even in situations where there are bright non-cell pixels such as an aggregate, an ROI selected by a human would avoid these pixels. Using this feature, a histogram can be constructed for each channel of all pixels fluorescence intensity (Fig. 3.1d), if the majority of the image is background then the mode of all pixels would be ideal for identifying an optimal background to subtract. This approach is used to convert the flat-field corrected image in Figure 3.1e to the subtracted image in 3.1f. A potential drawback to this approach is when cells are imaged at higher confluence; for this scenario an approximate percent of the image as background can be manually set then the median of that region of the histogram can be used as the background.

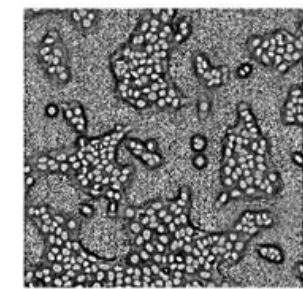
## **Segmentation**

For population analysis, an important next step is to segment cells from background. By the same logic as background detection, cells can be identified by their fluorescence intensity using a threshold to generate a binary image containing cells (Fig.3.1g) then multiplying it by the original image (Fig. 3.1 h). Simple morphological segmentation, such as size or shape of objects, is occasionally useful in these scenarios. For example, if a noisy background breaches the cell threshold, segmentation can be as simple as removing single pixel points or performing morphological erosions in the binary image. Once cells are segmented from background the population can be measured for whatever the assay requires, such as a ratio of FRET over CFP (Fig. 3.1i) or simple intensity measurements. If calculating a

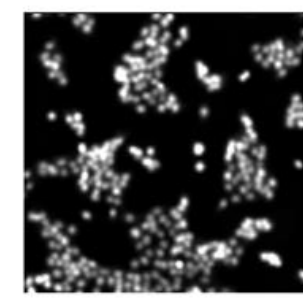
FRET ratio, it should be noted that cells with higher expression and therefore brighter pixels should not be exceptionally bright or dim in the ratio image (Fig. 3.1h-i) or there could be an artefact from not acquiring similar levels of light for each channel.

For quantification of signals from single cells, extra steps must be used for segmentation. Because each bright point generated from pixels of interest generate a point spread function around them, tightly packed cells as often seen in epithelial colonies, will appear merged together when using a simple intensity threshold (Fig. 3.2 a & d). To circumvent this problem, I've developed a method of performing Gaussian filtration with low standard deviation on the image (Fig. 3.2b), then dividing the image by this filter to generate an image with intensity equalized across the cells (Fig. 3.2c). I can then threshold the equalized image to create its own binary image, with well separated nuclei but poorly segmented background (Fig. 3.2e). Once the binary image from the original image and the binary from the equalized image are multiplied together, nuclei can be differentiated both from each other and from background (Fig. 3.2f). Once cells are segmented from each other they can be identified by the connected components in an image and analyzed in a loop for whatever the assay requires. Figure 3.2g shows an overlay of Hoechst dye in blue and EdU stained nuclei in red; each nucleus was identified and segmented with the DAPI channel then the average red fluorescence in its area measured and plotted in a histogram (Fig. 3.2h). Once a threshold is set to identify EdU positive cells, the cells can be treated as binary and the fraction of EdU positive cells identified (Fig. 3.2i).

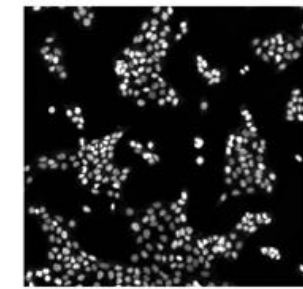
When dealing with epithelial cells forming tight colonies it is difficult to segment the cytoplasmic region of individual cells from one another. In HaCaT cells expressing



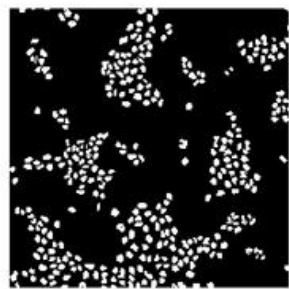
C



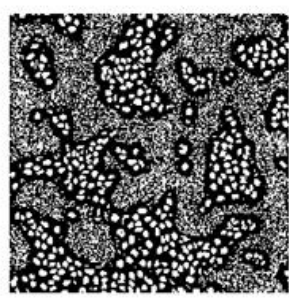
B



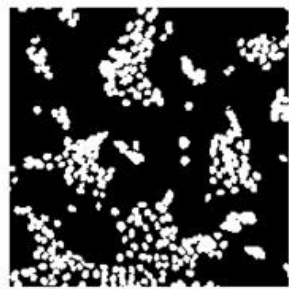
A



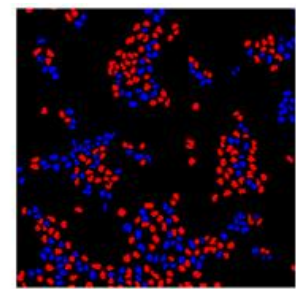
F



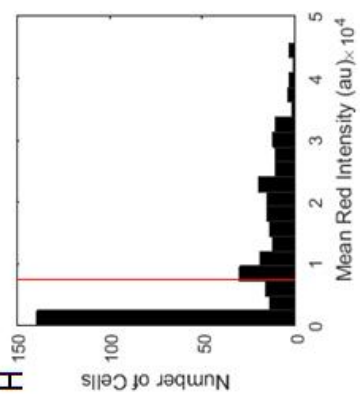
E



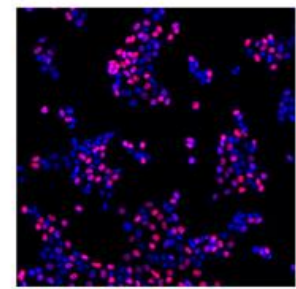
D



I



H



G

**Figure 3.2 Automated single cell segmentation techniques.** (A) Raw DAPI image of fixed HaCaT cells. (B) DAPI image passed through a Gaussian filter to blur the cells. (C) Equalized DAPI image generated by dividing the raw image by the blurred one. (D) Thresholded binary image from raw DAPI image. (E) Thresholded binary image from equalized DAPI image. (F) Product of binary images showing separation of nuclei and removal of background. (G) Overlay of DAPI channel in blue and Alexa-fluor attached to EdU in red. (H) Histogram of the average intensity of Alexa dye in each nucleus and the chosen threshold. (I) Cartoon with nuclei above threshold colored red and those below blue. Scale bar indicates 500  $\mu\text{m}$ .

both ERKTR in the cytoplasm and nucleus (Fig. 3.3a), TSen in the secretory pathway and plasma membrane (Fig. 3.3b), stained with Hoechst dye to label the nucleus (Fig. 3.3c), there was a need to segment apart each cell at the plasma membrane to track the activity reported by each sensor. To accomplish this, I separated the nuclei much like in the EdU example, then each channel is mathematically combined with the nuclei and cytoplasm as low points, and both channels for TSen were used to create high points at the junctions (Fig. 3.3d). I then imposed the segmented nuclei as minima and performed watershedding to determine the lowest points and the lines that separate them (Fig. 3.3e). Once the lines between cells are found, each cell is segmented and indexed for tracking through the experiment (Fig. 3.3f).

### **Tracking and Filtration**

Once the cells are segmented well enough that many can be detected consistently across timepoints, they can be tracked between time points. The tracking algorithm works by saving the pixels for each cell from the previous time point then comparing to the current time point and ordering the current cell index to match the old one. This begins by going through each cell one at a time. It first finds which cells are near the old cell by comparing the Euclidean distance of their centroids, this increases efficiency because only nearby cells must be compared. The tracking algorithm then finds which pixels of these nearby cells overlap with the pixels of the old cell and whichever has the most overlap is considered the same cell in both frames. This technique would not work if the time interval is too long for a given cell's motility, as another cell could move into its position. If no overlaps are found the algorithm then moves to find which centroids are the nearest, within a given threshold, and would

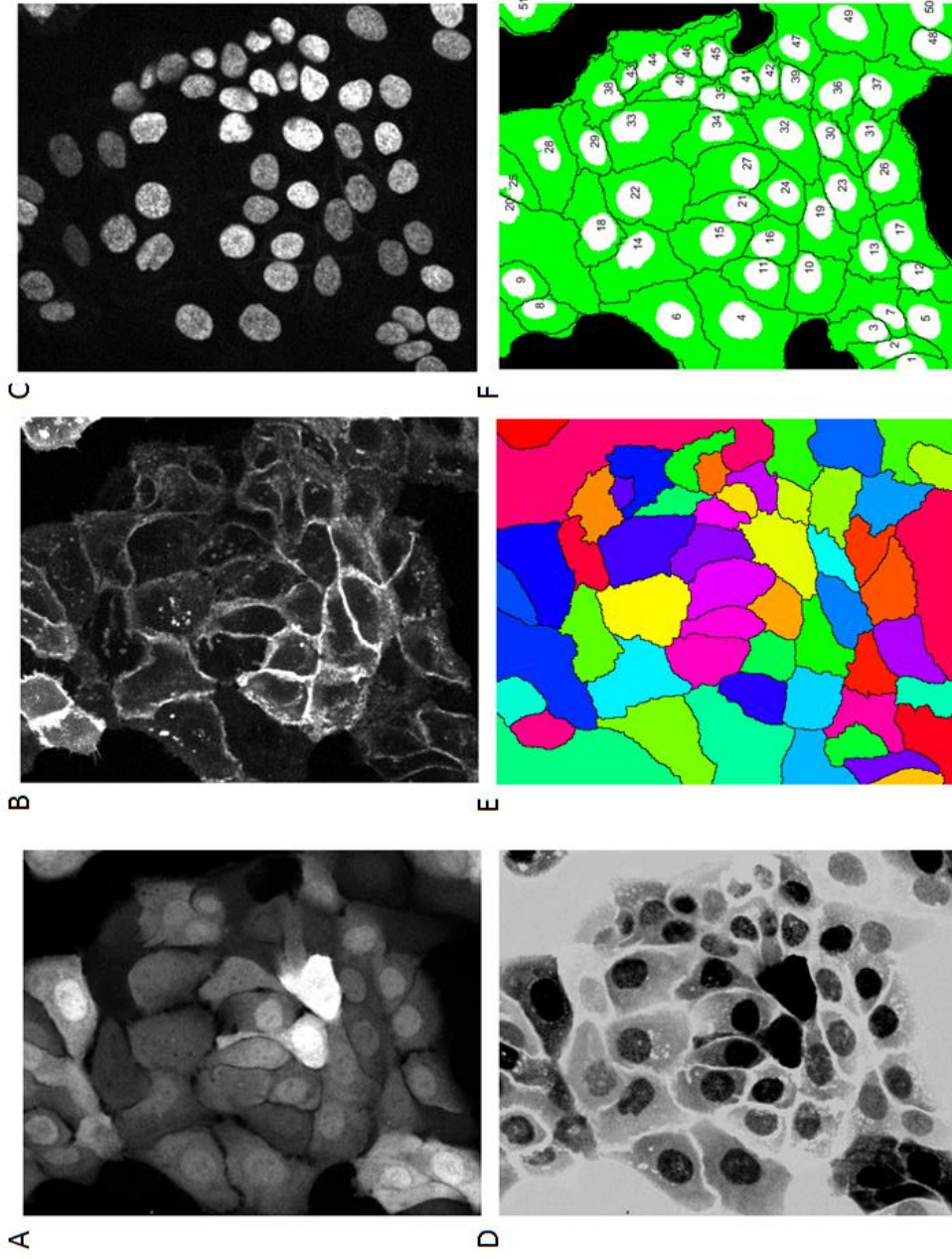


**Figure 3.3 Epithelial cell segmentation at cell junctions.** (A) Fluorescence image of HaCaT cells expressing ERKTR-mRuby2. (B) TSen viewed in the FRET channel. (C) Hoechst dye viewed in DAPI channel. (D) Combination image of TSen viewed as high but ERKTR and DAPI as low points. (E) Watershed segmentation of combination image. (F) Labeled and segmented cytosol and nuclei. Scale bar indicated 50  $\mu\text{m}$ .

consider that the most recent cell. Both loops have to consider which cells are already claimed – a cell from the last frame may see the most overlap with a cell from the current frame but that cell from the current frame may have a different cell from the last frame with more overlap. As a result, the algorithm cannot simply remove cells from the list as they are claimed but it finds the optimal pairing after recording all overlaps then repeats for distance. Once all cells have been paired between frames, any undocumented cells left over were written in as new cells and a new index was made to replace the current index, which then matched the index from the previous frame. As the analysis runs it can record any feature of the single cells desired – the centroid for location and speed, the CFP intensity, FRET intensity, cytoplasmic mRuby2, and nuclear mRuby2 were all measured in this example and the intensity of the nuclear stain could also be measured for detection of mitosis or apoptosis. Upon completion of the analysis, there are very large arrays for each measurement, largely due to error in segmentation leading to error in tracking. To create arrays that would be useful for display and analysis, these have to be filtered. First, the arrays are filtered by the number of frames for which each cell was tracked, then each cell is analyzed for missing numbers – if a single frame is missing for that cell it imputes the average of the frame before and the frame after. If two or more frames in a row are missing, that cell is filtered out. This leaves smaller arrays of cells that have values for all frames and can be used to generate heatmaps like those seen in Figure 3.4. If the time interval is too long then this approach would not generate points within a signaling event, but if the acquisition interval is well beneath the rate of signaling being observed then this

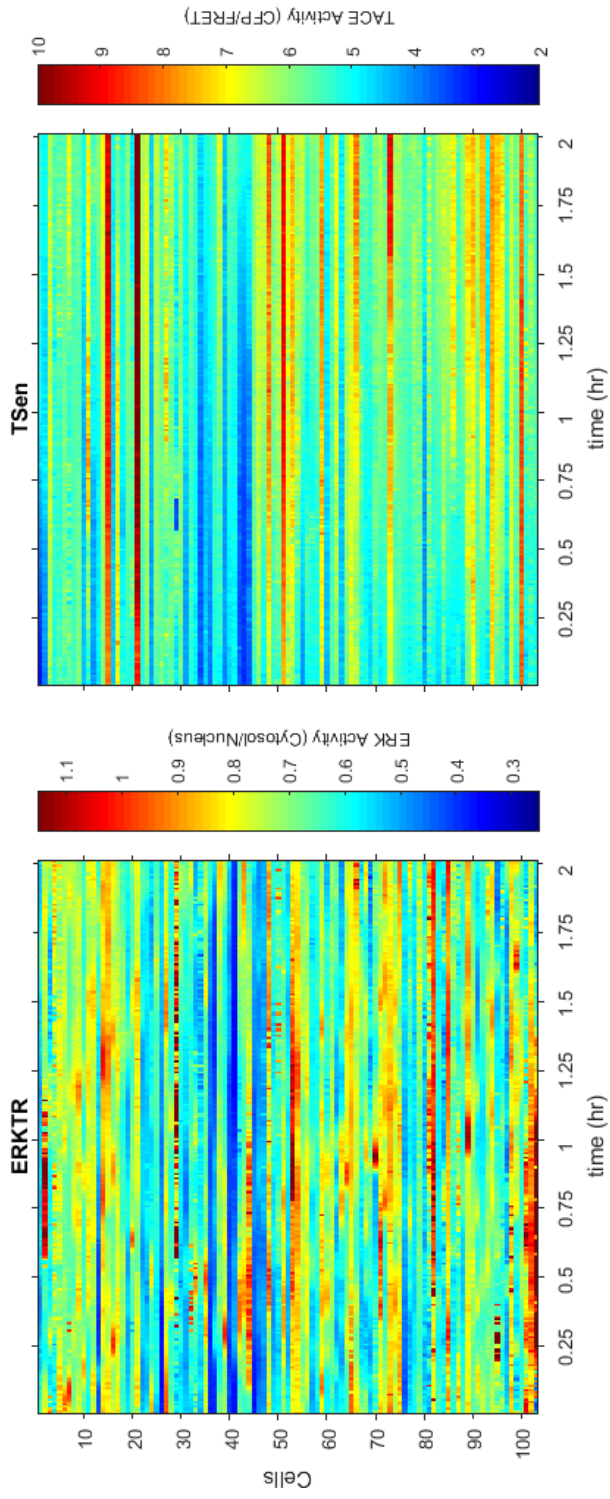


**Figure 3.4 Heat map display of reported ERK and TACE activity in single cells.** ERK activity reported with ERKTR or TACE activity reported with TSen is shown as single cell activity traces. The same cells are reported in each heat map.

approach can be useful in restoring data that would have been filtered out and increase sample size.

### **ERK Activity Pulses**

Signal noise caused by segmentation error or cellular shape change during acquisition can lead to sporadic peaks and troughs in the final quantification. Because I am interested in transient pulses of ERK activity, I need to segment biological signaling from artefacts introduced in both acquisition and analysis. To address the issue of identifying true activity pulses, I recorded both the cytoplasmic mRuby2 and nuclear mRuby2 signals rather than just the ratio of the two for each cell. The shape change of the cell or error in the focus of the microscope could potentially raise or lower both signals non-proportionally and lead to a positive change in ratio if each region changes differently. I used a peak detection algorithm on the ratio of the two then filtered it based on peaks discovered in the cytoplasmic signal and the negative of the nuclear signal for more robust detection of ERK pulses (Fig. 3.5). Filtering peaks from the ratiometric signal by both cytoplasmic and nuclear signals prevents both acquisition- and analysis-based peaks caused by disproportionate changes of each channel in the same direction.

Once ERK pulses were identified they could be correlated to the ERK pulses of neighbor cells as pulses tended to propagate from cell to neighbor cell<sup>46,108,116</sup>. Because the centroid of each cell was tracked as the activity was tracked, it was possible to identify which cells lay within a certain distance without rerunning any analysis. Once identified, pulses can be filtered by which neighbor cells have an identified ERK pulse in a similar time frame as the cell of interest. These pulsing

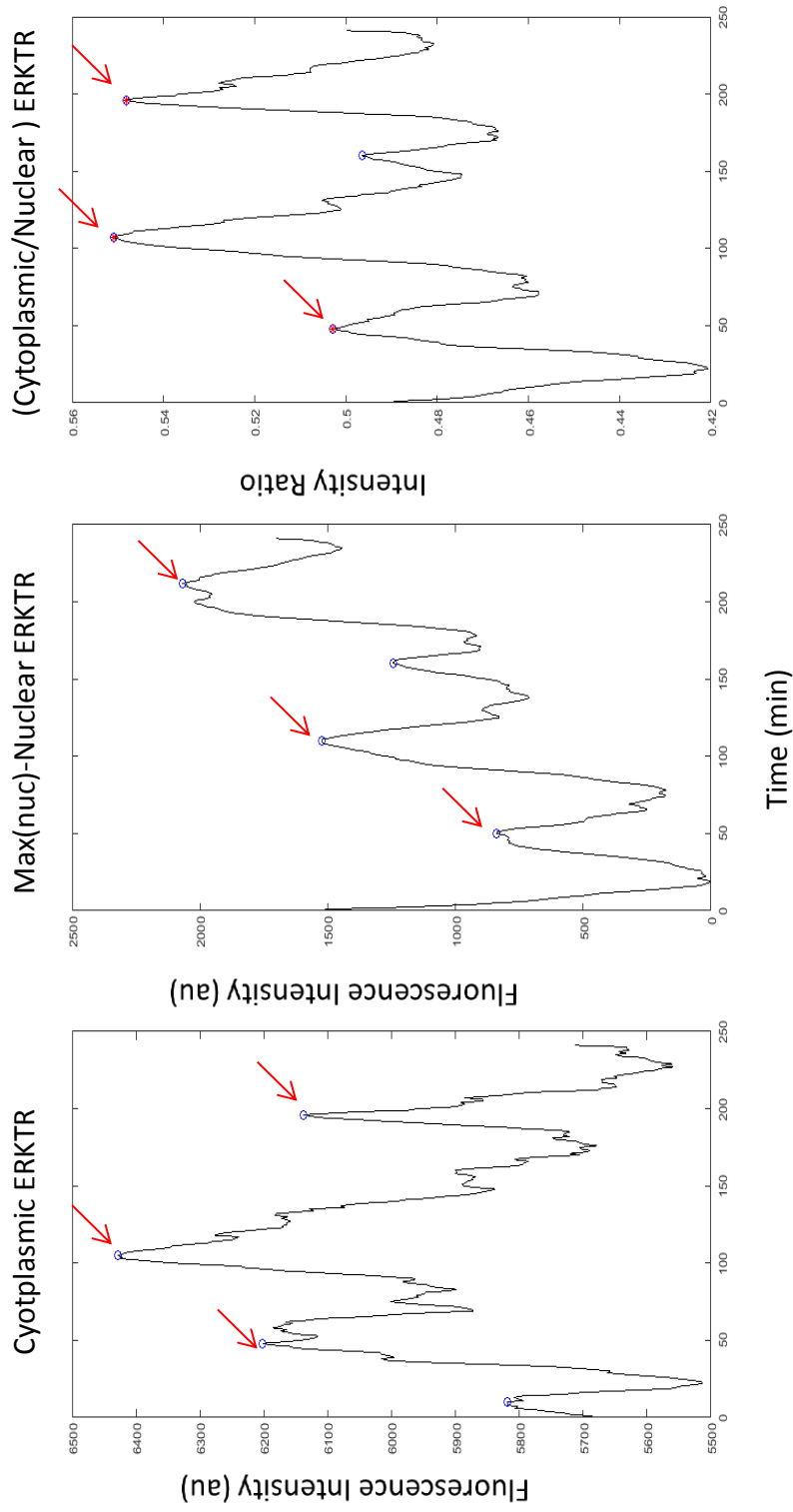


**Figure 3.5 Example of data traces obtained from ERKTR used to identify ERK activity pulses.** All identified peaks are circled in blue. Peaks found in the ratio of cytosolic to nuclear signal (right panel) are then compared to peaks in each individual segmentation. Those that overlap with peaks in both (red arrows, all frames) are considered activity spikes and the rest filtered out.

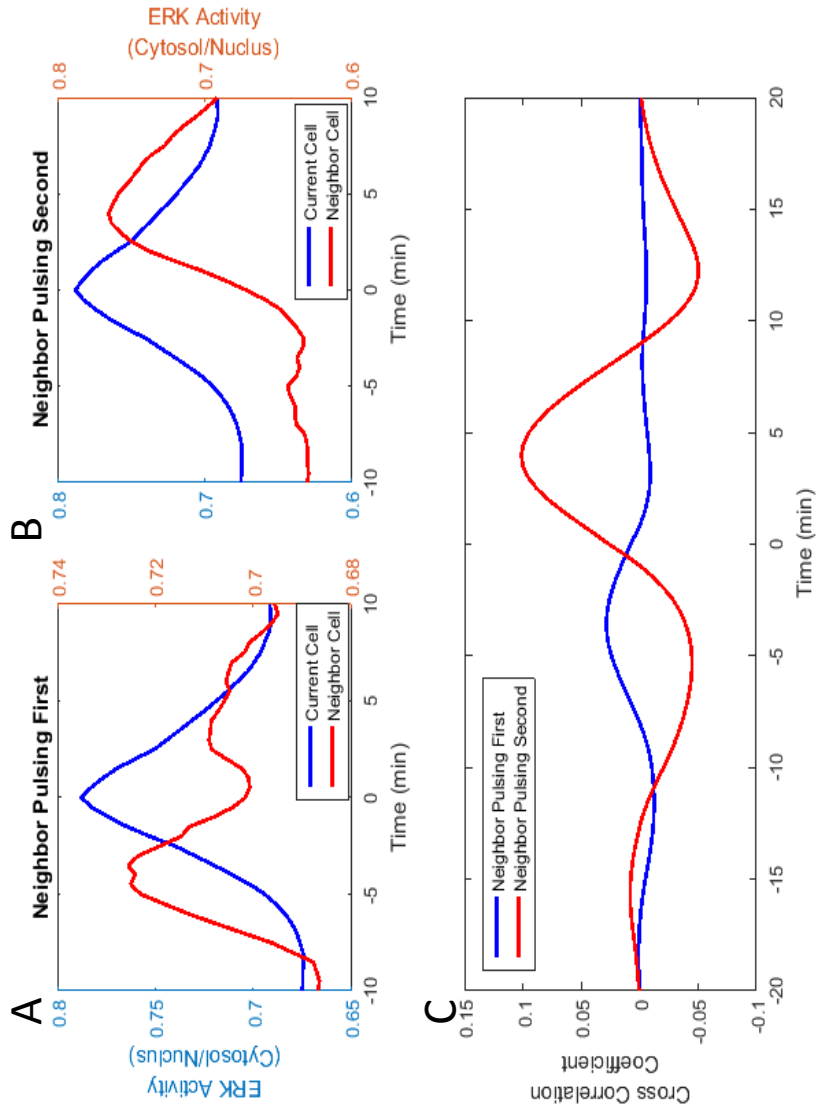


**Figure 3.6 Identified ERK pulses are compared to neighbor cell ERK pulses.** (A) Neighbor cells with an ERK pulse identified before the current cell pulse were averaged across the timeframe and plotted against the average ERK activity for the current cell. (B) Neighbor cells with an ERK pulse identified after the current cell pulse were averaged across the timeframe and plotted against the average ERK activity for the current cell. (C) Average cross-correlation of each group of pulsing neighbor cells vs. the current pulsing cell. Peak correlation times are at -4 and 3.5 minutes.

neighbor cells can then be segmented into two groups: those pulsing before the cell of interest and those pulsing after. With all pulses identified, and all pulsing neighbors identified, the average activities for each cell and neighbor cell can be displayed (Fig. 3.6a-b). For neighbor cells that pulse prior to the current cell, a large peak in activity was found approximately 4 minutes prior to the current cell and another peak after indicating a recurrent event in some cells (Fig. 3.6a). Neighbor cells pulsing after the current cell showed a similar time separation from the current cell, peaking around 4 or 5 minutes post-current cell (Fig. 3.6b). To further address the time separation of an ERK pulse from a neighbor cell's ERK pulse, I used cross-correlation upon each pair of pulse and neighbor pulse to assess their similarity as a function of time displacement. The average cross-correlation analysis shows that the peak to peak change in time is 3.5 minutes and 4 minutes for the pulsing before the current cell and the pulsing after the neighbor cell conditions, respectively. This corresponds to the 3-6 minute range seen previously<sup>46</sup> and is likely on the lower end of their findings because I monitored an ERK sensor while they compared the translocation of fluorescent-labeled ERK protein time separated from an upstream response. The comparable dynamics seen here indicate that the tracking and reporting of ERK pulses with ERKTR are consistent with past results.

### **Processing TSen**

TSen proved to be the more difficult sensor for measuring single cell activity. Both CFP and FRET channels, as well as the ratio of the two, were found to be exceptionally noisy, possibly because a large portion of this sensor is at the membrane and junctions between cells, and these pixels are shared between multiple cells. I

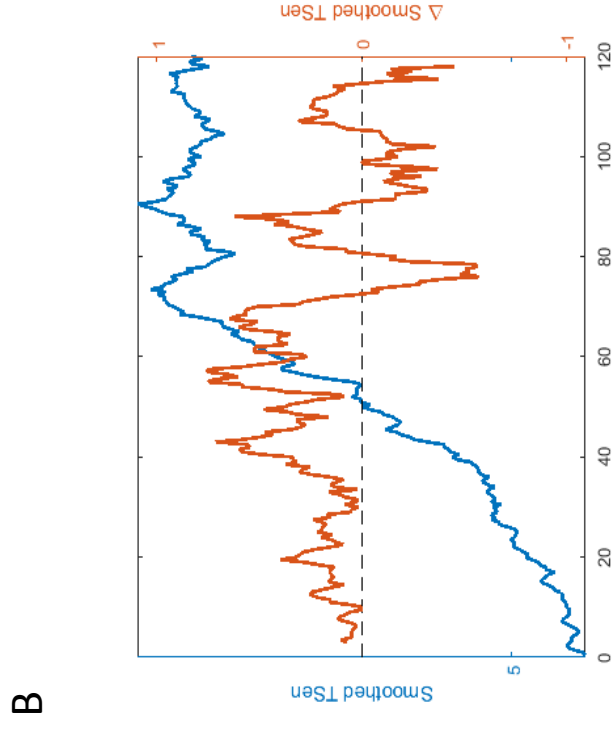
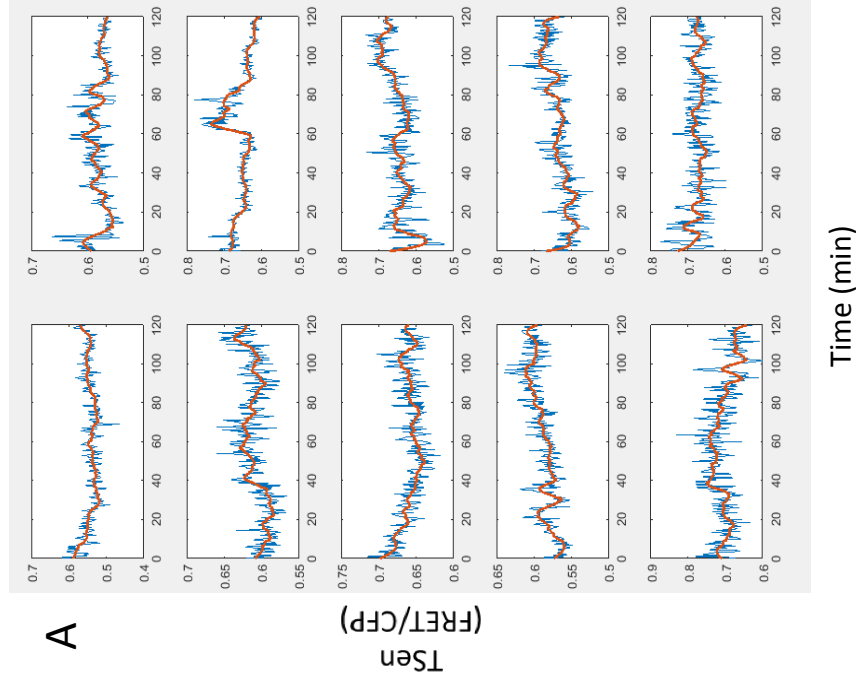


**Figure 3.7 Processing of TSen reported signal to gauge TACE activity.** (A) Reported TSen activity is shown in blue and the result of the Savitzky-Golay filter is overlaid in red. Each plot represents the trace from an individual cell. (B) Example trace of a single cell's smoothed activity in blue and its derivative in red.

found that simply smoothing each channel still lead to a large degree of noise, as a single frame spike or trough in signal is still averaged into the processed form as a more dispersed spike or trough. To address this issue, I used a Savitzky-Golay filter<sup>117</sup> to reduce noise by fitting adjacent frames with a low degree polynomial which is less likely distorted by large changes in a single frame and therefore generated more reliable trends (Fig. 3.7a). Once a more reliable signal was obtained for single-cell TSen, I needed its dynamics to be comparable to ERKTR to compare TACE activity to transient ERK activity pulses. Because TSen is a cleavage-based reporter it is non-reversible in its activity reporting, unlike EKAR or ERKTR which report a balance of kinase and phosphatase activity. This means that at any given point in time the CFP/FRET ratio is a combination of sensor molecules that are cleaved or intact. Therefore the sensor reports an integration of past TACE activity rather than its current rate of substrate cleavage. In order to use the dual-reporting system and simultaneously determine both ERK activity and TACE activity, the sensors had to have comparable dynamics. To determine the timing of TACE activity I used the rate of change of TSen (Fig. 3.7b); the derivative of its signal should provide information on its current rate of substrate cleavage.

To determine the rate of change in the population of TSen molecules, I calculated the first derivative of the filtered FRET ratio. The first derivative showed a pulsing activity at a similar time interval to ERKTR in fast-pulsing cells (Fig. 3.8). To address whether the apparent TACE activity pulses resulted as an artefact of data processing, a non-cleavable form of TSen (NCS) was analyzed in a similar manner in the presence or absence of EGF (Fig.2.1a). Fewer pulses were seen with NCS than

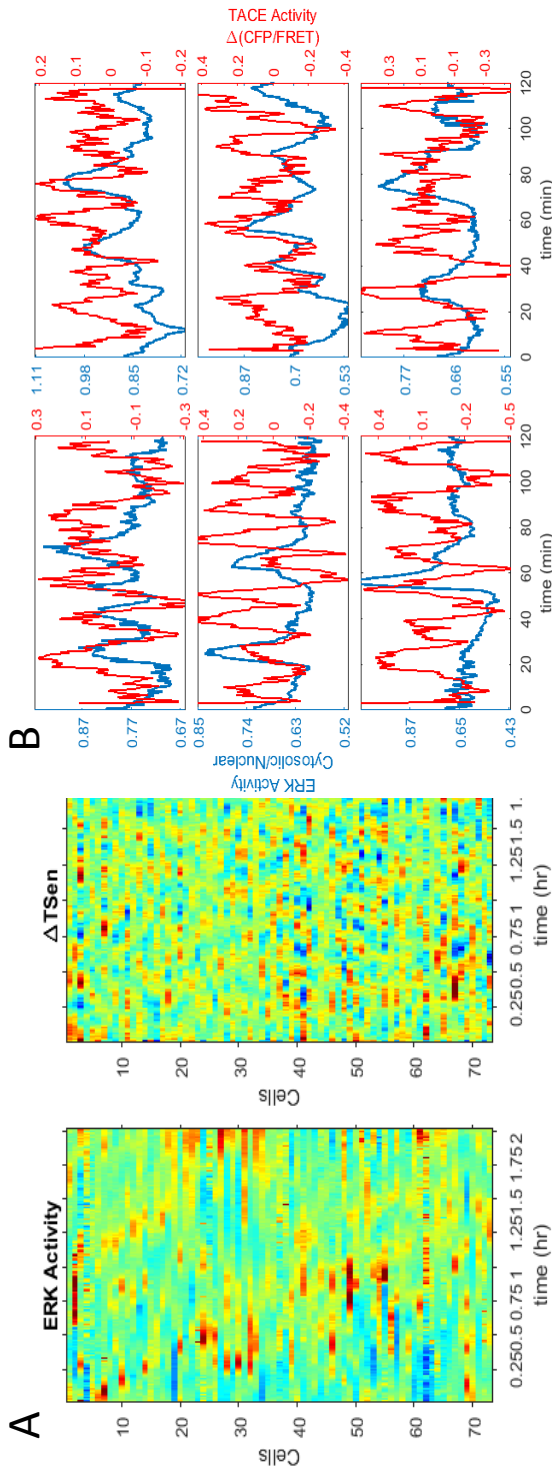


**Figure 3.8 Comparison of ERKTR reported ERK activity and processed Tsen reported TACE activity. (A)** Heat map display of reported ERK and Tsen processed by Savinsky-Golay and taken as a first derivative to report TACE activity in single cells. **(B)** Example of cells with ERK pulses and their reported TACE pulses plotted so that they can be compared across time.

with TSen and when EGF was added there was a large increase in the number of TSen pulses and only a marginal increase with NCS (Fig. 3.9). The marginal increase seen with NCS could be due to a higher rate of motility in the cells, which would lead to greater error in segmentation and tracking. The apparent pulsing activity is at the very least increased upon EGF treatment in TSen cells, this indicates that the pulse-like behavior of the sensor is likely recording actual biological activity overlaid with noise seen in NCS cells..

### **TSen and ERK Pulses**

To decipher if the apparent pulsing behavior of TSen is biologically relevant, I need to compare it to ERK activity, which lies both upstream and downstream of TACE in a feedback loop. Monitoring single cells in Figure 3.8 showed pulses both overlaid and uncorrelated with ERK pulses, presumably due to a combination of noise and relevant signal. To assess if there is a pulse in apparent TACE activity on a population level, I used the same strategy as before to compare ERK pulses to those of neighbor cells and determine if there is spike in apparent TACE activity occurring at a similar time to ERK pulses. First the TACE activity within the same cell as an ERK pulse was averaged across all instances (Fig. 3.10a) to reveal a strong peak approximately 8 minutes after the ERK pulse that begins rising around 3 minutes later. The pinnacle of this peak is so far from the ERK pulse it does not show up strongly in the averaged cross correlation (Fig. 3.10c), but instead it appears that many of the pulsing cells may have had a less prominent peak prior to the ERK pulse. Because TACE activity is expected to affect nearby cells in a paracrine manner as well as the cell of interest, I examined the TACE activity in all neighbors at the times around an ERK activity pulse

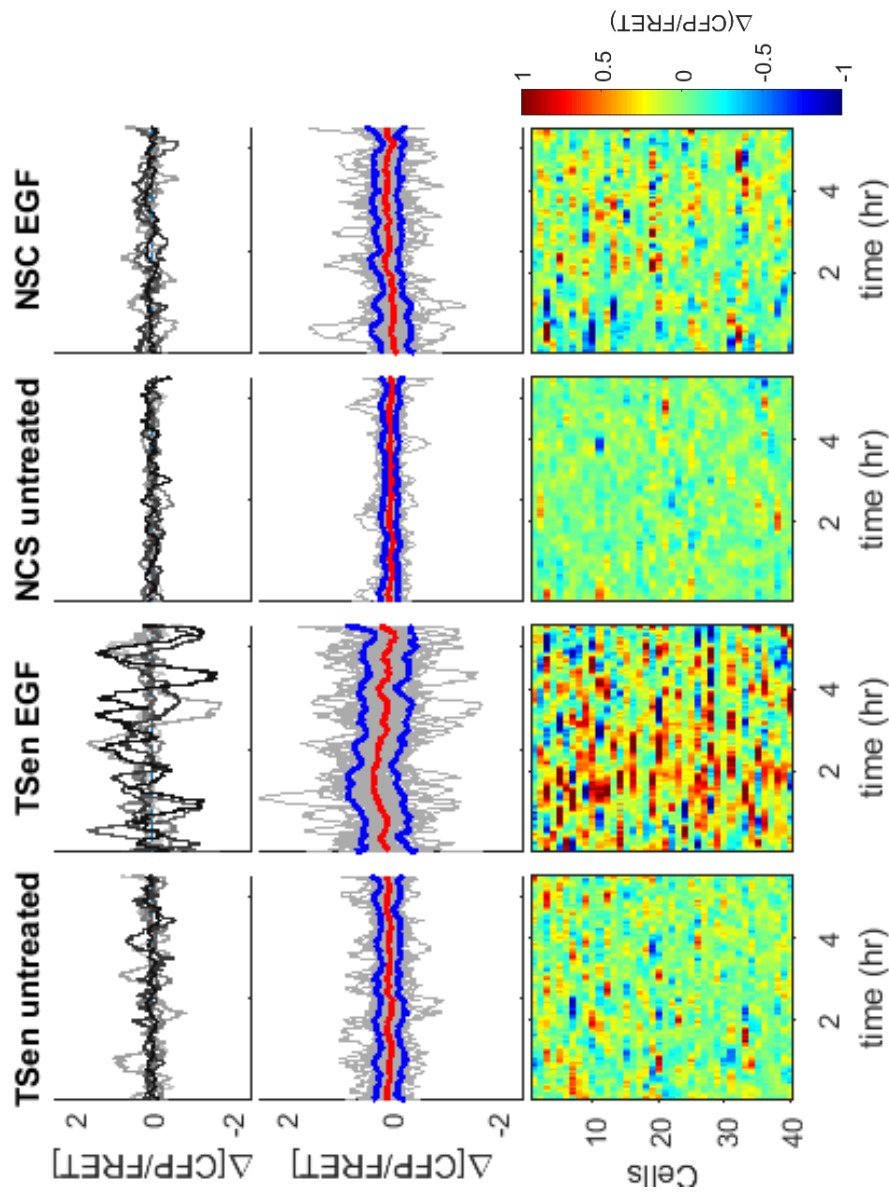


**Figure 3.9 Validation of TACE pulses with the non-cleavable sensor (NCS).** Ten example traces are plotted in the top panel. All traces are plotted in the middle panel in grey with their mean in red and one standard deviation above and below the mean displayed in blue. All traces are again displayed in the bottom panel as a heat map. TSen and NCS were each treated with 10 nM EGF to stimulate TACE activity.

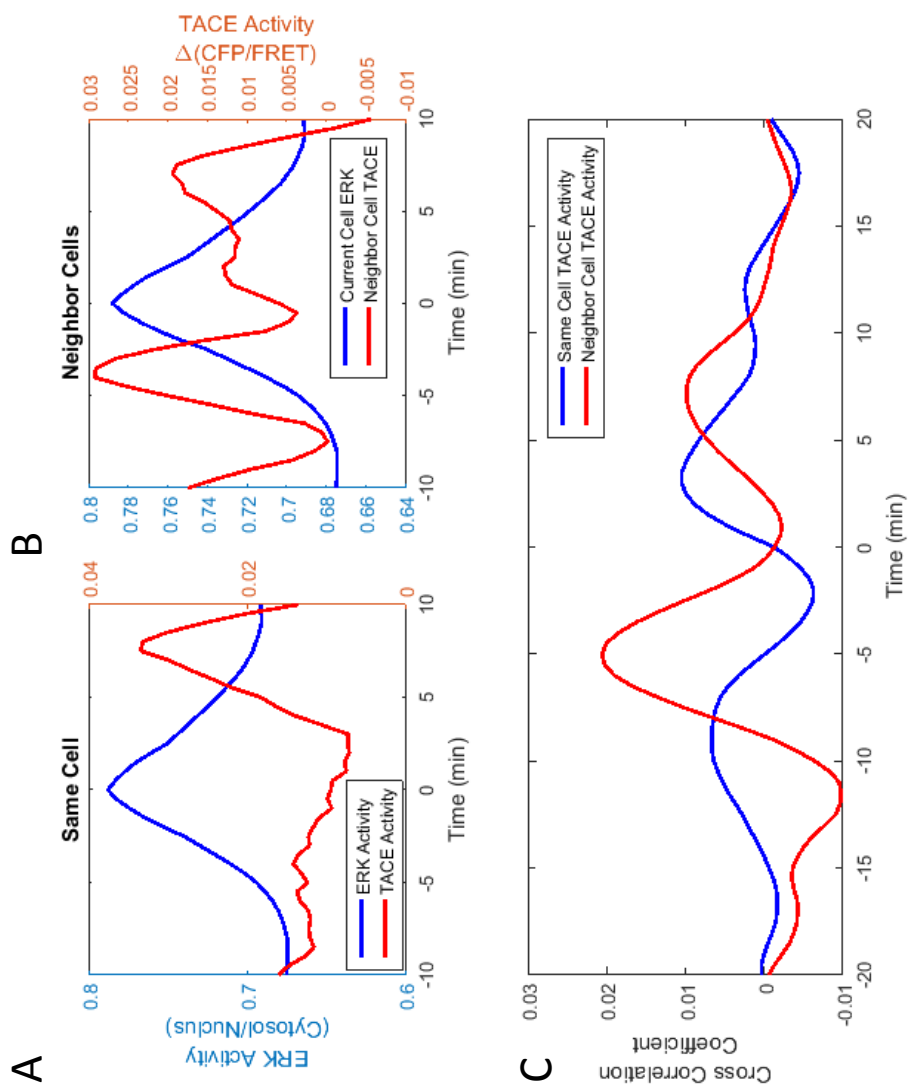


**Figure 3.10 Identified ERK pulses are compared to processed TSen in same cells and neighbor cells.** (A) Cells with an identified ERK pulse with processed TSen averaged across the timeframe and plotted against the average ERK activity for the current cell. (B) Neighbor cells processed TSen averaged across the timeframe and plotted against the average ERK activity for the current cell. (C) Average cross-correlation of either the current cell or neighbor cells. Peak correlation times are at -5 and 2.5 minutes.

and found a peak in TACE activity 4 minutes prior as well as apparently some cells pulsing afterward (Fig. 3.10b). The cross-correlation for this peak is slightly offset in time from the local maximum in average signal but still shows peaks for both neighbor cells having pulsing TACE activity before and after the current cell's ERK pulse (Fig.3.10c). These results indicate that there are changes in the TSen FRET ratio that correspond to a high TACE activity in a neighbor cell prior to an ERK pulse and a high TACE activity in the same cell after an ERK pulse.

To determine if the neighbor cells' ERK activity pulses are responsible for their spikes in apparent TACE activity, I once again identified neighbor cells with ERK activity pulses before the cell of interest and segmented them from those pulsing after. By averaging their processed TSen signal in this timeframe and plotting it against the ERK pulse of the cell of interest I can see that both cell pulsing in ERK before and after seem to have spikes in derivative TSen signal before and after in each segmented population (Fig. 3.11a-b). The averaged cross-correlation also showed each population having pulses before and after the ERK pulse, though perhaps slightly weighted toward the population with an ERK pulse afterward (Fig.3.11c). This result is somewhat confusing in that the apparent TACE pulses do not appear to originate in the same cell as an ERK pulse for propagation. This could be an issue of single cell TSen being noisy and possible artefacts overlaid in the smoothing process on top of real signal, or possibly due to the alternate methods of TACE being activated such as p38 phosphorylation<sup>63</sup> or actin remodeling as discussed in chapter 2. In either case, it does appear that TACE is showing some pulsing activity and that activity is somewhat correlated in time with ERK activity pulses. Unfortunately, without an orthogonal means to measure TACE activity

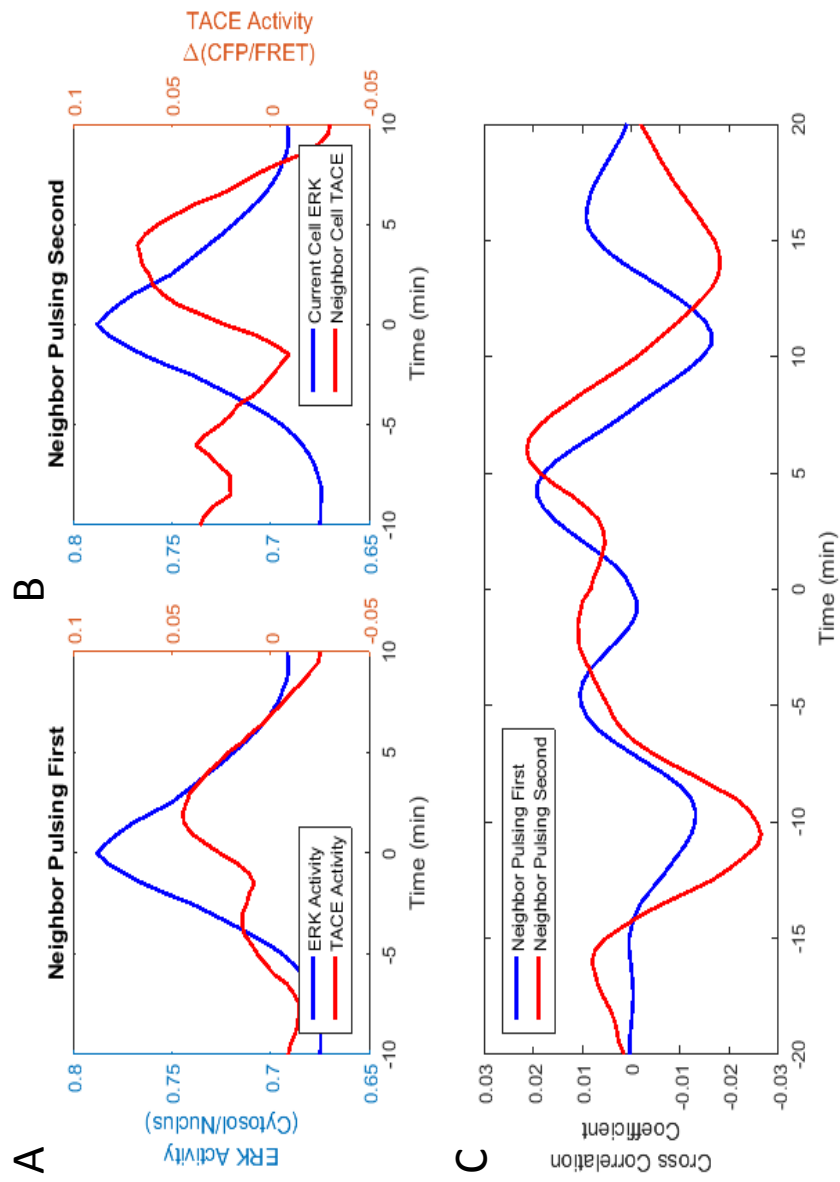


**Figure 3.11 Identified ERK pulses are compared to processed Tsen in neighbor cells identified for an ERK pulse in the timeframe.** (A) Neighbor cells with an ERK pulse identified before the current cell pulse were averaged for processed Tsen averaged across the timeframe and plotted against the average ERK activity for the current cell. (B) Neighbor cells with an ERK pulse identified after the current cell pulse were averaged for processed Tsen averaged across the timeframe and plotted against the average ERK activity for the current cell. (C) Average cross-correlation of each group of pulsing neighbor cells processed Tsen vs. the current pulsing cell. Peak correlation times are at -5, 4, and 6 minutes.

pulses it is hard to disprove that these are not an artefact of the analysis and this work must be verified by alternative means to be the focus of a publication.

## **Discussion**

I aimed to adapt, improve, and design image analysis techniques for automated analysis of cellular behavior. Many of these methods are useful for basic image processing and segmentation of pixels of interest while others are tailored to the more challenging problem of tracking individual epithelial cells. Once these techniques are employed, cell signaling can be interpreted from the image quantification. Elucidation of cell signaling is sometimes straightforward but in other cases requires heavy filtration and processing to reveal a biological response.

Many of the image analysis techniques used here are not new to the field, they are simply adapted to fit the research project using MATLAB as the processing platform. However, several of the basic components of this analysis are, to the best knowledge of the author, new methods in making image analysis automated. These techniques include using the pixel histogram for each channel then thresholding what fraction of the image is background and identify an optimal number to subtract. Also, using the same technique as flat-field correction, a Gaussian filter can be used to equalize the regional intensity of cell-sized objects and allow for easy segmentation between nearby bright objects; this is a simple method to utilize in practice and could easily be implemented in any MATLAB code.

ERK activity pulses are correlated with a cell's decision to proceed through the cell cycle<sup>45</sup> and their modulation can increase cell proliferation<sup>46</sup>. ERK activity pulses also

propagate from cell to cell in a wave-like behavior thought to be driven by ligand shedding through TACE or other proteases like it<sup>46,47</sup>. Using our novel biosensor for TACE activity in conjunction with the recently innovated translocation reporter for ERK activity, I was able to monitor single cell signaling for both TACE and ERK in real time. By identifying ERK pulses and comparing TACE activity, the dual-reporting of TSen and ERKTR in single cells has validated a time separated correlation between TACE and ERK activity as predicted. Unexpectedly, I found that processing TSen signal showed a pulse-like behavior. While these apparent TACE activity pulses are a novel observation, it is intuitive that an ERK activity pulse propagating to a nearby cell would require a temporal spike of ligand shedding. Because ERK phosphorylates TACE<sup>62</sup> to modulate its activity, it is expected that TACE activity would shortly follow an ERK pulse. Then, if there is a mechanism to lower TACE activity such as internalization or local depletion of substrate, that activity would lower and a pulse of TACE activity would release ligands to nearby cells.

Because TACE pulses have been found with a single sensor and cannot be validated by a population-based assay such as ELISA or western blot, this work remains unpublished. However, there are several exciting areas to test with this system and a potentially viable orthogonal method to see these pulses. I have generated HaCaT cells with a CRISPR-cas knockout of TACE to find that ERK activity and proliferation are lost but that rescue with wild-type TACE then restores the phenotype (See chapter 4). Furthermore, we have obtained DNA for TACE lacking the phosphorylation site for ERK and p38 at threonine 735<sup>62,63</sup>. Rescuing TACE with this phosphosite mutant will allow us to see if ERK pulse propagation still occurs without direct activation of ERK using

EKAR-ev as well as determining if there is still a time-offset correlation between TACE activity and ERK activity using ERKTR in conjunction with TSen. Furthermore, while writing this chapter we found that HaCaT cells expressing mRuby2 chimerically attached to TGF $\alpha$  between the signal sequence and the cleavage site (Fig. 4.9) showed an apparent pulsing behavior, with rise and loss of cell-accumulated fluorescence intensity. By repeating pulsing experiments with phosphomutants in parallel to ERK and p38 inhibitors, validating ERK effects with EKAR-ev, and validating TACE pulses with an alternate fluorescent TACE substrate this work will should reveal an exciting feature of autocrine and paracrine signaling in the near future.

## **Methods**

### **Cell culture**

HaCaT cells were cultured in DMEM supplemented with 2 mM L-glutamine, 100 U/mL penicillin, 100 U/mL streptomycin, and 10% (v/v) fetal bovine serum under 5% CO<sub>2</sub> at 37°C.

### **Cell Proliferation Assay**

The Click-IT EdU Alexa Fluor 647 Imaging Kit (Life Technologies) was used to stain dividing cells in the population. Cells were exposed to EdU (5-ethynyl-2'-deoxyuridine) for 4 hours.

### **Image Acquisition**

Population FRET measurements and Click-EdU experiments were imaged on a Molecular Devices ImageXpress MicroXL plate scanner. FRET measurements were

done with the following filters: FRET excitation 438/24-25, dichroic 520LP, emission 542/27-25; CFP excitation 438/24-25, dichroic 458LP, emission 483/32-25. EdU stain imaged with Alexa-647 using excitation 628/40-25, dichroic 660LP, emission 692/40-25. Hoechst dye imaged with excitation 377/50-25, dichroic 409LP, and emission 447/60-25.

Single cell tracking experiments with dual-sensor cells were done on a Nikon spinning disc confocal. Excitation for Hoechst, CFP and FRET, and mRuby2 were done with 405, 445, and 561 laser lines, respectively. Emission filters used were 447/38, 482/35, 540/30, and 620/60 for Hoechst, CFP, FRET, and mRuby2, respectively.

```

%This is example code for single timepoint population analysis for a FRET
%ratio

%Typical setup
clear,clc
curdir=pwd;
addpath C:\Users\LiuLab\Documents\MATLAB\functions

wavelengths=2;
sites=4;

%Identify media only wells
ye=1;
xe=2:4;

%Generate an average Vignette Image
wb=waitbar(0);
i=1;
for y=ye
    Row=char(y+64);
    for x=xe
        %int2strz is a function that can be accessed on the mathworks file
        %exchange
        Column=int2strz(x,2);
        for s=1:4
            imdir=dir([foldername,'\exp_name','_',Row,Column,'_s',int2str(s),'_*']);
            for w=1:wavelengths
                im=imread([foldername,'\imdir(w).name]);

                backall(:,w,i)=imgaussfilt(im,25);
                i=i+1;
            end
        end
    end
end
back=mean(double(backall),4);

%Read through wells of interest for analysis
for y=2:7
    Row=char(y+64);
    for x=2:11
        Column=int2strz(x,2);
        try,wb=waitbar(((y-2)*10+x-1)/60,wb,[Row,Column]);end
        for s=1:sites
            %Determine the image name to read
            imdir=dir([foldername,'\exp_name','_',Row,Column,'_s',int2str(s),'_*']);
            for w=1:wavelengths

```

```

%Read the image
im(:,:,w)=imread([foldername,'\',imdir(w).name]);

%Generate value to indicate if image is out of focus
if w==1
    r=corrcoef(double(imgaussfilt(im(:,:,w),5)),double(im(:,:,w)));
    ofi(y,x,s)=r(2);
end

%Flat-field Correct Image
im2(:,:,w)=uint16(double(im(:,:,w))./back(:,:,w)*mean(mean(back(:,:,w))));

%Background subtract
background=0.1;
imsort=sort(reshape(im2(:,:,w),numel(im2(:,:,w)),1));
imb=median(imsort(1:round(numel(imsort)*background)));
im3(:,:,w)=im2(:,:,w)-imb;
end

frt=im3(:,:,1);
cfp=im3(:,:,2);

%Remove any background pixels by intensity
frt_Thresh=500;
cfp_Thresh=500;
frt2=frt;
cfp2=cfp;
frt2(frt<frt_Thresh)=0;
cfp2(cfp<cfp_Thresh)=0;

%Generate a ratio image of the two channels
Ratio=double(frt2)./double(cfp2);
Ratio(isnan(Ratio))=0;
Ratio(isinf(Ratio))=0;

%Save the average ratio indexed by well and site
ratio(y,x,s)=sum(sum(Ratio))/nnz(Ratio);

end
end
end

```

```
%This is example code for a single timepoint to segment nuclei from each
%other and measure the average intensity of a second wavelength in those
%nuclei
```

```
%Typical setup
clear,clc
curdir=pwd;
addpath C:\Users\LiuLab\Documents\MATLAB\functions
```

```
wavelengths=2;
sites=4;
```

```
%Identify media only wells
ye=1;
xe=2:6;
```

```
%Generate an average Vignette Image
wb=waitbar(0);
i=1;
for y=ye
    Row=char(y+64);
    for x=xe
        %int2strz is a function that can be accessed on the mathworks file
        %exchange
        Column=int2strz(x,2);
        for s=1:sites;
            imdir=dir(['*_ ',Row,Column,'_s',int2str(s),'_*']);
            for w=1:wavelengths

                im=imread(imdir(w).name);

                backall(:,w,i)=imgaussfilt(im,25);

            end
            i=i+1;
        end
    end
end
back=mean(double(backall),4);
```

```
%Read through wells of interest for analysis
for y=4:7
    Row=char(y+64);
    for x=2:11
        Column=int2strz(x,2);
        wb=waitbar(((y-2)*10+x-1)/60,wb,[Row,Column]);
```

```

for s=1:sites
%Determine the image name to read
imdir=dir(['*_','_','Row,Column','_s',int2str(s),'_*']);
for w=1:wavelengths
%Read the image
im(:, :,w)=imread(imdir(w).name);

%Flat-field Correct Image
im2=uint16(double(im(:, :,w))./back(:, :,w)*mean(mean(back(:, :,w))));

%Background subtract
background=.25;
imsort=sort(reshape(im2,numel(im2),1));
imb=mode(imsort(1:round(numel(imsort)*background)));
im3(:, :,w)=im2-imb;

end
%Generate value to indicate if image is out of focus and move
%on to the next image if so
r=corrcoef(double(imgaussfilt(im(:, :,1),2.5)),double(im(:, :,1)));
ofi(y,x,s)=r(2);
if r(2)>0.99,continue,end

dap=im3(:, :,1);
edu=im3(:, :,2);

%Generate binary image based on intensity
bwd=im2bw(dap,2500/65535);

%Generate equalized image with a Gaussian filter
dapb=imgaussfilt(dap,4);
dape=uint16(double(dap)./double(dapb)*mean(mean(dapb)));

%Generate binary image based on equalized image and multiply it
%by the first binary image
bwe=im2bw(dape,graythresh(dape.*uint16(bwd))*1.75);
bw=bwe.*bwd;

%Remove anything from binary image less than a certain size
bw2=bwareaopen(bw,15);
bwf=bw2;
%mulitply the dapi image by the binary image
dapn=dap.*uint16(bwf);

%Find single cells using their connected components

```

```

cc=bwconncomp(bwf);
%Calculate average edu signal in each nucleus
clear edu_temp
parfor c=1:cc.NumObjects
    cell=zeros(size(bw));
    cell(cc.PixelIdxList{c})=1;

    edu_temp(c)=sum(sum(edu.*uint16(cell)))/nnz(cell);
end
%Determine number of objects in the image
cents=imextendedmax(imgaussfilt(dap,1),100).*bw;
cc_cents=bwconncomp(cents);
blah
%Save relevant information indexed for well and site, density
%measurements are to confirm cells are under same confluence
%conditions
edu{y,x,s}=edu_temp;
density_are(y,x,s)=nnz(bw);
density_int(y,x,s)=sum(sum(dap));
density_num(y,x,s)=cc_cents.NumObjects;
end
end
end

```

```

function [cells,cc_nuc,bwi3,bwnuc,bwcells2] = auto_segment_disc2(im3)

toolarge=1500;
toosmall=250;
firstgauss=7;

%segment the cells from background using the mRuby signal
bwm=im2bw(im3(:,:,3),1000/65535);
bwm3=imclose(bwm,strel('disk',3));
bwm4=imopen(bwm3,strel('disk',5));
bwm5=imclose(bwm4,strel('disk',10));
bwm6=bwareaopen(bwm5,1000);
bwcells=bwm6;

%segment nuclei from background and each other using a gaussian to blur
%them then find local maxima to impose a minimum for watershedding
irp=im3(:,:,4);
nucmax=imextendedmax(imgaussfilt(irp,firstgauss),10);
bwi=im2bw(imgaussfilt(irp,4),2000/65535);
bwi2=bwi;
irpb=imgaussfilt(irp,15);
irpe=uint16(double(irp)./double(irpb)*mean(mean(irpb)));
bwe=im2bw(irpe,1500/65535);
bwi2=bwi.*bwe;
bwi3=imopen(bwi2,ones(3,3));

%Use a distance matrix of how far the background has to reach into a
%nucleus to watershed apart elongated looking nuclei into more rounded
%shapes
ic=imcomplement(bwdist(~bwi3));
l_mod=imimposemin(ic,nucmax);
L = watershed(l_mod);
bwi4=bwi3;
bwi4(L==0)=0;

%Use the segmented cells to remove any nuclei not in bright enough regions
%for quantification
bwi5=bwi4.*bwcells;
bwi6=bwareaopen(bwi5,150);
bwi7=im2bw(bwi6-imdilate(~bwcells,ones(3,3)),0);

%Use the variable 'toolarge' to identify unreasonably large nuclei and
%repeat gaussian with smaller standard deviation to repeat watershedding
%with more minima
bwl=bwareaopen(bwi6,toolarge);
irp_large=irp.*uint16(bwl);
largemax=imextendedmax(imgaussfilt(irp_large,firstgauss-2),1);

```

```

ic=imcomplement(irp_large);
l_mod=imimposemin(ic,largemax);
L2 = watershed(l_mod);
bwl2=bwl;
bwl2(L2==0)=0;

%If any remain too large after second watershedding, repeat with distance
%matrix but with no imposed minima
bwl3=bwareaopen(bwl2,toolarge);
bwid=imdilate(bwl3,strel('disk',1));
bwid(L==0)=0;
d=bwdist(~bwid);
dn=-d;
dn(~bwid)=-Inf;
L2b=watershed(dn);
bwi8=bwi7;
cuts=true(size(bwi8));
cuts(L2==0)=0;cuts(bwl==0)=1;
cuts(L2b==0)=0;cuts(bwl==0)=1;
bwi8(cuts==0)=0;

%Remove anything too small to be a trackable nucleus and fill any holes in
%the nuclei
bwi8=bwareaopen(bwi8,toolsmall);
bwi9=imfill(bwi8,'holes');
bwnuc=bwi9;

%Generate a complement image of bright junctions using both channels of
%TSen and dim nuclei and cytosol then impose the segmented nuclei and
%watershed across cell junctions
ic3=imcomplement(uint16(double(im3(:,4))+double(im3(:,3))...
-double(im3(:,2))-double(im3(:,1))));
l_mod=imimposemin(ic3,~(bwcells)|bwnuc);
L3=watershed(l_mod);
bwcells2=bwcells;
bwcells2(L3==0)=0;

%Generate connected components for cells and nuclei
cc_nuc=bwconncomp(bwnuc);
cc_nuc.centroid=regionprops(cc_nuc,'Centroid');
cells=bwconncomp(bwcells2);
cells.centroid=regionprops(cells,'Centroid');

```

```

function [cc_new]=trackcellstest4(cc_new,cc_old)

old_index=zeros(1,cc_old.NumObjects);
new_cen=zeros(cc_new.NumObjects,2);
maxdist=100;
for c1=1:cc_new.NumObjects
    %Generate an array of all centroids in the new index and if it can't
    %find one, make a large number instead of 0
    try
        new_cen(c1,:)=cc_new.centroid(c1).Centroid;
    catch
        new_cen(c1,:)=[10000,10000];
    end
end
overlaps=zeros(cc_old.NumObjects,3);
dists=zeros(cc_old.NumObjects,cc_new.NumObjects);

%This for loop finds overlaps and dists by going through the last frames
%index
eucd=inf(cc_new.NumObjects,1);
for c2=1:cc_old.NumObjects
    %First it calculates the distance from the current centroid to all the
    %new centroids
    cur_cen=cc_old.centroid(c2).Centroid;
    if numel(cur_cen)==0;continue,end
    for c1=1:cc_new.NumObjects
        eucd(c1)=sqrt(sum((cur_cen - new_cen(c1,:)) .^ 2));
    end
    %It generates a matrix of all close centroids
    c1_idx=find(eucd<maxdist);

    %Calculates the overlap of the pixels indexes for each new cell to the
    %old cell
    overlap=zeros(max(c1_idx),1);
    for ctemp=1:numel(c1_idx)
        overlap(c1_idx(ctemp))=nnz(intersect(cc_new.PixelIdxList{c1_idx(ctemp)},cc_ol
d.PixelIdxList{c2}));
    end
    try
        overlaps(c2,1:numel(overlap))=overlap;
    end
    %And saves the distances of all cells within the threshold
    dists(c2,1:numel(eucd))=eucd;
end

%Once all overlaps and distances are saved for nearby cells to each cell in
%the old index it attempts to find the optimal overlap and optimal distance
%separately
overlaps2=zeros(size(overlaps));
dists2=zeros(size(dists));
ovmax=max(overlaps);
dsmin=min(dists);
for n=1:numel(ovmax)
    overlaps2(overlaps(:,n)==ovmax(n),n)=ovmax(n);
    dists2(dists(:,n)==dsmin(n),n)=dsmin(n);
end

```

```

end
dists2(dists2<maxdist)=0;

%Once the optimal overlap and distances are found, it saves the index for
%overlap and finds whichever cells lack an overlap and uses distance
%instead
ov_idx=logical(sum(overlaps2,2));
ds_idx=logical(sum(dists2,2).*~ov_idx);
[~,old_index(ov_idx)]=max(overlaps2(ov_idx,:),[],2);
[~,old_index(ds_idx)]=min(dists2(ds_idx,:),[],2);

%If a cell didn't show up within thresholds for distance as well as not
%having an overlap then it is appended to the end of the index
temp=ismember(1:cc_new.NumObjects,old_index);
undoc_index=find(temp==0);
n=1;
for u=find(undoc_index)
    old_index(cc_old.NumObjects+n)=undoc_index(u);
    n=n+1;
end

%Once all cells are accounted for a new connected components structure is
%generated with the index created
cur_idx=true(1,numel(old_index));
for c3=1:numel(old_index)
    if old_index(c3)>0
        cc_new.PixelIdxList{c3}=cc_new.PixelIdxList{old_index(c3)};
        cc_new.centroid(c3)=cc_new.centroid(old_index(c3));
        cc_new.cur_idx(c3)=1;
    else
        cc_new.PixelIdxList{c3}=cc_old.PixelIdxList{c3};
        cc_new.centroid(c3)=cc_old.centroid(c3);
        cc_new.cur_idx(c3)=0;
    end
end
end
cc_new.NumObjects=numel(cc_new.PixelIdxList);

```

```

clear,clc
addpath C:\Users\bunker\Documents\MATLAB\functions
addpath ..

%Load in the time-stamped matrix saved by the analysis code
load('tif_dump\2016    10    10    18    17    39')
try,close(wb),end

%There are a lot of arrays, etc. so all are cleared except the relevent
%ones
clearvars -except cyt2 nuc2 fret cfp centx centy tratio teratio

%It's optional here to filter based on all timepoints
timeframe=1:241;
figure
for site=2
    %Pull information into consolidated arrays, with the desired timeframe
    ratioall(timeframe,:,1)=cyt2(timeframe,:,site,1);
    ratioall(timeframe,:,2)=nuc2(timeframe,:,site,1);
    tsenall(timeframe,:,2)=fret(timeframe,:,site,1);
    tsenall(timeframe,:,1)=cfp(timeframe,:,site,1);
    centall(timeframe,:,1)=centx(timeframe,:,site,1);
    centall(timeframe,:,2)=centy(timeframe,:,site,1);
    tratiot(timeframe,:,1)=tratio(timeframe,:,site,1);

    clear filt_idx
    %the ratio is used to confirm that both segmentations detected
    %something to pass the filter
    ratio=ratioall(:, :, 1)./ratioall(:, :, 2);
    %An index is created for every cell to determine the number of Not a
    %Number (NaNs) and zeros
    clear nan_idx zer_idx
    for n=1:size(ratioall,2)
        nan_idx(n)=nnz(isnan(ratioall(:,n,1)));
        zer_idx(n)=nnz(ratioall(:,n,1)==0);
    end
    %A soft threshold of half the timepoints is used in this example, this
    %still removes many cells that appeared in just a few frames, likely as
    %error because of segmentation
    nan_idx(nan_idx<size(ratio,1)*.5)=0;
    filt_idx(1:nnz(~nan_idx.*~zer_idx))=find(~nan_idx.*~zer_idx);

    tsenf(:,1:nnz(filt_idx),:)=tsenall(:,filt_idx(1:nnz(filt_idx)),:);
    ratiof(:,1:nnz(filt_idx),:)=ratioall(:,filt_idx(1:nnz(filt_idx)),:);
    centf(:,1:nnz(filt_idx),:)=centall(:,filt_idx(1:nnz(filt_idx)),:);
    tratiof(:,1:nnz(filt_idx),:)=tratiot(:,filt_idx(1:nnz(filt_idx)),:);

    %Find data with only one frame missing, impute mean from frames around
missing point
    tsen_imp=tsenf;ratio_imp=ratiof;cent_imp=centf;tratio_imp=tratiof;
    clear idx n
    wb=waitbar(0);
    %n changes from cell to cell
    for n=1:size(tsenf,2)
        wb=waitbar(n/size(tsenf,2),wb);
        temp=ratiof(:,n,1)./ratiof(:,n,2);

```

```

if nnz(isnan(temp)==0)==numel(temp),idx(n)=1;continue,end
%Find the nans in each cell's timeframe
nans=find(isnan(temp));
%Find if the nans are adjacent to each other and only impute if not
nands=diff(nans);
if nnz(nands==1)>0
    idx(n)=0;
    continue
end
for i=1:numel(nans)
    %If the first point is missing a value, impute the second point.
    % This should not alter any pulsing information but still allow
    % that cell to be analyzed
    if nans(i)==1
        tsen_imp(nans(i),n,1)=tsenf(nans(i)+1,n,1);
        tsen_imp(nans(i),n,2)=tsenf(nans(i)+1,n,2);
        ratio_imp(nans(i),n,1)=ratiof(nans(i)+1,n,1);
        ratio_imp(nans(i),n,2)=ratiof(nans(i)+1,n,2);
        cent_imp(nans(i),n,1)=centf(nans(i)+1,n,1);
        cent_imp(nans(i),n,2)=centf(nans(i)+1,n,2);
        tratio_imp(nans(i),n,1,1)=tratiof(nans(i)+1,n,1,1);
        %If the last point is missing a value, impute the second point.
        % This should not alter any pulsing information but still allow
        % that cell to be analyzed
    elseif nans(i)==size(tsen_imp,1)
        tsen_imp(nans(i),n,1)=tsenf(nans(i)-1,n,1);
        tsen_imp(nans(i),n,2)=tsenf(nans(i)-1,n,2);
        ratio_imp(nans(i),n,1)=ratiof(nans(i)-1,n,1);
        ratio_imp(nans(i),n,2)=ratiof(nans(i)-1,n,2);
        cent_imp(nans(i),n,1)=centf(nans(i)-1,n,1);
        cent_imp(nans(i),n,2)=centf(nans(i)-1,n,2);
        tratio_imp(nans(i),n,1,1)=tratiof(nans(i)-1,n,1,1);
    else
        %If a point in the middle is missing a value, impute the mean
        %of the point before it and the point after it. With 30 second
        %timeframes this should allow for a near continuous view of
        %signaling changing and not miss any relevant information
        tsen_imp(nans(i),n,1)=mean([tsenf(nans(i)-
1,n,1),tsenf(nans(i)+1,n,1)]);
        tsen_imp(nans(i),n,2)=mean([tsenf(nans(i)-
1,n,2),tsenf(nans(i)+1,n,2)]);
        ratio_imp(nans(i),n,1)=mean([ratiof(nans(i)-
1,n,1),ratiof(nans(i)+1,n,1)]);
        ratio_imp(nans(i),n,2)=mean([ratiof(nans(i)-
1,n,2),ratiof(nans(i)+1,n,2)]);
        cent_imp(nans(i),n,1)=mean([centf(nans(i)-
1,n,1),centf(nans(i)+1,n,1)]);
        cent_imp(nans(i),n,2)=mean([centf(nans(i)-
1,n,2),centf(nans(i)+1,n,2)]);
        tratio_imp(nans(i),n,1,1)=mean([tratiof(nans(i)-
1,n,1,1),tratiof(nans(i)+1,n,1,1)]);
    end
    idx(n)=1;
end
end
close(wb)

```

```

%Use only the values that had no nans back to back
clear *all2
idx2=find(idx);
ratioall2(:,:,1)=ratio_imp(:,idx2,1);
ratioall2(:,:,2)=ratio_imp(:,idx2,2);
tsenall2(:,:,1)=tsen_imp(:,idx2,1);
tsenall2(:,:,2)=tsen_imp(:,idx2,2);
centall2(:,:,1)=cent_imp(:,idx2,1);
centall2(:,:,2)=cent_imp(:,idx2,2);
ratioall2(:,:,3)=ratioall2(:,:,1)./ratioall2(:,:,2);
tsenall2(:,:,3)=tratio_imp(:,idx2,:);

%Perform a Savitzky-Golay filter on the TSen signal (here using the
%mode of the ratio of the whole cell signal), then measure its binned
%change in time, and smooth it
bin=5;
smooth_num=10;
clear dsg dsgs
for n=1:size(tsenall2,2)
    sg(:,n)=sgolayfilt(tsenall2(:,n,3),3,25);
    temp=sg(:,n);
    dsg=temp(bin+1:end)-temp(1:end-bin);
    dsgs(:,n)=smooth(dsg,smooth_num);

    rationorm(:,n)=smooth(ratioall2(:,n,3)-median(ratioall2(:,n,3)),5);
end

%Because of the smoothed binned change in time, the binned tace
%activity has a different size than the ERKTR, this creates an array of
%same size
tab=dsgs;
tab2=NaN(size(tab,1)+bin,size(tab,2));
tab2(bin/2+1:size(tab,1)+bin/2,:)=tab;

tab3=tab2;
rat3=rationorm;

subplot(1,2,1)
ratio_image=shiftdim(rat3,1);
scale=[-.15 .15];
imagesc(ratio_image,scale)
colormap jet

set(gca,'xtick',0:60:241,'xticklabel',[[0:60:241]*.5]/60,'tickdir','out')
xlabel('time (hr)')
ylabel('Cells')
title('ERK Activity')

subplot(1,2,2)
tsen_image=shiftdim(tab3,1);
scale=[-0.5 0.5];
imagesc(tsen_image,scale)
colormap jet
set(gca,'xtick',1:60:241,'xticklabel',[[0:60:241]*.5]/60,'tickdir','out')

```

```
xlabel('time (hr)')  
ylabel('Cells')  
title('\DeltaTSen')
```

```
end
```

```

%This is example code for the single cell tracking of ERKTR/TSen HaCaT
%cells from exported tif images originally in an ND2 file generated by the
%spinning disc confocal. Frames were every 30 seconds and the wavelengths
%were 1-FRET, 2-CFP, 3-mRuby (TRITC), and 4-DAPI(Hoechst)

```

```

clear,clc
addpath C:\Users\LiuLab\Documents\MATLAB\functions
addpath ..
warning off

firstpoint=1;
timepoints=241;
sites=2;
background=0.05;

wb=waitbar(0);
curdir=pwd;
%Two new functions are used in this code and will be published adjacent to
%this code, one for segmentation and the other for tracking. The path
%added here is where they were stored during analysis
addpath([curdir, '\.'])

im_name='dms0';
for s=1:sites

    for t=firstpoint:timepoints

        try
            wb=waitbar((t+1-firstpoint)/(timepoints+1-firstpoint),wb,['site ',int2str(s),' t ',int2str(t)]);
        end

        imname=[im_name,'xy',int2str(s),'c*t',int2strz(t,3),'.tif'];
        imdir=dir(imname);
        for c=1:4
            temp=imread(imdir(c).name);
            %Because these images were obtained on the spinning disc
            %confocal there was no need for flatfield correction

            %It was found that the DAPI channel achieved higher success
            %with segmentation using a structuring element for background
            %subtraction. This channel is used for segmentation only and
            %it is irrelevant if a slightly incorrect number is used for
            %this subtraction.
            if c<4
                imsort=sort(reshape(temp,numel(temp),1));
                imb=mode(imsort(1:round(numel(imsort)*background)));
                im3(:,:,c)=temp-imb;
            else

```

```

        im3(:,:,c)=temp-imopen(temp,strel('ball',50,50));
    end
end
clear temp

%The auto segmentation function will be published adjacent to this
%script
[cells,cc_new,bwi3,bwnuc,bwcells2] = auto_segment_disc2(im3);

%For cell tracking, the first frame is matched to itself and all
%later frame to the frame previous
if t==firstpoint
    cc_old=cc_new;
    old_cells=cells;
end

%Tracking function will be published adjacent to auto segmentation
%function
cc_now=trackcellstest4(cc_new,cc_old);

%The centroids of all cells in this frame and last are recored
new_cen=zeros(cc_new.NumObjects,2);
clear cell_cen*
for c=1:cells.NumObjects
    cell_cen(c,:)=cells.centroid(c).Centroid;
end
for c=1:old_cells.NumObjects
    cell_cenold(c,:)=old_cells.centroid(c).Centroid;
end

%Centroids are used to calculate minimum distances to each current
%cell
clear idx idxold
for n=1:cc_now.NumObjects
    clear eucd eucdold
    cur_cen=cc_now.centroid(n).Centroid;
    if cc_now.cur_idx(n)==0,continue,end
    for c=1:cells.NumObjects
        eucd(c)=sqrt(sum((cur_cen - cell_cen(c,:)) .^ 2));
    end
    for c=1:old_cells.NumObjects
        eucdold(c)=sqrt(sum((cur_cen - cell_cenold(c,:)) .^ 2));
    end
    idx(n)=find(eucd==min(eucd));
    idxold(n)=find(eucdold==min(eucdold));
end

%The ratio of CFP over FRET is calculated pixel by pixel

```

```

Ratio=double(im3(:,:,2))./double(im3(:,:,1));
Ratio(isnan(Ratio))=0;
Ratio(isinf(Ratio))=0;
%Single cell quantification is done in parallel
clear array*
parfor n=1:numel(idx)
    %This tells it to ignore this cell if it wasn't tracked in the
    %current frame, all potentially useful information is stored
    if cc_now.cur_idx(n)==0,continue,end
    if idx(n)==0;continue,end

    %A binary image is created and the current cell set to 1
    curcell=zeros(size(im3(:,:,1)));
    curcell(cells.PixelIdxList{idx(n)})=1;

    %This moves through all cells in the last frame within a
    %certain distance and removes their pixels from the current
    %cell's binary image if they are not the same cell in an
    %attempt to remove noise from improperly segmenting the
    %membrane at the cell junctions
    tempold=idxold;tempold(n)=0;
    oldarray=tempold(tempold>0);
    for no=1:numel(oldarray)
        if no==n,continue,end
        curcell(old_cells.PixelIdxList{oldarray(no)})=0;
    end

    %This cleans up any stray pixels after removing other cells
    %overlapping pixels
    curcell=bwareaopen(curcell,50);

    %A binary image of the nucleus of the current cell is generated
    %and then a dilation and erosion made
    nuc=bwi3.*curcell;
    Nuc_d=imdilate(nuc,strel('disk',1));
    Nuc_e=imerode(nuc,strel('disk',1));

    %For analysis the nucleus is considered the more conservative,
    %eroded binary image and the cytoplasm a 6 pixel ring around the
    %dilated image
    Nuc=Nuc_e;
    Cyt2=(imdilate(Nuc_d,strel('disk',6))-Nuc_d).*curcell;

    %the pixel-by-pixel inverse fret ratio for current cell
    currat=logical((curcell==1).*(Ratio~=0));
    ratio=Ratio(currat);

    %The centroid of the cell is extracted from the structure

```

```

cent=cc_now.centroid(n).Centroid;

%The edge of the cell is a 5 pixel run near the side, excluding
%the nucleus because Hoechst could leak into the CFP channel
celledge=imdilate(bwperim(curcell),strel('disk',5)).*logical(curcell-Nuc_d);

%Within parallel loops, arrays can only be written to index
%based on that loop's variable. All single cell values were
%saved into temporary arrays then written into structures later
array1(n)=sum(sum(im3(:,,:3).*uint16(Cyt2)))/nnz(im3(:,,:3).*uint16(Cyt2));
array2(n)=sum(sum(im3(:,,:3).*uint16(Nuc_e)))/nnz(im3(:,,:3).*uint16(Nuc_e));

%Each channel for TSen is stored separately from the pixel by
%pixel ratio, also stored. These values are calculated at the
%cell membrane which has the most error in segmentation but was
%previously found to be where TSen measures TACE activity. An
%alternate means for ratio was to find where the peak of the
%histogram for that cell is,because changes along the outside
%of the cell would not shift the mode of all of the cells
%pixels. Because the mode itself could change slightly and add
%noise, the average of all pixels near the mode were used.
array3(n)=sum(sum(im3(:,,:1).*uint16(celledge)));
array4(n)=sum(sum(im3(:,,:2).*uint16(celledge)));
array5(n)=mean(ratio(find(round(ratio,2)==mode(round(ratio,2))))));

%MATLAB indexes by row then column, so x is 2 and y is 1
array6(n)=cent(2);
array7(n)=cent(1);
end

%Save all temporary array information into a structure with time,
%cell, and site information
cyt2(t+1-firstpoint,1:size(array1,2),s)=array1;
nuc2(t+1-firstpoint,1:size(array1,2),s)=array2;
fret(t+1-firstpoint,1:size(array1,2),s)=array3;
cfp(t+1-firstpoint,1:size(array1,2),s)=array4;
tratio(t+1-firstpoint,1:size(array1,2),s)=array5;
centx(t+1-firstpoint,1:size(array1,2),s)=array6;
centy(t+1-firstpoint,1:size(array1,2),s)=array7;

%Save the old connected components for this frame to be used for
%tracking in the next
cc_old=cc_now;
old_cells=cells;

%Binary choice to save images or not
if 0
    figure('visible','off')

```

```

%This shows both the nuclei and cytosol segmented for the
%current frame
imshowpair(bwcells2,bwnuc)
%This loop adds the cells' indexed number at its centroid
for n=1:cc_now.NumObjects
    if cc_now.cur_idx(n)==0;continue,end
    cent=cc_now.centroid(n).Centroid;
    try
        text(cent(1),cent(2),int2str(n))
    end

end

%Save the image in a folder named tracking, make the folder if
%it does not already exist
try
    saveas(gcf,['tracking\im_name','s ',int2str(s),'t ',int2strz(t,3)'.tif'])
catch
    mkdir('tracking')
    saveas(gcf,['tracking\im_name','s ',int2str(s),'t ',int2strz(t,3)'.tif'])
end
close(gcf)
end

end
end
close(wb)

%Save the script as a filename that will not overwrite an older version
save(int2str(clock))

```

```

function [fin_peaks, fin_locations]=pulse_peaks_spin_ERKraw(ratioall2)

%Generate a loop to analyze each cell
for cell=1:size(ratioall2,2)
    clear pk* *locs*
    %Smooth the signal in cytosolic (1), nuclear (2), and ratio (3)
    for i=1:3
        ratioall3(:,cell,i)=smooth(ratioall2(:,cell,i),5);
    end
    %Find peaks in all three dimensions but use the maximum-nuclear as we
    %want peaks for decreasing signal
    [~,locs,wds]=findpeaks(ratioall3(:,cell,3),'MinPeakProminence',...
        std(ratioall3(:,cell,3))/2,'minpeakdistance',20,...
        'minpeakheight',0.1);
    [pks1,locs1,wds1]=findpeaks(ratioall3(:,cell,1),'minpeakdistance',15,...
        'MinPeakProminence',std(ratioall3(:,cell,1))/2);
    [pks2,locs2,wds2]=findpeaks(max(ratioall3(:,cell,2))-(ratioall3(:,cell,2)),'minpeakdistance',20,...
        'MinPeakProminence',std(max(ratioall3(:,cell,2))-ratioall3(:,cell,2))/2);
    if numel(locs)==0 || numel(locs1)==0 || numel(locs2)==0,continue,end

    %Filter peaks in the ratiometric channel by their width
    locs_f1=locs;
    locs_f1(wds>40)=0;
    locs_f1(wds<3)=0;

    %For peaks for cytosol and nucleus, find region around each peak based
    %on its width
    for p=1:numel(pks1)
        if wds1(p)>30,wds1(p)=30;end
        temp=round(locs1(p)-wds1(p)/2:locs1(p)+wds1(p)/2);
        pkwds1(p,1:numel(temp))=temp;
    end
    for p=1:numel(pks2)
        if wds2(p)>30,wds2(p)=30;end
        temp=round(locs2(p)-wds2(p)/2:locs2(p)+wds2(p)/2);
        pkwds2(p,1:numel(temp))=temp;
    end

    %Find the overlap between the ratiometric peaks and the nuclear and
    %cytosolic peaks
    pkint1{numel(locs_f1),1}=[];pkint2=pkint1;
    for p=1:numel(locs_f1)
        if locs_f1(p)==0,continue,end
        temp=round(locs(p)-wds(p)/2:locs(p)+wds(p)/2);

        for p1=1:size(pkwds1,1)
            pkint1{p,p1}=intersect(temp(temp>0),pkwds1(p1,:));
        end
    end
end

```

```

    for p2=1:size(pkwds2,1)
        pkint2{p,p2}=intersect(temp(temp>0),pkwds2(p2,:));
    end
end

%Make it so each overlap only corresponds to the peak with maximum
%overlap for both nuclear and cytosolic peaks
pkint1_2=zeros(size(pkint1,1),size(pkint2,2));
for p1=1:size(pkint1,2)
    clear int_size*
    for p=1:size(pkint1,1)
        int_size1(p)=numel(pkint1{p,p1});
    end
    pkint1_2(logical(int_size1==max(int_size1)),p1)=max(int_size1);
end
pkint2_2=zeros(size(pkint2,1),size(pkint2,2));
for p2=1:size(pkint2,2)
    clear int_size*
    for p=1:size(pkint2,1)
        int_size2(p)=numel(pkint2{p,p2});
    end
    pkint2_2(logical(int_size2==max(int_size2)),p2)=max(int_size2);
end

%If a ratiometric peak still have overlap with peaks for cyotol and
%nucleus then consider it a real pulse
p2=0;locs_f=[];
for p=1:numel(locs_f1)
    if nnz(pkint1_2(p,:))>0 && nnz(pkint2_2(p,:))>0
        p2=p2+1;
        locs_f(p2)=locs(p);
    end
end
fin_locations(1:numel(locs_f),cell)=locs_f;
fin_peaks(1:numel(locs_f),cell)=ratioall3(round(locs_f),cell,3);

end

```

```

%Use the ratiometric (cyto/nuclear) dimension and smooth it
for c=1:size(ratioall2,2)
    rationorm2(:,c)=ratioall2(:,c,3);
    rationorm2(:,c)=smooth(rationorm2(:,c),5);
end

clear xc_* ERK_c* ERK_n* TACE_c* TACE_n*
self_i=1;
nehb_i=1;
nebp_i=1;
nebp2_i=1;
ts=20;
maxdist=35;
%loop for current cell
for c=1:size(tsenall2,2)
    n2=idx2(c);
    %loop for pulses in current cell
    for cp=1:nnz(e_locs(:,c))
        t=e_locs(cp,c);
        %Only acknowledge pulses well within timeframe
        if (t>ts && (t<=(size(ratioall2,1)-ts-1)))==0
            continue
        end

        %correlate self TACE to ERK
        norm1=rationorm2(t-ts:t+ts,c)-median(rationorm2(t-ts:t+ts,c));
        xc_self(:,self_i)=xcorr(norm1,tab2(t-ts:t+ts,c));
        TACE_curcell(:,self_i)=tab2(t-ts:t+ts,c);
        ERK_curcell(:,self_i)=rationorm2(t-ts:t+ts,c);
        self_i=self_i+1;

        %Find neighbors
        cur_cen=[centall2(t,c,1),centall2(t,c,2)];
        for c1=1:size(centall2,2)
            eucd(c1)=sqrt(sum((cur_cen - [centall2(t,c1,1),centall2(t,c1,2)]) .^ 2));
        end
        eucd(eucd==0)=Inf;
        c1_idx=find(eucd<maxdist);

        for n=1: numel(c1_idx)
            %correlate neighbor ERK and TACE to current ERK
            norm1=rationorm2(t-ts:t+ts,c)-median(rationorm2(t-ts:t+ts,c));
            norm2=rationorm2(t-ts:t+ts,c1_idx(n))-median(rationorm2(t-ts:t+ts,c1_idx(n)));
            xc_neb_erk(:,nehb_i)=xcorr(norm1,norm2);
            xc_neb_tace(:,nehb_i)=xcorr(norm1,tab2(t-ts:t+ts,c1_idx(n)));
            TACE_nebcell(:,nehb_i)=tab2(t-ts:t+ts,c1_idx(n));
            ERK_nebcell(:,nehb_i)=rationorm2(t-ts:t+ts,c1_idx(n));
        end
    end
end

```

```

nehb_i=nehb_i+1;

%For all neighbor pulses
np_idx=find(e_locs(:,c1_idx(n)));
for np=1:nnz(np_idx)

    tn=e_locs(np_idx(np),c1_idx(n));
    %Find neighbors that pulse after current cell
    if tn>t && tn<t+ts
        norm1=rationorm2(t-ts:t+ts,c)-median(rationorm2(t-ts:t+ts,c));
        norm2=rationorm2(t-ts:t+ts,c1_idx(n))-median(rationorm2(t-ts:t+ts,c1_idx(n)));
        %correlate neighbor ERK and TACE to current ERK
        xc_nebp_erk(:,nebp_i)=xcorr(norm1,norm2);
        xc_nebp_tace(:,nebp_i)=xcorr(norm1,tab2(t-ts:t+ts,c1_idx(n)));
        TACE_nebp2cell(:,nebp_i)=tab2(t-ts:t+ts,c1_idx(n));
        ERK_nebp2cell(:,nebp_i)=rationorm2(t-ts:t+ts,c1_idx(n));
        nebp_i=nebp_i+1;
    %Find neighbors that pulse before current cell
    elseif tn<t && tn>ts
        norm1=rationorm2(t-ts:t+ts,c)-median(rationorm2(t-ts:t+ts,c));
        norm2=rationorm2(t-ts:t+ts,c1_idx(n))-median(rationorm2(t-ts:t+ts,c1_idx(n)));
        xc_nebp2_erk(:,nebp2_i)=xcorr(norm1,norm2);
        xc_nebp2_tace(:,nebp2_i)=xcorr(norm1,tab2(t-ts:t+ts,c1_idx(n)));
        TACE_nebp2cell(:,nebp2_i)=tab2(t-ts:t+ts,c1_idx(n));
        ERK_nebp2cell(:,nebp2_i)=rationorm2(t-ts:t+ts,c1_idx(n));
        nebp2_i=nebp2_i+1;
    end
end
end
end
end
end

```

```

%This script was designed to be useful for sharing amongst the lab and
%anybody else who could use it.
%It rewrites the images produced by the image xpress in a format that would
%be readable by imageJ as an image stack, so that a video across time is
easily
%accessible for human truthing and fast observation of experimental
%conditions

clear,clc
curdir=pwd;

w=waitbar(0,'Deleting Thumbs');

direct=dir;
OriginalFolderCount=numel(direct)-2;
%The image xpress generates thumbnail versions of your images that retain
%no information of their own but can be used by metaxpress software. The
%retain all of the name information of the images for analysis but also
%contain the word "thumb", this piece deletes them.
for f=1:OriginalFolderCount
    cd(direct(f+2).name);
    delete('*thumb*');
    cd(curdir)
end

%this piece determines the experiment name provided by the image xpress, it
%is important that it does not change between timepoints
cd(direct(3).name)
subdirect=dir;
for i=1:numel(subdirect(3).name)
    if subdirect(3).name(i)=='_'
        m=i-1;
        break
    end
end
ExperimentName=subdirect(3).name(1:m);
cd(curdir)

%Because the experiment can have varied complexity and the image xpress
%changes the name based on the complexity, much of this code is redundantly
%written so that almost any experiment can be run through the same pipeline
if subdirect(3).name(m+5)~='_'
    %type 1 = one site one wavelength
    nametype=1;
elseif subdirect(3).name(m+6)=='s'
    if subdirect(3).name(m+9)~='w'
        %type 2 = multiple sites one wavelength
        nametype=2;
    else
        %type 4 = multiple sites multiple wavelengths
        nametype=4;
    end
elseif subdirect(3).name(m+6)=='w'
    %type 3 = one site multiple wavelengths
    nametype=3;
end

```

```

%This is so a pre-timepoint can be taken before adding any conditions to
%the cells and it is easily added to the image stack despite being from
%another experiment number
if numel(dir('TimePoint_0'))>0;
    firstpoint=0;
else
    firstpoint=1;
end

timepoints=OriginalFolderCount-1+firstpoint;
%The large if loops below were separated at the expense of brevity to
%increase the speed of running the reorganizer, each of the 4 if-loops is
%for a specific name type consisting of 1 or more wavelengths or sites
%nametype 1 is for one site one wavelength
if nametype==1
    for t=firstpoint:timepoints
        %This is the working piece of int2strz, a script on the mathworks
        %file exchange, extracted to that others could run the reorganizer
        %without obtaining that function. TimePoint then becomes '02'
        %instead of '2' in this case but retain '10' instead of '010'.
        if t==firstpoint, tic, w=waitbar(0,w,'Calculating Time
Remaining');end
        M = 1;
        xmax = double(max(abs(t(:)))));
        if xmax>=1
            M = M + floor(log10(xmax));
            if M<2, M = 2; end
        else
            M = M+1;
        end
        S = sprintf(['%0' int2str(M) '.0f'],round(t(:)));
        S = reshape(S,M,numel(t)).';clc
        Timepoint=S;

        %Determine the folder to read current images from
        timefolder=['TimePoint_',int2str(t)];

        cd(timefolder)
        %y being the column of a 96 or 384 well play
        for y=1:16 %A to P
            Row=char(y+64);
            rowname=[ExperimentName,'_',Row,'*'];
            %If the row does not exist in this experiment then keeping
            %moving to the next row or timepoint
            if numel(dir(rowname))>0
                %x is the row of a 96 or 384 well play
                for x=1:24
                    %Rerun the function part of int2strz to get '02' for x
                    %instead of '2' but retain '10' instead of '010'
                    M = 1;
                    xmax = double(max(abs(x(:)))));
                    if xmax>=1
                        M = M + floor(log10(xmax));
                        if M<2, M = 2; end
                    else

```

```

        M = M+1;
    end
    S = sprintf(['%0' int2str(M) '.0f'],round(x(:)));
    S = reshape(S,M,numel(x)).';
    Column=S;

    file=[ExperimentName, '_',Row,Column,'*'];
    %If the column does not exist in this experiment
    %then the file name will not exist keeping moving
    %to the next column or row
    if numel(dir(file))>0
        if t>firstpoint
            w=waitbar(t/timepoints,w,['estimated time
remaining: ',int2str(t1*timepoints*(1-(t/timepoints))/60),' minutes']);
        end
        %Generate a directory of image names
        imageD=dir(file);

        %Read the image
        image=imread(imageD(1).name);

        %If this is the first timepoint then create a
        %folder to place the image in based on the well
        if t<firstpoint+1
            cd(curdir)
            foldername=['well ',Row, Column];
            mkdir(foldername);
        end
        %Generate a new name for the image
        imagename=['t',Timepoint];

        %Move to the folder to write the image then
        %save it and move the directory back
        foldername=['well ', Row ,Column];
        cd(curdir);
        NewDirect=dir;
        cd (foldername)
        imwrite(image,[imagename,'.tif'])
        cd(curdir)
        cd(timefolder)
    end

    end
end
end
if t==firstpoint,t1=toc;end
cd(curdir)
end
%type 2 = multiple sites one wavelength
elseif nametype==2
    for t=firstpoint:timepoints
        if t==firstpoint, tic, w=waitbar(0,w,'Calculating Time
Remaining');end
        M = 1;
        xmax = double(max(abs(t(:))));
        if xmax>=1

```

```

        M = M + floor(log10(xmax));
        if M<2, M = 2; end
    else
        M = M+1;
    end
    S = sprintf(['%0' int2str(M) '.0f'],round(t(:)));
    S = reshape(S,M,numel(t)).';
    Timepoint=S;

timefolder=['TimePoint_',int2str(t)];

cd(timefolder)
for y=1:16 %A to P
    Row=char(y+64);
    rowname=[ExperimentName,'_',Row,'*'];
    if numel(dir(rowname))>0
        for x=1:24
            M = 1;
            xmax = double(max(abs(x(:))));
            if xmax>=1
                M = M + floor(log10(xmax));
                if M<2, M = 2; end
            else
                M = M+1;
            end
            S = sprintf(['%0' int2str(M) '.0f'],round(x(:)));
            S = reshape(S,M,numel(x)).';
            Column=S;

            file=[ExperimentName,'_',Row,Column,'_s*'];
            if numel(dir(file))>0
                if t>firstpoint
                    w=waitbar(t/timepoints,w,['estimated time
remaining: ',int2str(t1*timepoints*(1-(t/timepoints))/60),' minutes']);
                end
                NumberofSites=numel(dir(file));
                for s=1:NumberofSites
                    cd(curdir),cd(timefolder)

file=[ExperimentName,'_',Row,Column,'_s',int2str(s),'*'];
                    imageD=dir(file);
                    image=imread(imageD(1).name);
                    if t<firstpoint+1
                        if s<2
                            cd(curdir)
                            foldername=['well ',Row, Column];
                            mkdir(foldername);
                        end
                    end
                    imagename=['site ', int2str(s),'
t',Timepoint];

                    foldername=['well ', Row ,Column];
                    cd(curdir);
                    NewDirect=dir;
                    cd (foldername)
                    imwrite(image,[imagename,'.tif'])

```



```

        NumberofWavelengths=numel (imageD);

images=zeros ((length (imread (imageD(1) .name))),length ((imread (imageD(1) .name))
),NumberofWavelengths);

        for i=1:NumberofWavelengths
            images=uint16 (images);
            images (:,:,i)=imread (imageD(i) .name);
        end
        if t<firstpoint+1
            cd (curdir)
            foldername=['well ',Row, Column];
            mkdir (foldername);
        end
        for i=1:NumberofWavelengths
            imagename=['wavelength ',int2str(i), '
t',Timepoint];

            foldername=['well ', Row ,Column];
            image=images (:,:,i);
            cd (curdir);
            NewDirect=dir;
            cd (foldername)
            imwrite (image, [imagename, '.tif'])
        end
        cd (curdir)
        cd (timefolder)
    end
end
end
end
if t==firstpoint,t1=toc;end
cd (curdir)
end
%type 4 = multiple sites multiple wavelengths
elseif nametype==4
    for t=firstpoint:timepoints
        if t==firstpoint, tic, w=waitbar(0,w, 'Calculating Time
Remaining');end
        M = 1;
        xmax = double (max (abs (t (:)))));
        if xmax>=1
            M = M + floor (log10 (xmax));
            if M<2, M = 2; end
        else
            M = M+1;
        end
        S = sprintf (['%0' int2str (M) '.0f'],round (t (:)));
        S = reshape (S,M,numel (t)) .';
        Timepoint=S;

        timefolder=['TimePoint_',int2str (t)];

        cd (timefolder)
        for y=1:16 %A to P
            Row=char (y+64);
            rowname=[ExperimentName, '_', Row, '*'];
            if numel (dir (rowname))>0

```

```

for x=1:24
    M = 1;
    xmax = double(max(abs(x(:))));
    if xmax>=1
        M = M + floor(log10(xmax));
        if M<2, M = 2; end
    else
        M = M+1;
    end
    S = sprintf(['%0' int2str(M) '.0f'],round(x(:)));
    S = reshape(S,M,numel(x)).';
    Column=S;
    file=[ExperimentName, '_',Row,Column, '_s*_w1*'];
    if numel(dir(file))>0
        if t>firstpoint
            w=waitbar(t/timepoints,w,['estimated time
remaining: ',int2str(t1*timepoints*(1-(t/timepoints))/60), ' minutes']);
            end
            NumberofSites=numel(dir(file));
            for s=1:NumberofSites

file=[ExperimentName, '_',Row,Column, '_s',int2str(s), '_w*'];
            imageD=dir(file);
            NumberofWavelengths=numel(imageD);

images=zeros((length(imread(imageD(1).name))),length((imread(imageD(1).name))
),NumberofWavelengths);

            for i=1:NumberofWavelengths
                images=uint16(images);
                images(:, :, i)=imread(imageD(i).name);
            end
            if t<firstpoint+1
                if s<2
                    cd(curdir)
                    foldername=['well ',Row, Column];
                    mkdir(foldername);
                end
            end
            for i=1:NumberofWavelengths
                imagename=['site ', int2str(s), ' wavelength
',int2str(i), ' t',Timepoint];
                foldername=['well ', Row ,Column];
                image=images(:, :, i);
                cd(curdir);
                NewDirect=dir;
                cd (foldername)
                imwrite(image,[imagename, '.tif'])
            end
            cd(curdir)
            cd(timefolder)
        end
    end
end
end
end
cd(curdir)

```

```
        if t==firstpoint,t1=toc;end
    end
end
close(w)
%%
%This is an optional piece to delete the original timepoint folders and
%original images within.  This should not be done without those images
%backed up elsewhere but can consolidate space if they are.
try
    rmdir('*TimePoint*','s')
catch
    try
        rmdir('*TimePoint*','s')
    catch
        warning('Thumb.db could not be deleted at this time')
    end
end
end
```

## Chapter 4

### Loss of Junctions by $\alpha$ -catenin Silencing Enhances Proliferation and MAPK through Enhanced Ligand Shedding

#### Introduction

The vast majority of cancers are derived from epithelial cells<sup>35</sup>. The large occurrence of cancers from the epithelium is due to the nature of this tissue: it forms a constantly proliferating defense against the environment, with the basal layer generating cells to replenish the outer layers with a two week turnover<sup>34</sup>. Epithelial cells are connected by a combination of tight junctions, desmosomes, and adherens junctions to establish structural integrity throughout the tissue, create an osmotic barrier, and regulate signaling in the cells. One of the most important regulators of epithelial cells in retaining cell-cell junctions is E-cadherin; adherens junctions are essential to the formation of tight junctions<sup>118</sup> and lowered levels have long been correlated with tumor aggressiveness and metastasis<sup>23-25</sup>. The loss of E-cadherin in tumor metastasis is tied to epithelial to mesenchymal transition (EMT), the process of removing cell-cell junctions, losing apical-basal polarity, and generating morphological changes allowing for an invasive phenotype<sup>15</sup>.

E-cadherin is a calcium-dependent adhesion protein that binds another E-cadherin molecule on an adjacent cell with its ectodomain and forms a complex with catenin proteins with its cytoplasmic domain<sup>6</sup>. The catenin proteins  $\beta$ -catenin and p120 bind E-cadherin directly through armadillo repeats whereas  $\alpha$ -catenin binds  $\beta$ -catenin to join the complex<sup>1</sup>. E-cadherin silencing is sufficient to cause EMT in some model systems, but interestingly retaining its cytoplasmic region prevented a mesenchymal

morphology while still disrupting cell-cell junctions, implicating the catenin complex in this transition<sup>29</sup>. Only some of these changes were linked to  $\beta$ -catenin by silencing its expression in E-cadherin knockdown cells, while others remained elusive<sup>29</sup>.

E-cadherin silencing in MDCK cells failed to remove  $\beta$ -catenin at the membrane, apical-basal polarity, or tight junction integrity due to redundancy with Cadherin-6, whereas targeting the catenin complex by  $\alpha$ -catenin silencing, caused a mesenchymal phenotype with severe defects in both adherens and tight junctions, as well as loss of apical-basal polarity while not affecting  $\beta$ -catenin levels or localization<sup>31</sup>. When  $\alpha$ -catenin was ablated in mice the epidermis became thick and disordered with mitotic cells throughout all layers rather than being restricted to the basal layer, resembling a precancerous squamous cell carcinoma<sup>32</sup>. It is unclear how  $\alpha$ -catenin is capable of affecting signaling to create a hyper proliferative phenotype; an early result shows that  $\alpha$ -catenin null cells are more sensitive to insulin and only caused increased growth in its presence<sup>32</sup>, whereas another states that Yap1 dysregulation is responsible for increased proliferation<sup>119</sup>.

$\alpha$ -catenin also has a fundamental role in mediating actin dynamics, homodimers binding actin inhibit Arp2/3 activity and lower cytoskeletal dynamics<sup>9</sup>. In chapter 2 I helped find that actin depolymerizing agents are some of the strongest activators of TACE in both magnitude and kinetics that we have seen. Because TACE is a primary regulator of growth in epithelial cells by activation of the epidermal growth factor receptor (EGFR) through ligand cleavage, I hypothesize that loss of  $\alpha$ -catenin causes an increase in ligand shedding responsible for a hyper proliferative phenotype.

## Results

## Silencing $\alpha$ -Catenin in HaCaT Keratinocytes

To address the role of  $\alpha$ -catenin in a keratinocytes model, I transfected a short hairpin RNA (shRNA) for  $\alpha$ -catenin in HaCaT cells and achieved efficient knockdown of protein levels (Fig. 4.1a). Silencing of  $\alpha$ -catenin caused a significant morphological change in HaCaT cells as seen by fibroblast morphology and spreading from distinct colonies (Fig. 4.1b). Because  $\alpha$ -catenin knockdown causes a mesenchymal morphology, I treated control cells treated with TGF- $\beta$  for 48 hours to cause EMT and compared mesenchymal and epithelial protein markers (Fig. 4.1a). I found that there is a marginal decrease in  $\beta$ -catenin and epithelial marker E-cadherin, as well as a slight increase in mesenchymal marker vimentin in  $\alpha$ -catenin knockdown cells, which was mild compared to TGF- $\beta$  treatment. I used immunofluorescence to image  $\beta$ -catenin to determine if it was localized to the nucleus or to cell-cell junctions and found its localization was unperturbed by  $\alpha$ -catenin silencing (Fig. 4.2). Because E-cadherin levels were mostly unaffected upon  $\alpha$ -catenin knockdown, I performed immunofluorescence on E-cadherin and found that most of the protein was not at cell junctions as those junctions did not exist (Fig. 4.1d). These results are in agreement with past studies in other epithelial cell models<sup>29-32</sup> in that the effects of  $\alpha$ -catenin silencing show sufficient loss of junctions and change in morphology to appear mesenchymal but do not show an EMT phenotype when observing protein markers.

The epidermis of mice with a double knockout of  $\alpha$ -catenin showed hyper proliferation throughout its layers<sup>32</sup>. To test for this phenotype within our model system, I used EdU to stain cells proceeding through S phase in a four hour period and found a significantly higher fraction of EdU positive cells in HaCaT cells with reduced  $\alpha$ -catenin

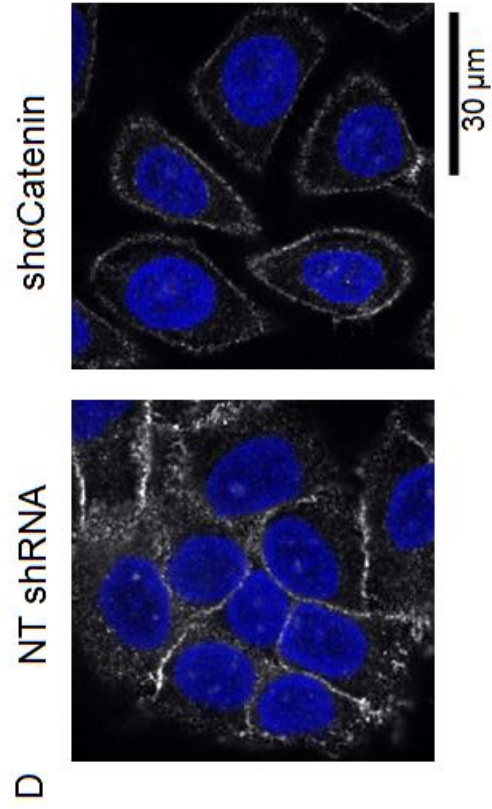
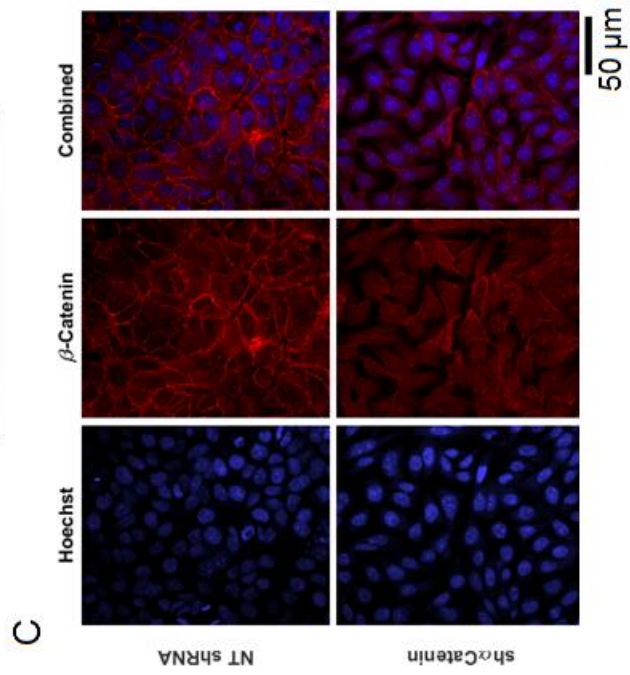
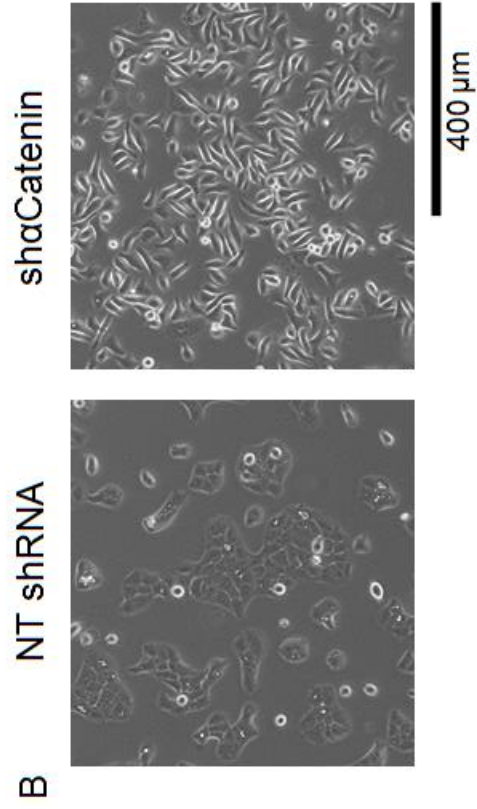
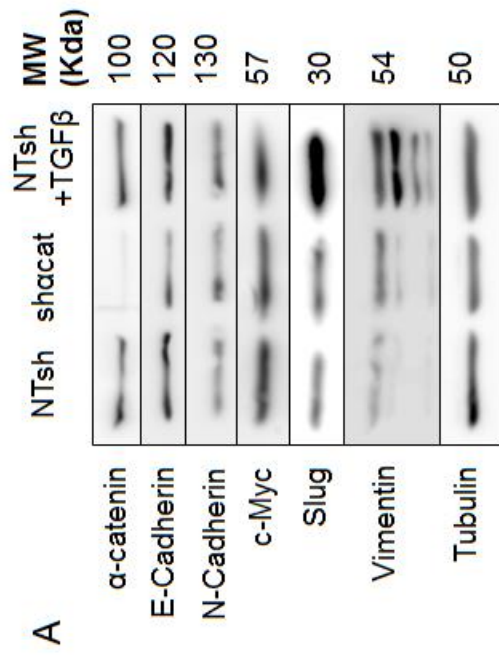


**Figure 4.1  $\alpha$ -Catenin knockdown causes scattering in HaCaT cells.** (A) Western blot of  $\alpha$ -catenin cells compared to non-targeting shRNA with or without TGF $\beta$  for 48 hours. Tublin used as loading control. (B) DIC images show the morphological change of  $\alpha$ -catenin knockdown in HaCaT cells. Images contrasted identically. (C) Immunofluorescence of  $\beta$ -catenin shows that it has not translocated to the nucleus in response to  $\alpha$ -catenin knockdown. Images contrasted identically. (D) Immunofluorescence for E-cadherin shows it remains at the membrane but there are no cell-cell junctions. Images contrasted identically.

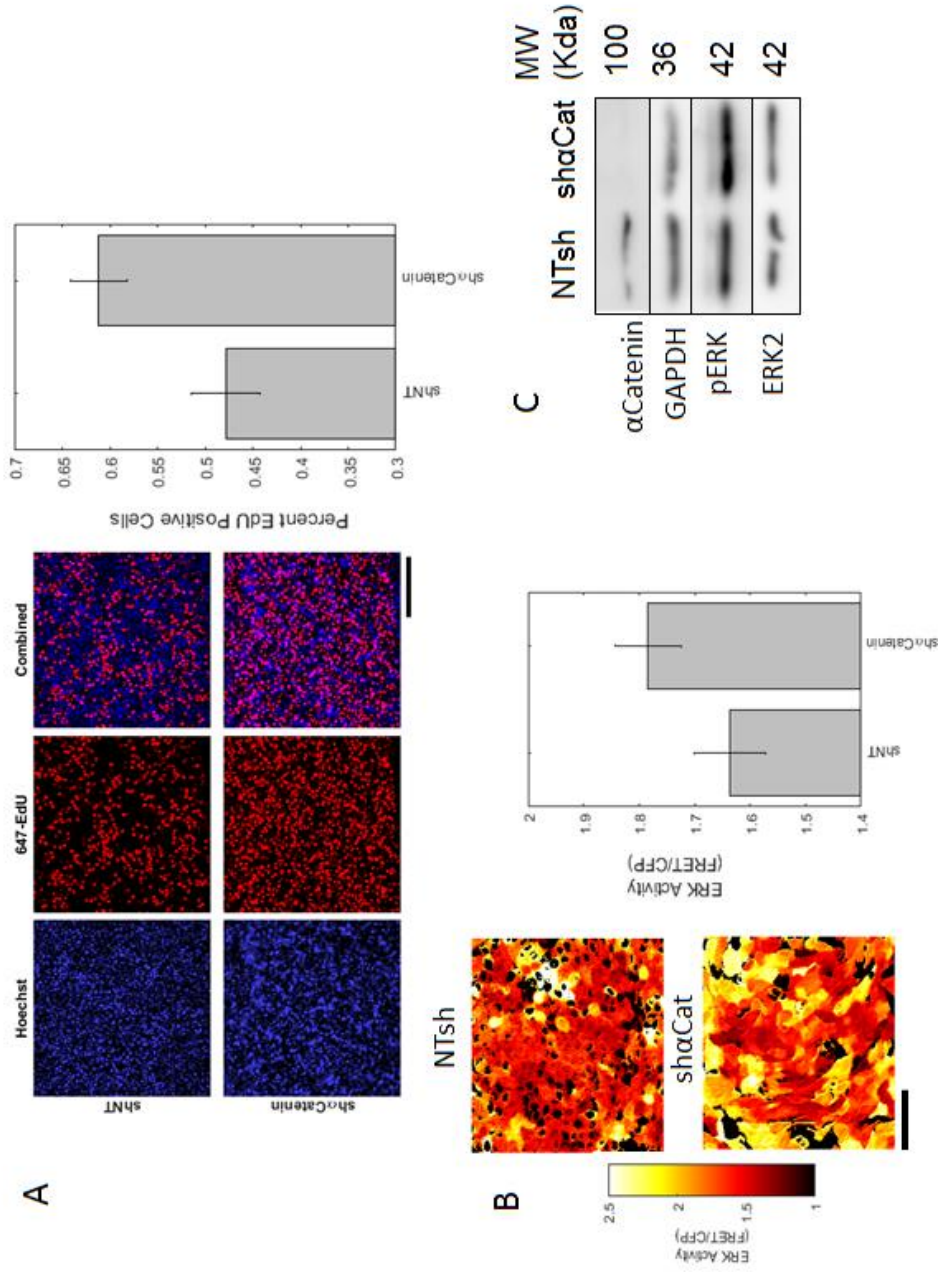


**Figure 4.2 Phenotype of HaCaT cells with  $\alpha$ -catenin knockdown.** (A)  $\alpha$ -catenin silencing causes a significant increase in cell proliferation in HaCaT cells. Images contrasted identically. Scale bar indicates 500  $\mu$ m. (B) ERK activity reported by EKAR is increased with  $\alpha$ -catenin knockdown. Scale bar indicates 80  $\mu$ m. (C) p-ERK detected by western blot is increased upon  $\alpha$ -catenin knockdown. Over 500 cells quantified for each image, performed in triplicate with error bars representing standard deviation.

compared to control cells (Fig. 4.2a), verifying this effect in our model system. I then began to interrogate the signaling responsible for proliferation and aimed to determine if ERK activity was affected by this knockdown. I used the FRET-based ERK sensor EKAR-ev to measure a large increase in the ratio of FRET to CFP in  $\alpha$ -catenin knockdown cells (Fig. 4.2c), indicative of increased ERK activity. I then validated this increase with a western blot and found a noticeable increase in phosphorylated ERK in  $\alpha$ -catenin knockdown cells compared to control cells (Fig. 4.2b). It appears that the mechanism by which  $\alpha$ -catenin silencing increases proliferation could be through activation of ERK signaling.

### **HaCaT Cell ERK Activity and Proliferation**

To understand how  $\alpha$ -catenin may be affecting proliferation, it is important to understand how growth is normally regulated in HaCaT cells. I began by characterizing ERK activity with EKAR and found that it can be successfully blocked by the EGFR inhibitor Gefitinib (Fig. 4.3a). TACE inhibitor BMS-561392<sup>120</sup> is capable of lower ERK activity to a similar level as Gefitinib (Fig. 4.3a). Depleted activity from both EGFR and TACE inhibition indicates that ERK activity is a function of ligand shedding through TACE to activate EGFR. I used neutralizing antibodies to further isolate signaling components and found that blocking EGFR with Cetuximab led to a similar decrease in ERK activity as a neutralizing antibody for the EGFR ligand transforming growth factor alpha (TGF $\alpha$ ) (Fig.4.3b), connecting a specific TACE substrate to EGFR activation. Because ERK activity pulses have been implicated in proliferation<sup>45,46</sup>, I tracked single cells expressing EKAR-ev and found that TACE inhibition with BMS is capable of blocking most activity pulses while EGFR inhibition appears to remove practically all

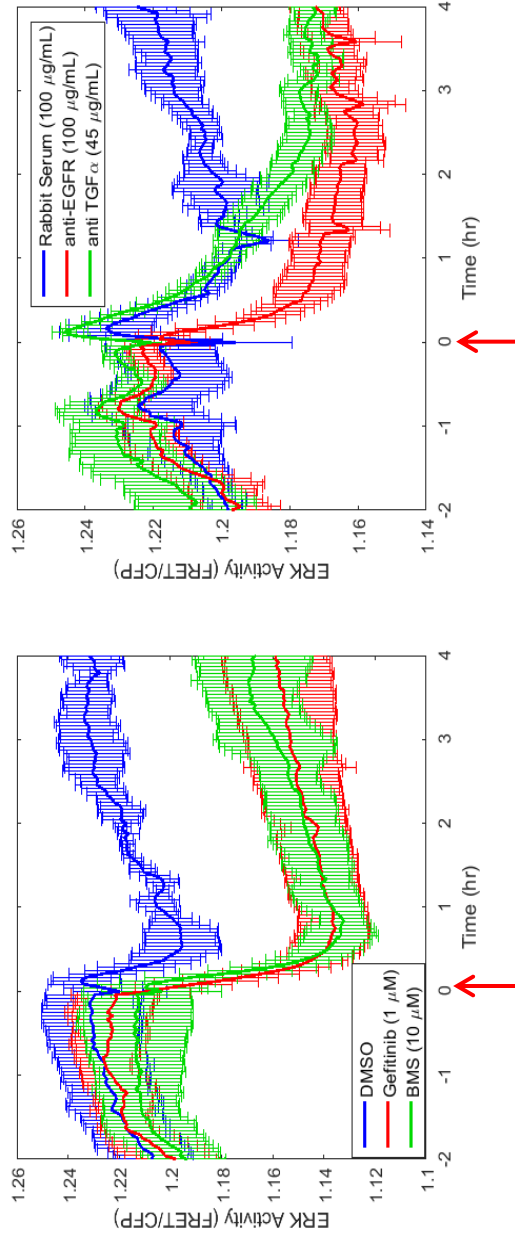


**Figure 4.3 HaCaT cells require TACE activity for TGF $\alpha$  shedding** (A) EKAR reported ERK activity with EGFR and TACE inhibition by Gefitinib and BMS, respectively (B) EKAR reported ERK activity with neutralizing antibodies for EGFR or TGF $\alpha$ . Conditions added at 0 hours, indicated with red arrows. Over 500 cells quantified in each image, performed in triplicate with error bars representing standard deviation.

activity pulses (Fig. 4.4). The near complete loss of ERK pulses with an EGFR inhibitor validates a dependence on receptor activity found in a different cell model<sup>47</sup>. The reduction of ERK pulses upon TACE inhibition is likely due to reduced pulse propagation from cell to cell, a process thought to act through ligand shedding<sup>46,47</sup>. Both population and single cell results show a strong connection between ERK signaling and TACE-mediated ligand shedding to EGFR.

Because TACE appears intricately tied to ERK signaling in HaCaT cells, I used a genetic approach to validate and further assess the scope of its regulation. I generated a CRISPR-cas knockout of TACE in HaCaT cells grown from a single clone in EGF-supplemented media (Fig. 4.5a). I used several known activators of TACE in cells with or without a TACE knockout. Surprisingly, I found that TSen in HaCaT cells appears to be much less specific than the cell lines we measured in chapter 2 (mouse embryonic fibroblasts and HeLa cells). Treatment with the TACE activator Cytochalasin D in the absence of TACE is still capable of causing a large increase in TSen cleavage, though it does not remain high compared to wild-type cells (Fig. 4.5b). TGF $\beta$  treatment causes a short-term pulse in TACE activity as seen in sensor cleavage in wild type but not TACE null cells. After fifteen hours, however, TGF $\beta$  shows approximately the same amount of sensor cleavage. This sensor-reported activity is presumably through the TGF $\beta$ -induced increased expression of other membrane proteases (reviewed in <sup>71</sup>).. It is also notable that BMS, thought to be a specific inhibitor of TACE<sup>120</sup>, lowered sensor cleavage in both wild-type and TACE knockout cells, showing that whatever leads to this reduction in activity is both inhibited by BMS and capable of cleaving TSen, while not being TACE=. Though there also appear to be several contexts in which TACE is crucial for

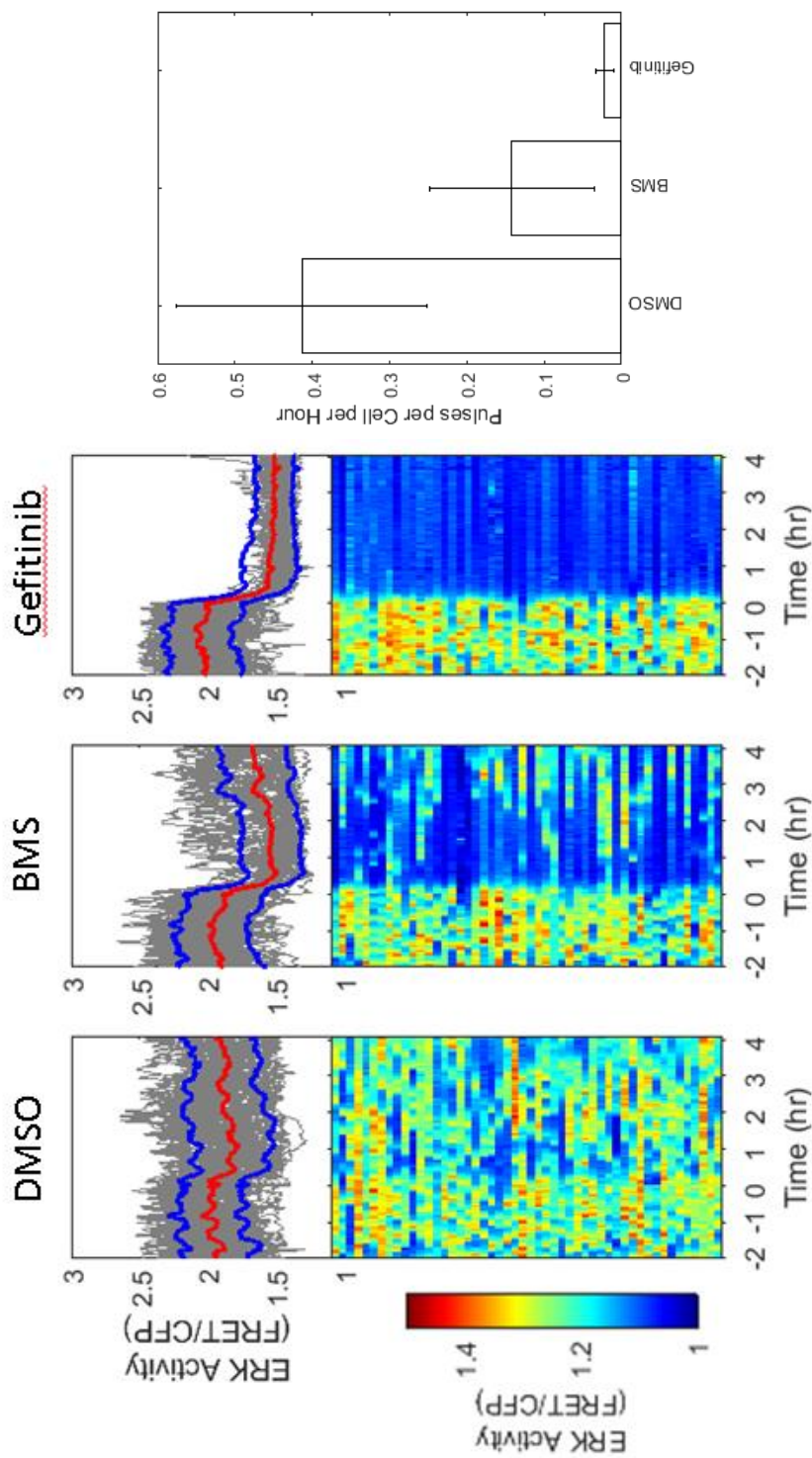


**Figure 4.4 ERK pulses require EGFR activity and ligand shedding.** FRET ratio of EKAR displayed as grey traces for individual cells, red trace for population average, and blue traces for one standard deviation above and below the mean for combined cell populations (>200 cells). Heat maps show individual cells and the pulse frequency was calculated after inhibitor or vehicle treatment (0 hr). Pulse frequency was calculated with a peak detection algorithm then normalized to cell number and frames per hour. Over 50 cells were quantified in each image, performed in triplicate with error bars indicating standard deviation.

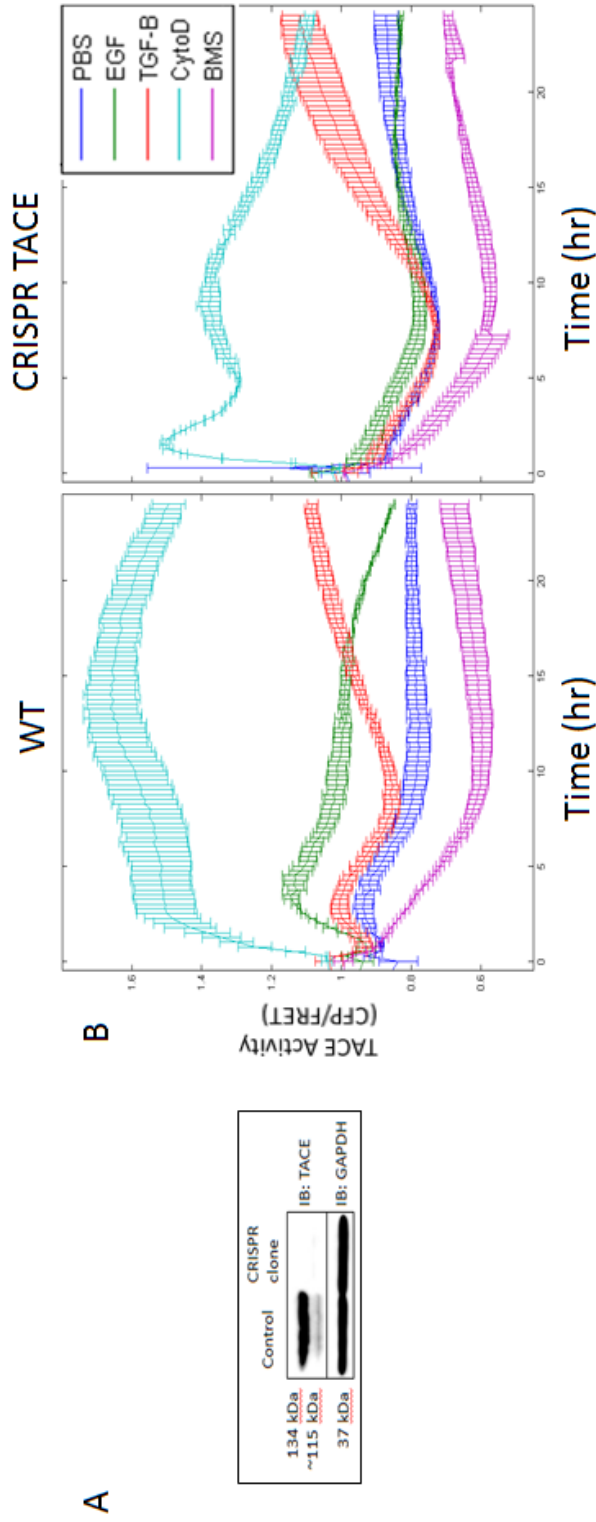


**Figure 4.5 CRISPR-Cas knockout of TACE in HaCaT cells does not prevent TSen cleavage under all conditions.** (A) Complete knockout of TACE in clonal expansion of HaCaT cells. (B) TSen in wild-type HaCaT cells or clonally expanded TACE knockout cells in sheets treated with PBS as control, EGF, TGF- $\beta$ , or Cytochalasin D as activators, or BMS as a TACE inhibitor. Over 1000 cells quantified per image, performed in triplicate with error bars indicating standard deviation.

TSen cleavage; EGF did not cause any reported activity increase in TACE null cells, TGF $\beta$  lacked an early peak in activity, and Cytochalasin D did not cause as lasting of an effect. Based on the EGF result, it is possible that kinases are responsible for the TACE-dependent cleavage of TSen in HaCaT cells and that the early peak from TGF $\beta$  is due to kinase activity and the extended activity of Cytochalasin D is due to feedback through ERK.

I then used this knockout cell line to measure downstream pathways and determine if TSen is cleaved non-specifically or if HaCaT cells maintain redundant proteases for EGFR activation. The FRET sensor EKAR-ev showed that there is a large reduction of ERK activity, as indicated by a change in FRET over CFP (Fig. 4.6a). CRISPR TACE cells showed a marked reduction in phosphorylated ERK that can be restored when TACE is rescued in these cells (Fig. 4.6b). The reduction in phosphorylated ERK closely matched the phosphorylated ERK seen cells incubated with the MMP and ADAM inhibitor TMI-1 on both wild-type and rescue cells, showing that blocking ligand shedding either genetically through TACE or by inhibition of the protein family had the same result. I tracked single cells expressing EKAR-ev and monitored their pulsing behavior to find an almost complete reduction of ERK activity pulses in the TACE knockout cells (Fig. 4.7). The TACE knockout cells showed pulsing behavior between TACE inhibited and EGFR inhibited levels (Fig. 4.7 vs 4.4), suggesting that BMS had previously caused an incomplete blockage of ligand shedding but that there is still a dependence on EGFR activity not accounted for with TACE. To determine the effect of TACE knockout downstream of ERK activity pulses, I measured proliferation with an EdU assay after four days of not supplementing media with EGF

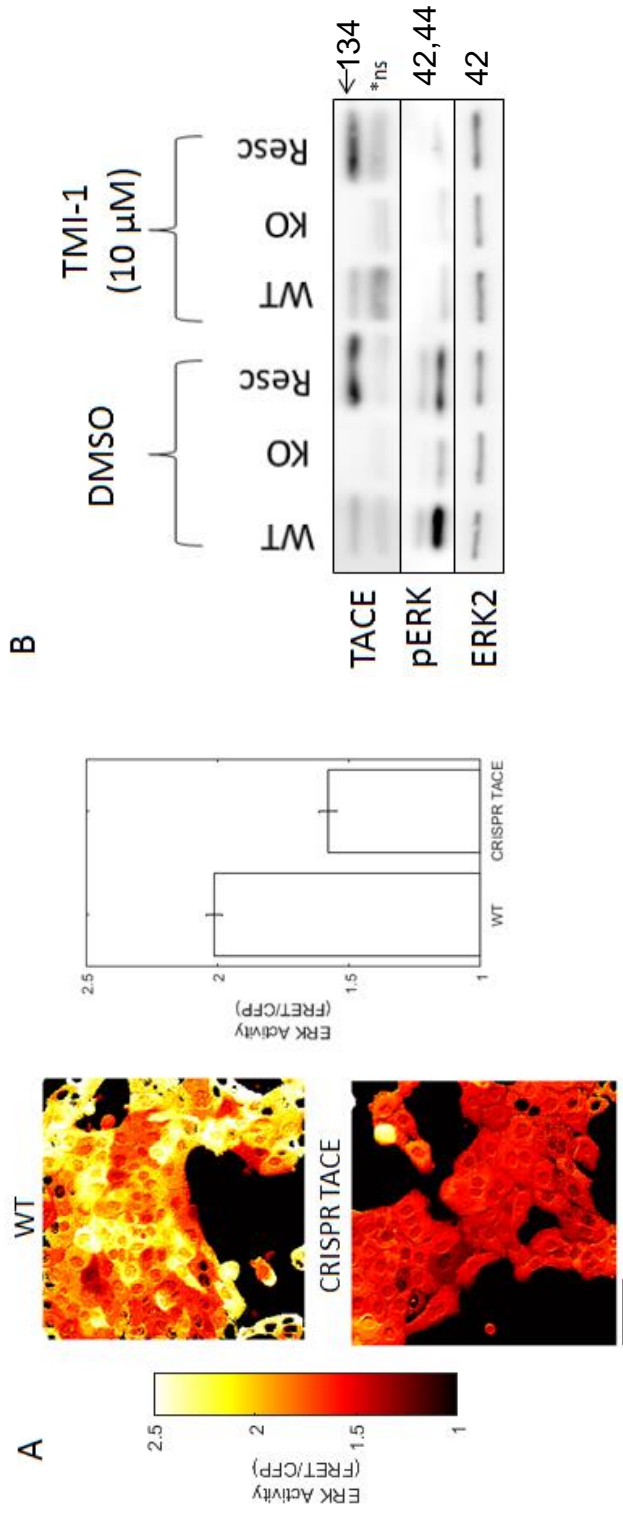


**Figure 4.6 ERK activity is lost upon TACE knockout in HaCaT cells.** (A) Pseudo-colored FRET ratio images for WT (top) and CRISPR TACE knockout cells (bottom). The FRET ratio is decreased in TACE knockout cells indicating lower ERK activity in clonally expanded TACE knockout cells. Over 500 cells quantified per image in triplicate with error bars indicating standard deviation. Scale bar indicated 80  $\mu$ m. (B) pERK is reduced in HaCaT cells with TACE knockout and restored upon TACE rescue. Treatment with MMP inhibitor TMI-1 removes pERK in all three cell lines. Arrow indicates TACE, ns - nonspecific band.

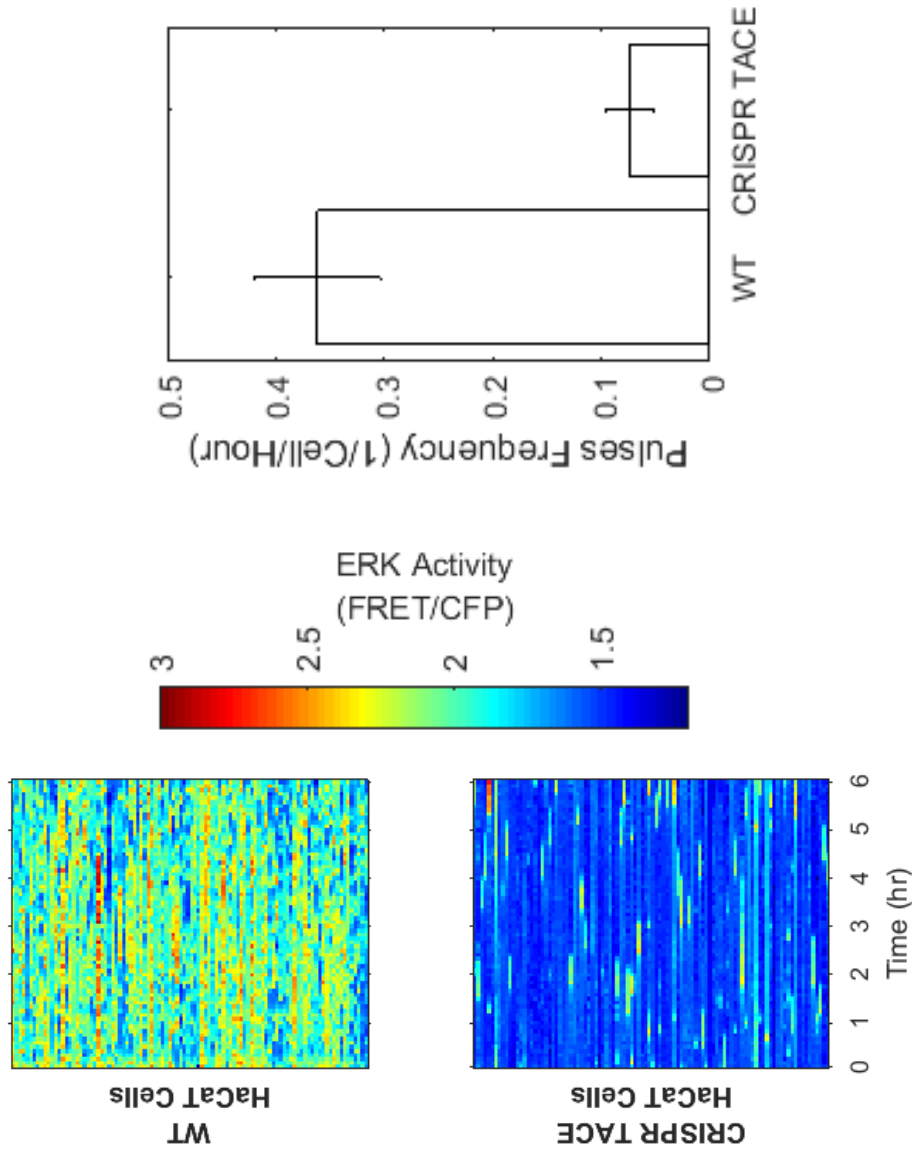


**Figure 4.7 ERK pulses are almost completely lost in HaCaT cells with a TACE knockout.** Single cell traces of FRET ratio are displayed for WT (top) and CRISPR TACE knockout cells (bottom). A large reduction in FRET ratio indicates lower ERK activity in knockout cells. A peak-detection algorithm was used to identify ERK pulses which were normalized to cell number and frames per hour, showing a large reduction in pulses upon knockout. Over 100 cells were quantified per image, performed in triplicate with error bars indicating standard deviation.

and using comparable cell densities at the time of EdU treatment. Complete knockout of TACE protein appears to almost completely abolish mitosis in HaCaT cells as shown by a vastly decreased fraction of cells with EdU incorporation (Fig. 4.8). Decreased EdU incorporation was rescued by expression of TACE in these cells. While TSen is cleaved non-specifically by proteases other than TACE, these results suggest that downstream signaling is massively perturbed by TACE knockout. Overall, these results support a model that HaCaT cells rely on TACE activity to cleave TGF $\alpha$ , activate EGFR, activate ERK and ERK pulses, as well as to proliferate.

### **Ligand Shedding in Sh $\alpha$ -catenin Cells**

Because ERK activity and proliferation in HaCaT cells appear to be directly tied to TACE-dependent ligand shedding of TGF $\alpha$ , I aimed to determine if the phenotype seen in  $\alpha$ -catenin silenced cells is due to increased TACE activity. I first used the TACE sensor TSen to find that there is a marked increase in cleavage of the sensor with  $\alpha$ -catenin knockdown as shown by CFP/FRET (Fig. 4.9a). Because I found that other proteases cleave TSen in HaCaT cells (Fig. 4.5), that TACE null cells appear to have no activation of ERK or proliferation (Fig. 4.6-8), and that ERK activity appears to depend on TGF $\alpha$  (Fig. 4.3b), I expect that TGF $\alpha$  is cleaved exclusively by TACE in this model system. I aimed to validate the increased activity seen by TSen by generating a fluorescent chimera of TGF- $\alpha$ , by inserting mRuby2 and Gaussia luciferase between the signal sequence and TACE cleavage site (Fig. 4.9b). A fluorescent TGF- $\alpha$  construct allows for TACE activity detection by monitoring loss of fluorescence on cells by microscopy or detection of shed ligand by fluorescence or luciferase activity in the media. I incubated control and  $\alpha$ -catenin knockdown cells for 18 hours then measured

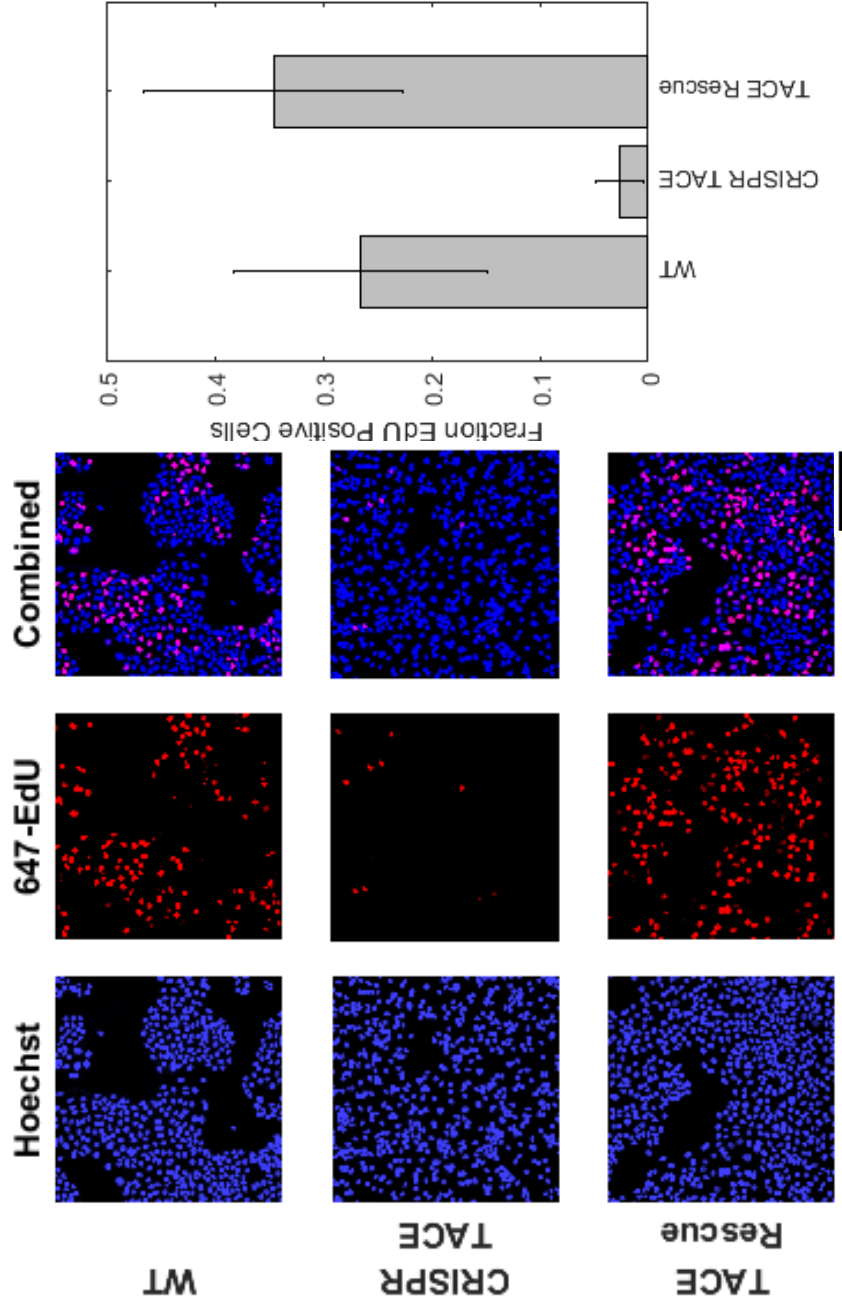


**Figure 4.8 HaCaT cells cease almost all proliferation in the absence of TACE.** Hoechst dye (blue) used to label all nuclei and EdU (red) labeling cells that entered S-phase in a 4 hour period. WT (top) shows a large fraction of EdU positive cells compared to CRISPR TACE knockout (middle) and TACE rescue (bottom) shows restoration of EdU in population. Single cell quantification shows a vastly reduced fraction of EdU positive cells in TACE null cells. At least 100 cells quantified per image, performed in triplicate with error bars indicating standard deviation. Scale bar indicates 500  $\mu\text{m}$ .

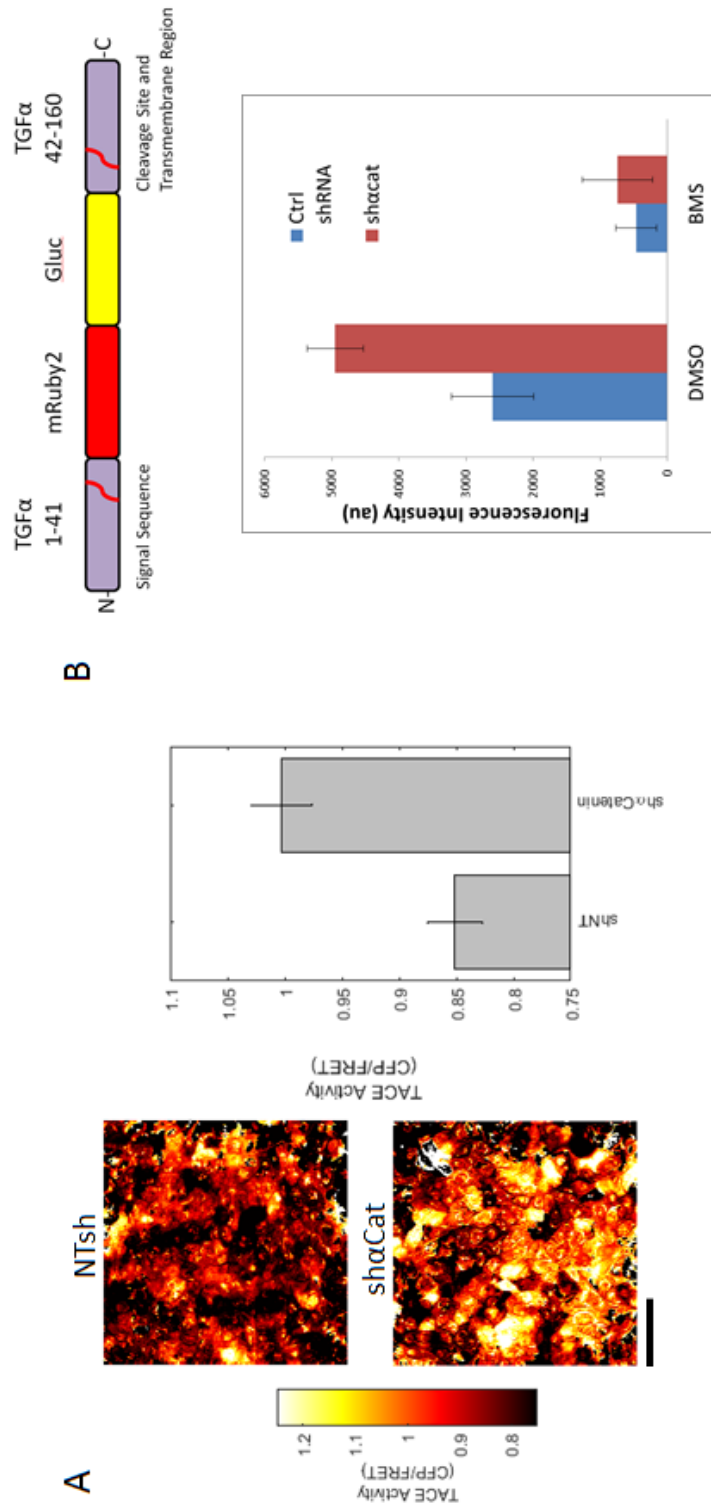


**Figure 4.9  $\alpha$ -catenin knockdown increases ligand shedding in HaCaT cells.**

(A) Inverse FRET ratio images of TSen show increased CFP/FRET sh $\alpha$ -catenin cells (bottom) compared to control (top) indicating increased TACE activity upon knockdown. Over 500 cells quantified in each image, performed in triplicate with error bars indicating standard deviation. Scale bar indicates 80  $\mu$ m. (B) Chimeric TGF $\alpha$ -mRuby2 construct (top) as a secondary reporter of ligand shedding with mRuby2 and Gaussia luciferase inserted between the signal sequence and TACE cleavage site. Red lines indicate cleavage sites. Measuring the media for fluorescence after 18 hours shows a roughly two-fold increase in fluorescence from sh $\alpha$ -catenin cells compared to control and fluorescence from both cell lines was reduced with a TACE inhibitor (BMS). Media extracted from wells in sextuplicate, error bars indicate standard deviation.

fluorescence in the media and saw an almost two-fold increase in fluorescence upon  $\alpha$ -catenin silencing. The fluorescence in media was dramatically reduced by inhibiting TACE in either cell line, which supports the concept that TACE activity is responsible for increased fluorescence. The nearly two-fold change in fluorescence marks the strongest effect I have seen with  $\alpha$ -catenin knockdown in HaCaT cells short of the striking morphological changes in figure 4.1 and implicates ligand shedding through TACE as the most likely mechanism for how silencing  $\alpha$ -catenin increases proliferation.

To test the hypothesis that increased ligand shedding through TACE causes a hyper proliferative phenotype, I repeated the stable transfection of  $\alpha$ -catenin shRNA in TACE null cells (Fig. 4.10a). Silencing  $\alpha$ -catenin causes a prominent change in morphology in the presence or absence of TACE (Fig. 4.10b), though I found that there is no longer an increase in vimentin in a TACE knockout background. I then used EdU staining to determine if the hyper proliferative phenotype of  $\alpha$ -catenin silencing depended on TACE. As seen in figure 4.11, the decrease in proliferation in the absence of EGF supplement was observed in TACE null cells, even upon  $\alpha$ -catenin knockdown. This result shows that  $\alpha$ -catenin ablation leads to increased proliferation by means of ligand shedding through TACE in HaCaT cells.

## **Discussion**

There is a striking dysregulation of epithelial cells when  $\alpha$ -catenin is silenced; all mitotic cells in all layers of the epidermis shows a hyper proliferative phenotype and hair defects indicate a lack of cooperation between mesenchymal and epithelial cells<sup>32</sup>. It is apparent that loss of  $\alpha$ -catenin is associated with loss of cell-cell junctions<sup>31</sup>(Fig. 4.1b and d) and a cellular change of this magnitude could be responsible for a proliferative

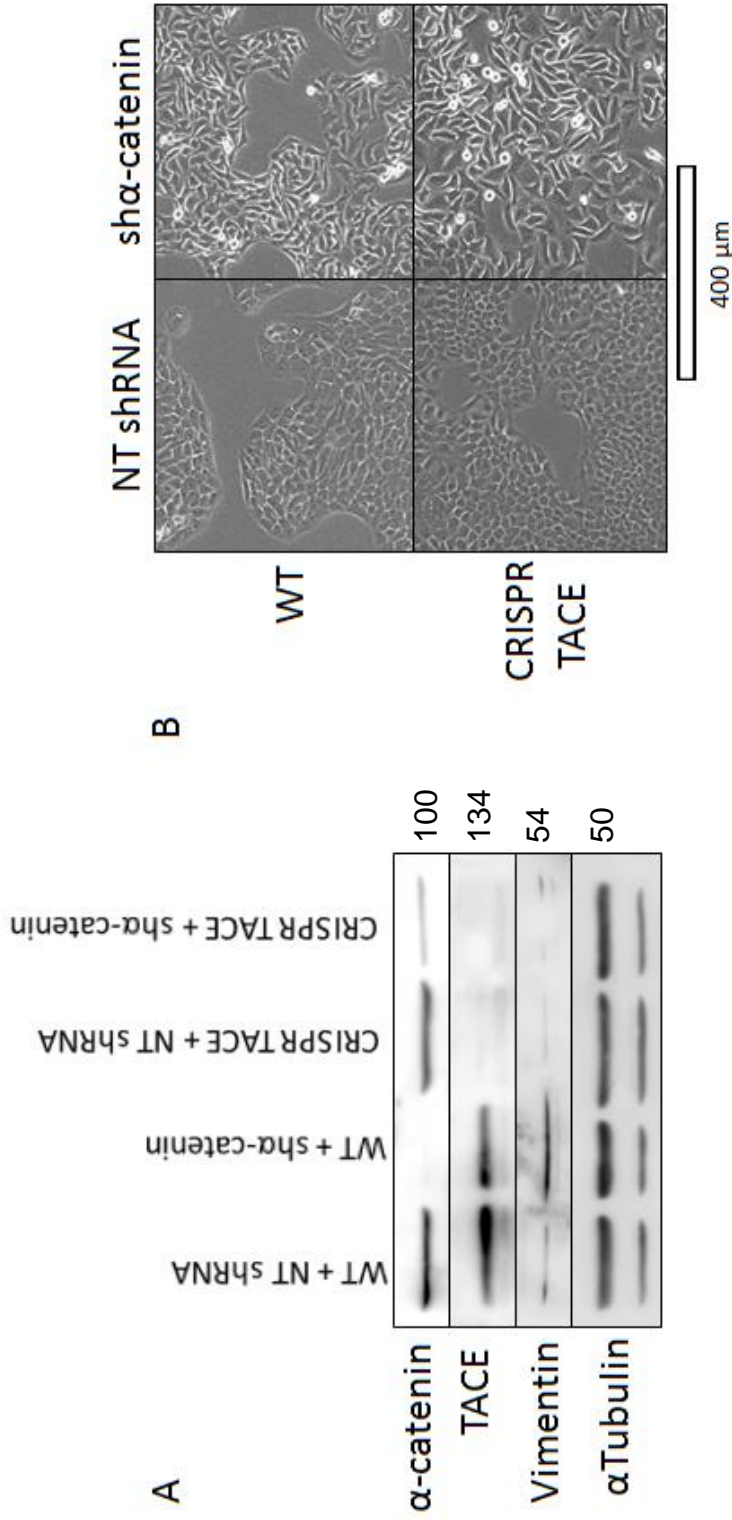


**Figure 4.10 Silencing  $\alpha$ -catenin in a TACE null background** (A) Western blot shows  $\alpha$ -catenin knockdown in cells expressive TACE or with TACE knockout.  $\alpha$ -catenin knockdown in CRISPR TACE cells achieved almost as low protein levels as in the presence of TACE but did not show an increase in vimentin. (B) DIC images of  $\alpha$ -catenin knockdown in the WT (top) or TACE null cells (bottom) showed a morphological change with  $\alpha$ -catenin silencing occurs in the presence or absence of TACE.

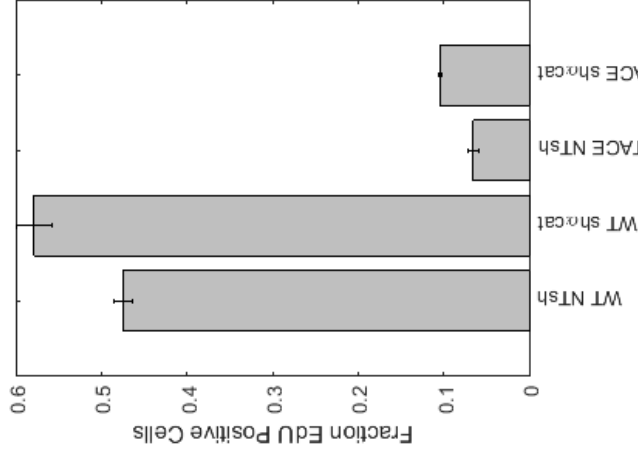
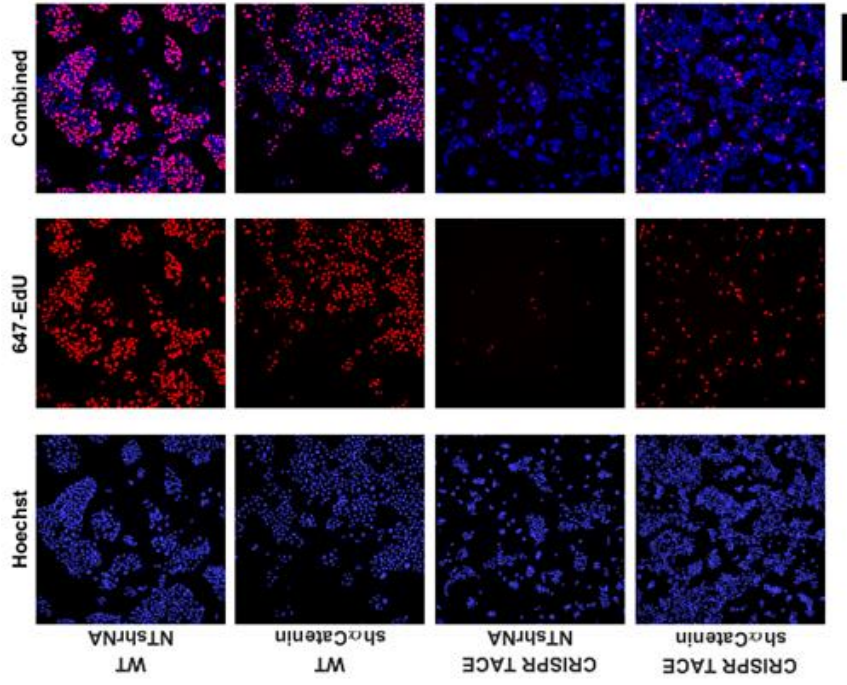


**Figure 4.11 Knocking down  $\alpha$ -catenin increases proliferation in wild-type cells but retains a negligible fraction of dividing cells in a TACE null background.** Hoechst dye (blue) is used to stain all nuclei and EdU stain (red) to show cells that entered S-phase in a 4 hour period. WT cells expressing either control or shRNA for  $\alpha$ -catenin (top two rows) show a large number of EdU positive cells compared to TACE null cells (bottom two rows). Single cell quantification shows a very low fraction EdU positive cells in the absence of TACE. At least 50 cells were quantified per image, performed in triplicate with error bars indicating standard deviation. Scale bar indicates 500  $\mu$ m.

phenotype. In fact, similar results have been shown with E-cadherin loss<sup>30</sup> and in some epithelial models loss of E-cadherin has generated full EMT<sup>29</sup>. While loss of E-cadherin is a key component of EMT and has been correlated with aggressive tumors and metastases<sup>14,23-25</sup>, in some cells instead causes an event called scattering, which is characterized by loss of junctions but not transcriptional changes associated with EMT<sup>29,121</sup>. The lack of transcriptional changes is possibly due to  $\beta$ -catenin retention at the plasma membrane in some epithelial models, but nuclear localization in others<sup>29,31</sup> and could be due to a redundant cadherin in some systems. While E-cadherin is primarily viewed as an adherence protein, EMT induced by loss of E-cadherin did not occur if the cytosolic region was retained, but instead cell-cell junctions were lost and transcription unaffected. This is in-part due to  $\beta$ -catenin binding the cytosolic region causing membrane retention, but not all signaling changes were due to  $\beta$ -catenin activity<sup>29</sup>. While I did not observe full EMT or translocation of  $\beta$ -catenin (Fig. 4.1 a and c), I did observe a striking change in morphology and loss of cell junctions (Fig. 4.1 b and d) paired with phenotypic changes in signaling (Fig. 2). This implicates  $\alpha$ -catenin in the  $\beta$ -catenin-independent signaling regulation caused by the E-cadherin cytosolic domain as  $\beta$ -catenin levels and localization were unaffected upon knockdown but a strong phenotype was still generated.

I found an epithelial cell model in which the ERK signaling cascade and proliferation are controlled by a specific string of proteins: HaCaT cells mediate TGF- $\alpha$  release through the membrane protease TACE, which leads to activation of EGFR in the same and nearby cells, giving rise to ERK activation and subsequent cell cycle-progression. This model system allowed me to examine the effect of  $\alpha$ -catenin silencing

and shed light on how a hyper proliferative phenotype can form in epithelial cells and perhaps how this phenotype found in mice<sup>32</sup> is controlled. I validated that  $\alpha$ -catenin knockdown caused increased growth in HaCaT cells (Fig. 4.2) and that there is an increase in the activity of key cell-cycle regulator ERK<sup>38</sup>. Because I tied ERK activity to TACE activity in HaCaT cells, I proceeded to detect the rate of ligand shedding using TSen and fluorescent-tagged TGF $\alpha$ . Indeed, using two fluorescence reporters for TACE activity, I found that knocking down  $\alpha$ -catenin causes a drastic increase in TACE activity, consistent with ligand shedding (Fig 4.9). The mechanism of  $\alpha$ -catenin silencing leading to hyper proliferation appears to be tied to the increased activity of TACE at the membrane and subsequent EGFR and ERK activation.

How  $\alpha$ -catenin alters TACE activity is not entirely clear. Several possibilities currently exist; core amongst them is that loss of  $\alpha$ -catenin induces loss of junctions, which could fundamentally alter TACE regulation. The morphological changes caused by silencing  $\alpha$ -catenin are dramatic and likely accompanied by large-scale changes in cellular trafficking and organization of membrane proteins. Because a key component of TACE regulation is its trafficking from the endoplasmic reticulum<sup>58</sup> and presumably its endocytosis from the plasma membrane, it is possible that increased ligand shedding observed is due to its localization. It is equally likely that substrate trafficking is altered and this accounts for increased activity, or even that an alternate regulator is affected that could alter its state at the plasma membrane<sup>66,68</sup>. Even if TACE protein levels at the membrane remained the same, there is a large change in the distribution of proteins when junctions are removed, as TJs no longer maintain apical-basal polarity<sup>1</sup> and polarity is lost upon  $\alpha$ -catenin silencing<sup>31</sup>. Because of this protein redistribution, it is

possible that TACE gains access to its substrates when polarity is lost, as they may be sequestered in different regions in healthy epithelium.

The function of  $\alpha$ -catenin at the membrane is both to generate a link between cadherin-cadherin junctions by binding actin and vinculin under tension<sup>10-13</sup> and to form homodimers capable of binding actin filaments<sup>8,9</sup> (Fig. 4.12). These homodimers are capable of altering actin dynamics by inhibiting Arp2/3 activity, thus preventing actin branching and lamellipodia formation at sites of high  $\alpha$ -catenin concentrations<sup>8,9</sup>. The inhibitory effect of  $\alpha$ -catenin on actin dynamics would explain how it mediates ligand shedding. One of the strongest activators of TACE activity is actin depolymerization as indicated by treatment with depolymerizing agents Cytochalasin D and Latrunculin B (Fig. 2.6 and 2.7). While it is unclear how changes in the cytoskeleton are altering TACE activity, it is one of the largest effects seen. It is possible that this is how  $\alpha$ -catenin regulates TACE, as cytoskeletal changes and MAPK signaling are themes throughout EMT and there is a gap in understanding as to how the cytoplasmic domain of E-cadherin regulates this process.

## **Methods**

### **Cell Culture**

HaCaT cells were cultured in DMEM supplemented with 2 mM L-glutamine, 100 U/mL penicillin, 100 U/mL streptomycin, and 10% (v/v) fetal bovine serum under 5% CO<sub>2</sub> at 37°C. HaCaT cells with a CRISPR-cas knockout of TACE were cultured in 6 pM EGF until TACE was rescued.

### **Cell Proliferation Assays**

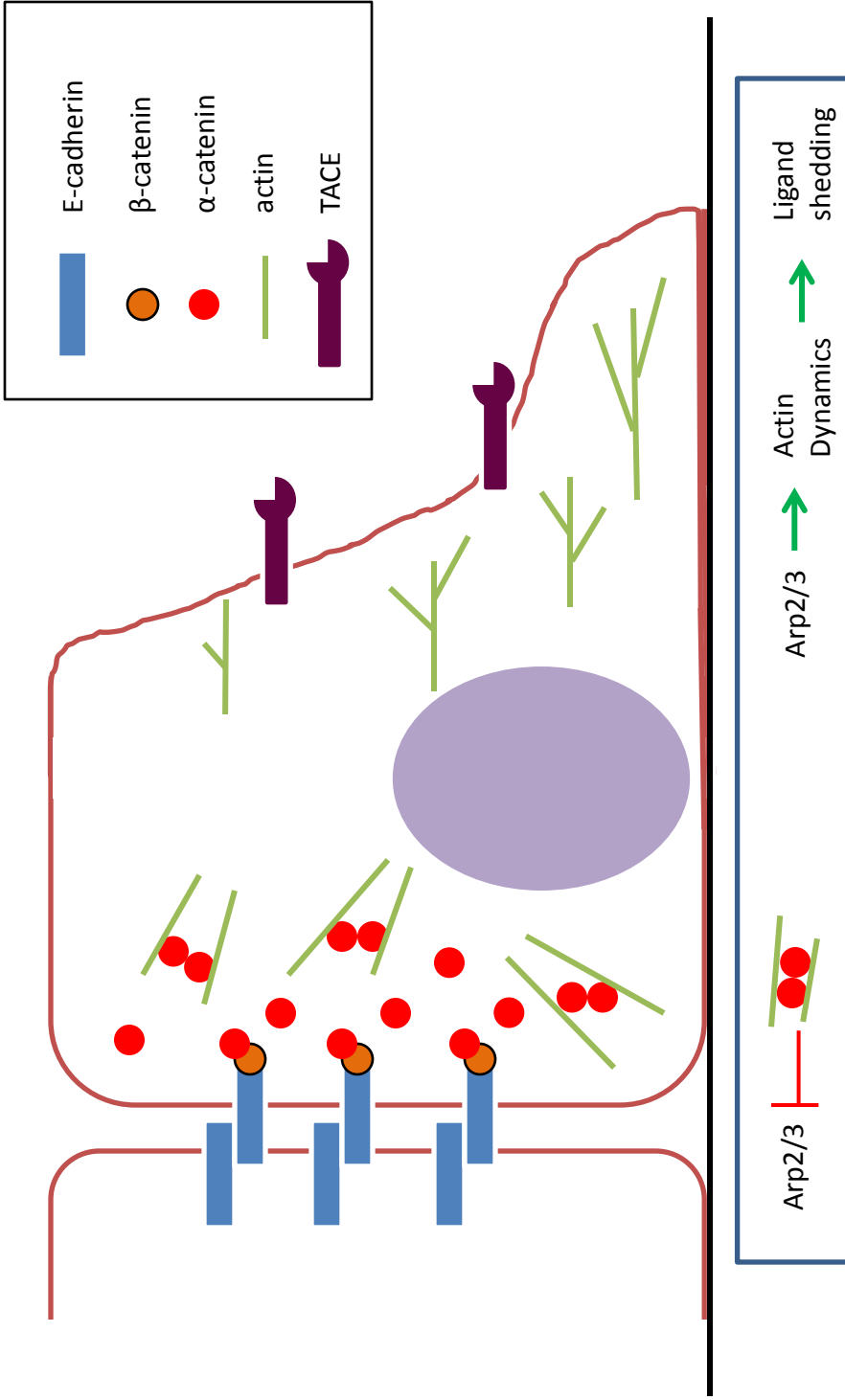


**Figure 4.12 Representation of increased ligand shedding upon loss of cell junctions.** When cadherins collect at the border between cells,  $\alpha$ -catenin levels are locally increased and homodimers bind actin at levels such that Arp2/3 is inhibited. When  $\alpha$ -catenin is not present, Arp2/3 causes actin branching and lamellipodia formation. Increased cytoskeletal changes activate TACE-mediated ligand shedding to regulate MAPK in the front cell and others nearby.

Cells were exposed to 5-ethynyl-2'-deoxy-uridine (EdU) for 4 hours before fixation with 4% paraformaldehyde for 5 minutes then treated as per the instructions in the Click-IT EdU Alexa Fluor 647 Imaging Kit (Life Technologies) used to determine the percentage of cells proliferating. Analysis was done as described in chapter 3 (Fig. 3.2). Assays performed with CRISPR-cas knockout of TACE were withheld EGF supplement for five days prior to treatment with EdU.

### **Western Blotting**

Whole-cell lysates of  $1.25 \times 10^6$  cells in a six-well plate were prepared in radioimmunoprecipitation assay buffer [25 mM tris-HCl (pH 7.4), 150 mM NaCl, 1% sodium deoxycholate, 1% Triton X-100, 0.1% SDS, 1 mM EDTA, 1 mM phenylmethylsulfonyl fluoride (PMSF), 30 mM NaF, 1 mM sodim orthovanadate]. Antibodies used for Western blots were against TACE (Ab39162, Abcam), Slug (9585T, Cell signaling), Vimentin (GTX100619, Genetex), ERK2 (sc-1647, Santa Cruz Biotechnologies), p-ERK (sc-7383, Santa Cruz Biotechnologies),  $\alpha$ Tubulin (sc-12462, Santa Cruz Biotechnologies), c-Myc (sc-40, Santa Cruz Biotechnologies),  $\alpha$ E-Catenin (sc-7894, Santa Cruz Biotechnologies), E-cadherin (sc-71008, Santa Cruz Biotechnologies), N-cadherin (sc-393933, Santa Cruz Biotechnologies), and GAPDH (sc-47724, Santa Cruz Biotechnologies).

### **Neutralizing Antibodies**

Cetuximab was a gift from Gail Eckhardt and antiTGF $\alpha$  (ab9585) was purchased from Abcam and were used at 100  $\mu$ g/mL and 45  $\mu$ g/mL, respectively.

### **Stable shRNA expression**

Stable shRNA knockdown of  $\alpha$ -catenin was achieved using TRC Lentiviral shRNA (Thermo) with the construct TRCN0000234534 and control by SHC016 and lentiviral transduction. Cell lines were selected by 1  $\mu$ g/mL puromycin treatment for three days. Lentiviral manufacturing was done in 293T cells with pHCMV-VSVg, pMDLg, and pREV vectors.

### **CRISPR-cas Knockout**

CRISPR-cas knockout of TACE was performed by cloning the sequence CACCGCCAATTCATGAGTTGTAACC as the guide RNA into LentiCRISPR (pXPR\_001)<sup>122</sup> and using lentiviral transduction as a delivery system. The cells were then selected with 0.5  $\mu$ g/mL puromycin for three days then allowed to recover in 6 pM EGF before diluting to single cells per well in 96 well plates. Single cells were grown into large colonies in 6 pM EGF before moving into larger dishes. Clonally expanded populations were measured for TACE levels by western blot (not shown).

### **Fluorescent protein secretion experiments**

mRuby2-TGF $\alpha$  secretion experiments were conducted by transferring the media from a 96-well plate (Costar) containing cells for 18 hours to a 96-well PCR plate, centrifuging at 233 RCF for 5 minutes, then transferring 100  $\mu$ L of the total 150  $\mu$ L to a round-bottomed 96 well plate (Corning 4520). The Fluorescence of the media was then measured using a Tecan Microplate reader with an excitation of 570/10 nm and emission of 610/5 nm.

### **FRET data analysis and fluorescence spectroscopy**

Cells were incubated and imaged in Corning 3603 96 well plates. Filters used for FRET measurements were the following: FRET excitation 438/ 24-25, dichroic 520LP, emission 542/27-25 (Semrock MOLE-0189); CFP excitation 438/24-25, dichroic 458LP, emission 483/32-25 (Semrock CFP- 2432B-NTE-Zero). Measurements were done in triplicate with 10x magnification. For images displayed, 40x magnification was used.

## Chapter 5

### Discussion

#### Significance

The epidermis is the primary barrier between an organism and the environment. Maintenance of the epidermis occurs through constant proliferation of keratinocytes in the basal layer that then differentiate as they progress toward the exterior. These cells not only proliferate at an extremely high rate, with a cellular turnover every two weeks, but must be primed to increase growth even higher and become migratory upon wounding<sup>34</sup>. Because cellular programs regulating motility and proliferation remain active long after embryogenesis and growth, it is understandable that basal-cell and squamous-cell carcinomas are some of the most common cancers that occur<sup>35</sup>.

Cells in the epidermis fulfill their role in protecting the body by forming a series of cell-cell junctions to strengthen the skin and provide a barrier for osmosis<sup>1</sup>. These cell-cell junctions also inhibit adverse signaling, as their loss is strongly correlated with aggressive cancers and metastases<sup>14,23–25</sup>, and can cause scattering or even EMT<sup>29,30</sup>. Some of this signaling can be linked to the cadherin-catenin complex;  $\beta$ -catenin release and subsequent translocation to the nucleus up-regulates mesenchymal genes. But there are a number of changes that occur in the absence of  $\beta$ -catenin for which there remains no explanation<sup>29</sup>. Removal of  $\alpha$ -catenin from the cadherin-catenin complex generates a hyper proliferative phenotype that resembles a squamous-cell carcinoma without altering  $\beta$ -catenin interactions with E-cadherin,<sup>32</sup> but the signaling pathways that induce increased proliferation remain unclear.

Because growth of epithelial cells is commonly dysregulated to create uncontrolled growth and these cells are capable of forming aggressive and invasive cancers, it is imperative that we understand the signaling and regulation of proliferative pathways. A major hub for signaling is the mitogen activated protein kinase (MAPK) pathway, specifically the extracellular signal-regulated kinase (ERK) cascade which can regulate motility and survival as well as progression through the cell cycle to proliferate<sup>37,38</sup>. A primary mechanism of triggering the ERK cascade in epithelial cells is activation of epithelial growth factor receptor (EGFR). EGFR ligands such as HB-EGF, amphiregulin, and transforming growth factor alpha (TGF $\alpha$ ) can be cleaved from a pro-form into an active one by membrane-bound proteases such as TNF $\alpha$ -converting enzyme (TACE). TACE has been found to be critical for cell motility, survival, and proliferation in many scenarios as well as being a major player in immune responses<sup>63,69,71,73</sup>. While TACE has been found to be fundamental for epithelial migration in development<sup>54,77</sup>, there is a great deal of debate as to its regulation – there are conflicting results as to the role of trafficking, phosphorylation, redox state, and lipid binding in how TACE is regulated<sup>58,62,63,65–68</sup>. In this work, I aim to create a better understanding its role in epithelial maintenance and disease.

### **A Biosensor for TACE Activity**

To determine how TACE regulates its various substrates it is important to measure TACE activity in live cells. This allows for real-time detection of stimulated changes as well as the potential for understanding spatial changes both at a subcellular level and across a population. The design of a TACE sensor is aimed to be specific for TACE over other MMPs and ADAM proteins as possible while maintaining plasma

membrane localization for optimal detection of ligand shedding activity. To create such a sensor (TSen), we used the TNF $\alpha$  cleavage site, which TACE cleaves efficiently and specifically,<sup>93,123</sup> as well as the PDGFR transmembrane region commonly used to localize a protein to the plasma membrane. To ensure that TSen localized to a region where TACE would likely be active, the signal sequence for TGF $\alpha$  was used as well as dual valine residues on the C-terminus required for TGF $\alpha$  maturation<sup>92</sup>. While the chosen cleavage sequence appears to be specific for TACE over ADAM10<sup>57</sup>, the non-catalytic domains of TACE are also important for achieving substrate specificity<sup>56</sup>. It would be difficult to generate a fluorescent probe without altering adjacent domains of a TACE substrate and fortunately the chimeric nature of this sensor did not interfere with its cleavage by TACE.

Once validated, I was able to use TSen to dissect the signaling networks that regulate TACE activity. The phorbol ester PMA is often used to activate TACE and has been proposed to operate either through PKC or directly on the ectodomain<sup>65,124</sup>. I used kinase inhibitors to show that p38 and ERK activities are necessary for full activation of TACE, though the degree that they regulate PMA-induced activation varies in different cell lines. I then used EGF to induce MAPK signaling and monitored TACE activity in the presence or absence of kinase inhibitors. I found that the activation of TACE differed greatly in different cell lines, indicating that the signaling networks responsible for TACE activation vary upon EGF stimulation. Furthermore, activating TACE with EGF would presumably release more EGFR ligands generating a positive feedback loop in these cells. This sort of response could potentially be used in epithelial cells to

stimulate wound healing by promoting both motility and increased proliferation upon either stress or release of EGFR ligands from other cells.

I was also able to use TSen to screen for novel modulators of TACE activity. I detected several potentially interesting compounds and pursued one: Cytochalasin D. The actin depolymerizing action of Cytochalasin D was found to be a major activator of TACE activity, both in magnitude and kinetics. The mechanism of how actin depolymerization is able to activate TACE to such a high degree is currently unclear, but I found an increased amount of TACE on the plasma membrane compared to the interior of the cell. This change in trafficking is potentially an off-target effect of inhibiting endocytosis or may be related to the regulation of TACE trafficking from the ER. Because there is debate as to how TACE is regulated in general – trafficking from the ER<sup>58</sup>, dimerization and inhibition<sup>67</sup>, phosphorylation<sup>60,62,63,67,125</sup>, redox state<sup>66</sup>, or binding to phosphatidylserine<sup>68</sup> – it is difficult to predict the precise role of actin. I predict that this activity is specific, as it is a very strong activator in several cell lines but has no effect on TACE activity in HeLa cells. In cell lines where actin depolymerization does cause TACE activation, the effect is very large in magnitude and there is potentially an independent mechanism for TACE activation not known in the literature.

### **Autocrine and Paracrine TACE signaling**

To further development of projects across the lab, I adapted image analysis techniques into automated fashion using MATLAB. This has been an extended undertaking to constantly improve efficiency and accuracy of many types of analysis and experimental designs. The algorithms developed in this project span from the simple reorganizing of images into a useful arrangement to tracking cells and

deciphering their signaling through signal processing techniques. Some of the basic tools developed here are, to the knowledge of the author, novel techniques for the field and could be potentially useful for other researchers, such as using the pixel histogram for background subtraction or generating an equalized image with a low deviation Gaussian for segmentation purposes.

To put these techniques to use for finding novel signaling in cells, I generated an epithelial line of HaCaT cells stably expressing both TSen and ERKTR, each a recently developed sensor. I was then able to use this cell line and automated image analysis techniques to track and monitor single cells activities of ERK and TACE simultaneously in single cells for the first time. This process unearthed several unforeseen challenges, such as the substantial amount of noise in the TSen reported signal for any given cell. I was also challenged by many foreseeable issues such as segmenting HaCaT cells from each other when the cell-cell junctions share the same pixels between cells and that the two sensors have fundamentally different dynamics as one is based on cleavage and the other on phosphorylation.

Upon processing the TSen signal into comparable dynamics to ERKTR, I observed single cell pulses of sensor cleavage. This is a novel finding – ligand shedding has never been reported as single cell pulses. It is intuitive that ligand shedding could occur in spikes; if ERK activity occurs in pulses and is also able to activate TACE, then it is expected that at least the activation of TACE could occur with a rapidity of a pulse. As long as there is a somewhat rapid mechanism for the downregulation of TACE activity such as endocytosis or local depletion of ligand, it can be expected that ligand shedding would occur in spikes at the single cell level.

I validated the propagation of ERK pulses to nearby cells using ERKTR and cross correlation identified a similar time separation as seen previously<sup>46</sup>. I then used the processed TSen signal to determine when pulses of sensor cleavage occur compared to ERK pulses. I find that after an ERK pulse, there is a spike in apparent TACE activity that begins to rise shortly before neighbor cells have an ERK pulse but reaches its peak afterward. This offset of timing could be an inaccuracy in the smoothing and binning of TSen signal used to predict its activity. Alternatively, it could be an issue with the sensitivity of TSen compared to TGF $\alpha$  and the neighbor cell's EGFR; TGF $\alpha$  may be cleaved in enough abundance at the rise in activity to generate an ERK pulse rather than at its peak. I was also able to detect neighbor cell pulses in sensor cleavage adjacent in time to an ERK pulse but did not find an increased correlation when I filtered the neighbors based on which one had an ERK pulse prior to the cell of interest. This result is confusing; I expect a cell to have an ERK pulse then stimulate TACE, which then stimulates an ERK pulse in a neighbor cell and thus propagates the signal. Perhaps the TSen signal is noisy enough that actual activity is hidden beneath the noise and larger sample sizes are required, or perhaps one of the other activators of TACE such as p38 or actin depolymerization are playing a large enough role in TACE activity that observing only ERK is insufficient to show the predicted peaks.

Despite the concept of pulsing TACE activity being an intuitive addition to the propagation of ERK pulses, describing them as a novel mechanism in cellular signaling requires multiple lines of evidence, especially in the case of pulses appearing only after signal processing. However, pulses of ligand shedding were seen during the writing of

this thesis using the mRuby-TGF $\alpha$  construct (described in Fig. 4.9), and it appears that an orthogonal approach to this conclusion could be forthcoming. Another exciting contribution to this work is that a CRISPR-Cas knockout of TACE was generated in HaCaT cells that showed almost no pulses of ERK activity (Fig. 4.7), and that this line is primed for expression of TACE mutants lacking the phosphorylation site for ERK. In the near future, I hope to identify if this phosphosite is necessary for ERK pulse propagation and if TACE pulses still occur in conjunction with ERK pulses.

### **Ligand shedding is increased upon $\alpha$ -catenin knockdown**

Using HaCaT keratinocytes as a model system, I was able repeat a hyper proliferative phenotype seen in the literature<sup>32</sup> and tease apart the underlying signaling responsible for this proliferative phenotype. Using neutralizing antibodies and small molecule inhibitors, I found that TACE appears to act through TGF $\alpha$  to activate EGFR and ERK in HaCaT cells. I then used CRISPR-cas to generate a TACE knockout like to show that HaCaT cells rely on TACE for nearly all ERK activity and proliferation. With this knowledge, I was able to hypothesize that  $\alpha$ -catenin knockdown increases ligand shedding through TACE activation and this triggers the proliferative phenotype. I did indeed find that HaCaT cells with reduced  $\alpha$ -catenin have increased proliferation, ERK activity, and ligand shedding. I repeated the sh $\alpha$ -catenin knockdown using HaCaT cells clonally expanded with a CRISPR-Cas knockout of TACE, a cell line that does not grow without supplementing with EGF. I found that  $\alpha$ -catenin silencing in the absence of TACE has the same effect on morphology and junctions as with TACE, but that the marked increase in proliferation has been removed. This causally links the decreased  $\alpha$ -catenin to increased ligand shedding as a mechanism for increasing proliferation.

The more detailed mechanism of how  $\alpha$ -catenin is able to modulate TACE activity is the next un-solved issue. The most striking features of  $\alpha$ -catenin knockdown are the morphological change and the loss of cell-cell junctions. Both of these features are large cellular changes and likely have many underlying effects in the cell, including trafficking. It is very likely that the regulation of protein movement from the ER to the cell surface is altered when cell shape changes from a tight epithelial colony to a spread out mesenchymal morphology; this alone could account for increased TACE on the surface and could also affect the substrates themselves. Another possibility is that because cell-cell junctions are lost, TJs are no longer able to establish apical-basal polarity on the cell membrane and sequestered plasma membrane proteins may be allowed to diffuse freely. This means that TACE at the membrane could have increased access to its substrates without intracellular trafficking being the underlying mechanism.

Another role of  $\alpha$ -catenin is to form homodimers that bind actin filaments and inhibit Arp2/3-mediated actin branching. While it is difficult to tie this role directly to TACE activity, I have seen that one of the strongest activators of TACE is the actin depolymerizing agent Cytochalasin D. The mechanism of activating TACE through the actin cytoskeleton is not known, but if changes in cytoskeletal dynamics are capable of altering TACE activity then the mechanism of  $\alpha$ -catenin knockdown could very well be in relieving its inhibitory effect on Arp2/3. Regardless of mechanism, I have found that  $\alpha$ -catenin knockdown directly influences proliferation, which could further influence EMT. Tying  $\alpha$ -catenin to ligand shedding also helps explain how loss of E-cadherin, but not E-cadherin's cytoplasmic domain, is able to cause EMT<sup>29</sup>.

TACE plays a fundamental role in the epithelium. In this model system, I have found that this protease is required for the core signaling pathway ending with ERK and its activity pulses, as well as proliferation. TACE regulation is also connected to the actin cytoskeleton in epithelial cells and this connection possibly explains how it performs its role in the epithelium. I found a large increase in ligand shedding when cell-cell junctions were removed by loss of  $\alpha$ -catenin; this could act as a mechanism of wound sensing as an opening is created in the epidermis. Also, because TACE acts through both an autocrine and paracrine manner, this would propagate the signal to cells not adjacent to the wound. EGF treatment causes increased ligand shedding which generates a positive feedback loop in the population and would aid in generating increased proliferation and motility until the wound is sealed. I also expect that increased motility would affect actin dynamics and potentially activate TACE through an alternate mechanism; this is another potential feedback loop which would aid in wound healing. If this mechanism is in place then it would not only be a powerful tool for wound healing but also for cancer progression. This provides a possible mechanism of cancer cells gaining aggressive behavior upon loss of junctions, as well as tying MAPK signaling to this phenotype.

## Citations

1. Niessen, C. M. Tight Junctions/Adherens Junctions: Basic Structure and Function. *J. Invest. Dermatol.* **127**, 2525–2532 (2007).
2. Pasti, G. & Labouesse, M. Epithelial junctions, cytoskeleton, and polarity. *WormBook* 1–35 (2014). doi:10.1895/wormbook.1.56.2
3. With, A. E. M., The Integrated Graduate Program in the Life Sciences, Department of Medicine, N. U. F. S. of M. & , David E. Escobar, C. J. G. in *Subcellular Biochemistry* 171–196 (2012).
4. Daniel D Bikle, Zhongjian Xie, and C.-L. T. Calcium regulation of keratinocyte differentiation. *Expert Rev. Endocrinol. Metab.* **7**, 461–472 (2012).
5. Irie, K., Shimizu, K., Sakisaka, T., Ikeda, W. & Takai, Y. Roles and modes of action of nectins in cell-cell adhesion. *Semin. Cell Dev. Biol.* **15**, 643–656 (2004).
6. Ivanov, D. B., Philippova, M. P. & Tkachuk, V. A. Structure and functions of classical cadherins. *Biochem.* **66**, 1174–1186 (2001).
7. Green, K. J. & Simpson, C. L. Desmosomes: New Perspectives on a Classic. *J. Invest. Dermatol.* **127**, 2499–2515 (2007).
8. Yamada, S., Pokutta, S., Drees, F., Weis, W. I. & Nelson, W. J. Deconstructing the cadherin-catenin-actin complex. *Cell* **123**, 889–901 (2005).
9. Drees, F., Pokutta, S., Yamada, S., Nelson, W. J. & Weis, W. I.  $\alpha$ -catenin is a molecular switch that binds E-cadherin- $\beta$ -catenin and regulates actin-filament assembly. *Cell* **123**, 903–915 (2005).
10. Buckley, C. D. *et al.* The minimal cadherin-catenin complex binds to actin filaments under force. *Science* (80-. ). **346**, 1254211–1254211 (2014).
11. Yao, M. *et al.* Force-dependent conformational switch of  $\alpha$ -catenin controls vinculin binding. *Nat. Commun.* **5**, (2014).
12. Rangarajan, E. S. & Izard, T. The cytoskeletal protein a-catenin unfurls upon binding to vinculin. *J. Biol. Chem.* **287**, 18492–18499 (2012).
13. Rangarajan, E. S. & Izard, T. Dimer asymmetry defines  $\alpha$ -catenin interactions. *Nat. Struct. Mol. Biol.* **20**, 188–193 (2013).
14. Yu, Y. & Elble, R. C. Homeostatic Signaling by Cell-Cell Junctions and Its Dysregulation during Cancer Progression. *J. Clin. Med.* **5**, 1–20 (2016).
15. Thiery, J. P. Epithelial–mesenchymal transitions in tumour progression. *Nat. Rev. Cancer* **2**, 442–454 (2002).
16. Stoker, M. & Perryman, M. An epithelial scatter factor released by embryo fibroblasts. *J. Cell Sci.* **77**, 209–23 (1985).
17. Thiery, J. P., Acloque, H., Huang, R. Y. J. & Nieto, M. A. Epithelial-Mesenchymal

- Transitions in Development and Disease. *Cell* **139**, 871–890 (2009).
18. Edme, N., Downward, J., Thiery, J.-P. & Boyer, B. Ras induces NBT-II epithelial cell scattering through the coordinate activities of Rac and MAPK pathways. *J. Cell Sci.* **115**, 2591–601 (2002).
  19. Janda, E. *et al.* Ras and TGF $\beta$  cooperatively regulate epithelial cell plasticity and metastasis: Dissection of Ras signaling pathways. *J. Cell Biol.* **156**, 299–313 (2002).
  20. Stefan, M. *et al.* Src Homology 2-containing Inositol 5-Phosphatase 1 Binds to the Multifunctional Docking Site of c-Met and Potentiates Hepatocyte Growth Factor-induced Branching Tubulogenesis. *J. Biol. Chem.* **276**, 3017–3023 (2001).
  21. Mancini, a, Koch, a, Wilms, R. & Tamura, T. The SH2-containing inositol 5-phosphatase (SHIP)-1 is implicated in the control of cell-cell junction and induces dissociation and dispersion of MDCK cells. *Oncogene* **21**, 1477–1484 (2002).
  22. Oft, M., Akhurst, R. J. & Balmain, A. Metastasis is driven by sequential elevation of H-ras and Smad2 levels. *Nat. Cell Biol.* **1**, 487–494 (2002).
  23. Oka, H. *et al.* Expression of E-cadherin cell adhesion molecules in human breast cancer tissues and its relationship to metastasis. *Cancer Res* **53**, 1696–1701 (1993).
  24. Umbas, R. *et al.* Decreased E-cadherin expression is associated with poor prognosis in patients with prostate cancer. *Cancer Res.* **54**, 3929–3934 (1994).
  25. Schipper, J. R. *et al.* E-Cadherin Expression in Squamous Cell Carcinomas of Head and Neck: Inverse Correlation with Tumor Dedifferentiation and Lymph Node Metastasis. *Cancer Res.* **51**, 6328–6337 (1991).
  26. Graff, J. R. *et al.* E-Cadherin Expression Is Silenced by DNA Hypermethylation in Human Breast and Prostate Carcinomas Advances in Brief E-Cadherin Expression Is Silenced by DNA Hypermethylation in Human Breast and Prostate Carcinomas1. 5195–5199 (1995). doi:10.1210/ME.7.2.232
  27. Strathdee, G. Epigenetic versus genetic alterations in the inactivation of E-cadherin. *Semin. Cancer Biol.* **12**, 373–9 (2002).
  28. Tam, W. L. & Weinberg, R. A. The epigenetics of epithelial-mesenchymal plasticity in cancer. *Nat. Med.* **19**, 1438–1449 (2013).
  29. Onder, T. T. *et al.* Loss of E-cadherin promotes metastasis via multiple downstream transcriptional pathways. *Cancer Res.* **68**, 3645–3654 (2008).
  30. Qin, Y., Capaldo, C., Gumbiner, B. M. & Macara, I. G. The mammalian Scribble polarity protein regulates epithelial cell adhesion and migration through E-cadherin. *J. Cell Biol.* **171**, 1061–1071 (2005).
  31. Capaldo, C. T. & Macara, I. G. Depletion of E-cadherin disrupts establishment but not maintenance of cell junctions in Madin-Darby canine kidney epithelial cells.

- Mol. Biol. Cell* **18**, 189–200 (2007).
32. Vasioukhin, V., Bauer, C., Degenstein, L., Wise, B. & Fuchs, E. Hyperproliferation and defects in epithelial polarity upon conditional ablation of  $\alpha$ -catenin in skin. *Cell* **104**, 605–617 (2001).
  33. Weis, W. I. & Nelson, W. J. Re-solving the cadherin-catenin-actin conundrum. *J. Biol. Chem.* **281**, 35593–35597 (2006).
  34. Fuchs, E. & Raghavan, S. Getting Under the Skin of Epidermal Morphogenesis. *Nat. Rev. Genet.* **3**, 199–209 (2002).
  35. Alam, M. & Ratner, D. Cutaneous Squamous-Cell Carcinoma. *N. Engl. J. Med.* **344**, 975–983 (2001).
  36. Khavari, T. A. & Rinn, J. Ras/Erk MAPK signaling in epidermal homeostasis and neoplasia. *Cell Cycle* **6**, 2928–2931 (2007).
  37. Chang, L. & Karin, M. Mammalian MAP kinase signalling cascades. *Nature* **410**, 37–40 (2001).
  38. Meloche, S. & Pouysségur, J. The ERK1/2 mitogen-activated protein kinase pathway as a master regulator of the G1- to S-phase transition. *Oncogene* **26**, 3227–3239 (2007).
  39. Traverse, S. *et al.* EGF triggers neuronal differentiation of PC12 cells that overexpress the EGF receptor. *Curr. Biol.* **4**, 694–701 (1994).
  40. Asthagiri, a R., Reinhart, C. a, Horwitz, a F. & Lauffenburger, D. a. The role of transient ERK2 signals in fibronectin- and insulin-mediated DNA synthesis. *J. Cell Sci.* **113 Pt 24**, 4499–4510 (2000).
  41. Cai, L., Dalal, C. K. & Elowitz, M. B. Frequency-modulated nuclear localization bursts coordinate gene regulation. *Nature* **455**, 485–90 (2008).
  42. Hao, N. & O’Shea, E. K. Signal-dependent dynamics of transcription factor translocation controls gene expression. *Nat. Struct. Mol. Biol.* **19 VN-r**, 31–39 (2012).
  43. Lahav, G. *et al.* Dynamics of the p53-Mdm2 feedback loop in individual cells. *Nat. Genet.* **36**, 147–150 (2004).
  44. Tay, S. *et al.* Single-cell NF-kappaB dynamics reveal digital activation and analogue information processing. *Nature* **466**, 267–71 (2010).
  45. Albeck, J. G., Mills, G. B. & Brugge, J. S. Frequency-Modulated Pulses of ERK Activity Transmit Quantitative Proliferation Signals. *Mol. Cell* **49**, 249–261 (2013).
  46. Aoki, K. *et al.* Stochastic ERK Activation Induced by Noise and Cell-to-Cell Propagation Regulates Cell Density-Dependent Proliferation. *Mol. Cell* 1–12 (2013). doi:10.1016/j.molcel.2013.09.015
  47. Sparta, B. *et al.* Receptor level mechanisms are required for epidermal growth

- factor (EGF)-stimulated extracellular signal-regulated kinase (ERK) activity pulses. *J. Biol. Chem.* **290**, 24784–24792 (2015).
48. Shankaran, H. *et al.* Rapid and sustained nuclear-cytoplasmic ERK oscillations induced by epidermal growth factor. *Mol. Syst. Biol.* **5**, 332 (2009).
  49. Nakayama, K., Satoh, T., Igari, A., Kageyama, R. & Nishida, E. FGF induces oscillations of Hes1 expression and Ras/ERK activation. *Curr. Biol.* **18**, 332–334 (2008).
  50. Lemmon, M. A. & Schlessinger, J. Cell signaling by receptor tyrosine kinases. *Cell* **141**, 1117–1134 (2010).
  51. Kao, S. C., Jaiswal, R. K., Kolch, W. & Landreth, G. E. Identification of the Mechanisms Regulating the Differential Activation of the MAPK Cascade by Epidermal Growth Factor and Nerve Growth Factor in PC12 Cells. *J. Biol. Chem.* **276**, 18169–18177 (2001).
  52. Gooz, M. ADAM-17: the enzyme that does it all. *Crit. Rev. Biochem. Mol. Biol.* **45**, 146–169 (2010).
  53. Edwards, D. R., Handsley, M. M. & Pennington, C. J. The ADAM metalloproteinases. *Mol. Aspects Med.* **29**, 258–289 (2009).
  54. Peschon, J. J. *et al.* An essential role for ectodomain shedding in mammalian development. *Science (80- )*. **282**, 1281–1284 (1998).
  55. Arribas, J. & Esselens, C. ADAM17 as a therapeutic target in multiple diseases. *Curr. Pharm. Des.* **15**, 2319–35 (2009).
  56. Stawikowska, R. *et al.* Activity of ADAM17 (a disintegrin and metalloprotease 17) is regulated by its noncatalytic domains and secondary structure of its substrates. *J. Biol. Chem.* **288**, 22871–22879 (2013).
  57. Tucher, J. *et al.* LC-MS based cleavage site profiling of the proteases ADAM10 and ADAM17 using proteome-derived peptide libraries. *J. Proteome Res.* **13**, 2205–2214 (2014).
  58. Adrain, C., Zettl, M., Christova, Y., Taylor, N. & Freeman, M. Tumor Necrosis Factor Signaling Requires iRhom2 to Promote Trafficking and Activation of TACE. *Science* **335**, 225–228 (2012).
  59. Schlöndorff, J., Becherer, J. D. & Blobel, C. P. Intracellular maturation and localization of the tumour necrosis factor alpha convertase (TACE). *Biochem. J.* **347 Pt 1**, 131–8 (2000).
  60. Niu, A. *et al.* Src mediates the mechanical activation of myogenesis by activating TNF $\alpha$ -converting enzyme. *J. Cell Sci.* **126**, 4349–57 (2013).
  61. Lemjabbar-Alaoui, H., Sidhu, S. S., Mengistab, A., Gallup, M. & Basbaum, C. TACE/ADAM-17 phosphorylation by PKC-epsilon mediates premalignant changes in Tobacco smoke-exposed lung cells. *PLoS One* **6**, (2011).

62. Soond, S. M., Everson, B., Riches, D. W. H. & Murphy, G. ERK-mediated phosphorylation of Thr735 in TNF $\alpha$ -converting enzyme and its potential role in TACE protein trafficking. *J. Cell Sci.* **118**, 2371–80 (2005).
63. Xu, P. & Derynck, R. Direct activation of TACE-mediated ectodomain shedding by p38 MAP kinase regulates EGF receptor-dependent cell proliferation. *Mol. Cell* **37**, 551–66 (2010).
64. Joslin, E. J. *et al.* Structure of the EGF receptor transactivation circuit integrates multiple signals with cell context. *Mol. Biosyst.* **6**, 1293–1306 (2010).
65. Le Gall, S. M. *et al.* ADAM17 is regulated by a rapid and reversible mechanism that controls access to its catalytic site. *J. Cell Sci.* **123**, 3913–3922 (2010).
66. Willems, S. H. *et al.* Thiol isomerases negatively regulate the cellular shedding activity of ADAM17. *Biochem. J.* **428**, 439–450 (2010).
67. Xu, P., Liu, J., Sakaki-Yumoto, M. & Derynck, R. TACE Activation by MAPK-Mediated Regulation of Cell Surface Dimerization and TIMP3 Association. *Science Signaling* **5**, ra34-ra34 (2012).
68. Sommer, A. *et al.* Phosphatidylserine exposure is required for ADAM17 sheddase function. *Nat. Commun.* **7**, 11523 (2016).
69. Xiao, L.-J. *et al.* ADAM17 targets MMP-2 and MMP-9 via EGFR-MEK-ERK pathway activation to promote prostate cancer cell invasion. *Int. J. Oncol.* **40**, 1714–24 (2012).
70. Wang, S. E. *et al.* Transforming growth factor beta engages TACE and ErbB3 to activate phosphatidylinositol-3 kinase/Akt in ErbB2-overexpressing breast cancer and desensitizes cells to trastuzumab. *Mol. Cell. Biol.* **28**, 5605–20 (2008).
71. Lu, Y. *et al.* TGF- $\beta$ 1 promotes motility and invasiveness of glioma cells through activation of ADAM17. *Oncol. Rep.* **25**, 1329–35 (2011).
72. Miller, M. A. *et al.* Reduced Proteolytic Shedding of Receptor Tyrosine Kinases Is a Post-Translational Mechanism of Kinase Inhibitor Resistance. *Cancer Discov.* **6**, 382–99 (2016).
73. Miller, M. a *et al.* ADAM-10 and -17 regulate endometriotic cell migration via concerted ligand and receptor shedding feedback on kinase signaling. *Pnas* **110**, E2074-83 (2013).
74. Black, R. A. *et al.* A metalloproteinase disintegrin that releases tumour-necrosis factor- $\alpha$  from cells. *Nature* **385**, 729–733 (1997).
75. Li, Y., Brazzell, J., Herrera, A. & Walcheck, B. ADAM17 deficiency by mature neutrophils has differential effects on L-selectin shedding. *Blood* **108**, 2275–2279 (2006).
76. Maretzky, T. *et al.* Migration of growth factor-stimulated epithelial and endothelial cells depends on EGFR transactivation by ADAM17. *Nat. Commun.* **2**, 229

- (2011).
77. Hassemer, E. L. *et al.* ADAM17 transactivates EGFR signaling during embryonic eyelid closure. *Invest. Ophthalmol. Vis. Sci.* **54**, 132–140 (2013).
  78. Giricz, O., Calvo, V., Peterson, E. A., Abouzeid, C. M. & Kenny, P. A. TACE-dependent TGF $\alpha$  shedding drives triple-negative breast cancer cell invasion. *Int. J. Cancer* **133**, 2587–95 (2013).
  79. Scheller, J., Chalaris, A., Garbers, C. & Rose-John, S. ADAM17: A molecular switch to control inflammation and tissue regeneration. *Trends Immunol.* **32**, 380–387 (2011).
  80. Lee, D. C. *et al.* TACE/ADAM17 processing of EGFR ligands indicates a role as a physiological convertase. *Ann. N. Y. Acad. Sci.* **995**, 22–38 (2003).
  81. Nakamura, Y., Sotozono, C. & Kinoshita, S. The Epidermal Growth Factor Receptor (EGFR): Role in Corneal Wound Healing and Homeostasis. *Exp. Eye Res.* **72**, 511–517 (2001).
  82. Blobel, C. P. ADAMs: key components in EGFR signalling and development. *Nat. Rev. Mol. Cell Biol.* **6**, 32–43 (2005).
  83. Murphy, G. Regulation of the proteolytic disintegrin metalloproteinases, the ‘Sheddases’. *Semin. Cell Dev. Biol.* **20**, 138–145 (2009).
  84. Gonzales, P. E. *et al.* Inhibition of the tumor necrosis factor- $\alpha$ -converting enzyme by its pro domain. *J. Biol. Chem.* **279**, 31638–31645 (2004).
  85. Srour, N. *et al.* TACE/ADAM-17 maturation and activation of sheddase activity require proprotein convertase activity. *FEBS Lett.* **554**, 275–283 (2003).
  86. Díaz-Rodríguez, E., Montero, J. C., Esparís-Ogando, A., Yuste, L. & Pandiella, A. Extracellular signal-regulated kinase phosphorylates tumor necrosis factor  $\alpha$ -converting enzyme at threonine 735: a potential role in regulated shedding. *Mol. Biol. Cell* **13**, 2031–44 (2002).
  87. Fan, H. & Derynck, R. Ectodomain shedding of TGF- $\alpha$  and other transmembrane proteins is induced by receptor tyrosine kinase activation and MAP kinase signaling cascades. *Embo J* **18**, 6962–6972 (1999).
  88. Gechtman, Z., Alonso, J. L., Raab, G., Ingber, D. E. & Klagsbrun, M. The shedding of membrane-anchored heparin-binding epidermal-like growth factor is regulated by the Raf/mitogen-activated protein kinase cascade and by cell adhesion and spreading. *J. Biol. Chem.* **274**, 28828–35 (1999).
  89. Maretzky, T., Zhou, W., Huang, X.-Y. & Blobel, C. P. A transforming Src mutant increases the bioavailability of EGFR ligands via stimulation of the cell-surface metalloproteinase ADAM17. *Oncogene* **30**, 611–8 (2011).
  90. Zhang, Q. *et al.* Phosphorylation of TNF- $\alpha$  converting enzyme by gastrin-releasing peptide induces amphiregulin release and EGF receptor activation.

- Proc. Natl. Acad. Sci. U. S. A.* **103**, 6901–6906 (2006).
91. Ouyang, M. *et al.* Simultaneous Visualization of Protumorigenic Src and MT1-MMP Activities with Fluorescence Resonance Energy Transfer. *Cancer Res.* **70**, 2204–2213 (2010).
  92. Briley, G. P., Hissong, M. A., Chiu, M. L., Lee, D. C. & Carolina, N. The Carboxyl-Terminal Valine Residues of ProTGF $\alpha$  Are Required for Its Efficient Maturation and Intracellular Routing. *Mol. Biol. Cell* **8**, 1619–1631 (1997).
  93. Mohan, M. J. *et al.* The Tumor Necrosis Factor- $\alpha$  Converting Enzyme (TACE): A Unique Metalloproteinase with Highly Defined Substrate Selectivity. *Biochemistry* **41**, 9462–9469 (2002).
  94. Jin, G. *et al.* A continuous fluorimetric assay for tumor necrosis factor- $\alpha$  converting enzyme. *Anal. Biochem.* **302**, 269–75 (2002).
  95. Lelimosin, M. *et al.* Intrinsic Dynamics in ECFP and Cerulean Control Fluorescence Quantum Yield. *Biochemistry* **48**, 10038–10046 (2009).
  96. M. Grootveld, M. F. M. BMS-561392 Bristol-Myers Squibb. *Curr. Opin. Investig. Drugs* **4**, 598–602 (2003).
  97. Alvarez-Iglesias M., Wayne G, O’Dea KP, Amour A, T. M. Continuous real-time measurement of tumor necrosis factor- $\alpha$  converting enzyme activity on live cells. *Lab. Investig.* **85**, 1440–1448 (2005).
  98. Armstrong, L. & Godinho SI, Uppington KM, Whittington HA, M. A. Tumour necrosis factor- $\alpha$  processing in interstitial lung disease: a potential role for exogenous proteinase-3. *Clin. Exp. Immunol.* **156**, 336–343 (2009).
  99. Hu, J., Steen, P. E. Van Den, Dillen, C. & Opdenakker, G. Targeting neutrophil collagenase / matrix metalloproteinase-8 and gelatinase B / matrix metalloproteinase-9 with a peptidomimetic inhibitor protects against endotoxin shock. *Biochem. Pharmacol.* **70**, 535–544 (2005).
  100. Wang, Y., Robertson, J. D. & Walcheck, B. Different signaling pathways stimulate a disintegrin and metalloprotease-17 (ADAM17) in neutrophils during apoptosis and activation. *J. Biol. Chem.* **286**, 38980–38988 (2011).
  101. Harvey, C. D. *et al.* A genetically encoded fluorescent sensor of ERK activity. *Proc. Natl. Acad. Sci. U. S. A.* **105**, 19264–9 (2008).
  102. Boulant, S., Kural, C., Zeeh, J.-C., Ubelmann, F. & Kirchhausen, T. Actin dynamics counteract membrane tension during clathrin-mediated endocytosis. *Nat. Cell Biol.* **13**, 1124–1131 (2011).
  103. Kelley, L. C., Hayes, K. E., Ammer, A. G., Martin, K. H. & Weed, S. A. Cortactin phosphorylated by ERK1/2 localizes to sites of dynamic actin regulation and is required for carcinoma lamellipodia persistence. *PLoS One* **5**, (2010).
  104. Han, M.-Y., Kosako, H., Watanabe, T. & Hattori, S. Extracellular Signal-Regulated

- Kinase/Mitogen-Activated Protein Kinase Regulates Actin Organization and Cell Motility by Phosphorylating the Actin Cross-Linking Protein EPLIN. *Mol. Cell. Biol.* **27**, 8190–8204 (2007).
105. Martinez-Quiles, N., Ho, H.-Y. H., Kirschner, M. W., Ramesh, N. & Geha, R. S. Erk/Src phosphorylation of cortactin acts as a switch on-switch off mechanism that controls its ability to activate N-WASP. *Mol. Cell. Biol.* **24**, 5269–80 (2004).
  106. Kelley, L. C., Hayes, K. E., Ammer, A. G., Martin, K. H. & Weed, S. A. Revisiting the ERK/Src cortactin switch. *Commun. Integr. Biol.* **4**, 205–207 (2011).
  107. Chapnick, D. a & Liu, X. Leader cell positioning drives wound-directed collective migration in TGF $\beta$ -stimulated epithelial sheets. *Mol. Biol. Cell* **25**, 1586–93 (2014).
  108. Nikolić, D. L., Boettiger, A. N., Bar-Sagi, D., Carbeck, J. D. & Shvartsman, S. Y. Role of boundary conditions in an experimental model of epithelial wound healing. *Am. J. Physiol. Cell Physiol.* **291**, C68-75 (2006).
  109. Komatsu, N. *et al.* Development of an optimized backbone of FRET biosensors for kinases and GTPases. *Mol. Biol. Cell* **22**, 4647–56 (2011).
  110. Lakowicz, J. R. in *Principles of Fluorescence Spectroscopy* 367–394 (1999).
  111. Miyawaki, A. Visualization of the spatial and temporal dynamics of intracellular signaling. *Dev. Cell* **4**, 295–305 (2003).
  112. Miyawaki, A. *et al.* Fluorescent indicators for Ca<sup>2+</sup> based on green fluorescent proteins and calmodulin. *Nature* **388**, 882–887 (1997).
  113. Regot, S., Hughey, J. J., Bajar, B. T., Carrasco, S. & Covert, M. W. High-sensitivity measurements of multiple kinase activities in live single cells. *Cell* **157**, 1724–1734 (2014).
  114. Souchier, C., Brisson, C., Batteux, B., Robert-Nicoud, M. & Bryon, P. A. Data reproducibility in fluorescence image analysis. *Methods Cell Sci.* **25**, 195–200 (2004).
  115. Leong, F. J. W.-M., Brady, M. & McGee, J. O. Correction of uneven illumination (vignetting) in digital microscopy images. *J. Clin. Pathol.* **56**, 619–21 (2003).
  116. Matsubayashi, Y., Ebisuya, M., Honjoh, S. & Nishida, E. ERK Activation Propagates in Epithelial Cell Sheets and Regulates Their Migration during Wound Healing. *Curr. Biol.* **14**, 731–735 (2004).
  117. Savitzky, A. & Golay, M. J. E. Smoothing and Differentiation of Data by Simplified Least Squares Procedures. *Anal. Chem.* **36**, 1627–1639 (1964).
  118. Tunggal, J. A. *et al.* E-cadherin is essential for in vivo epidermal barrier function by regulating tight junctions. *EMBO J.* **24**, 1146–1156 (2005).
  119. Silvis, M. R. *et al.* -Catenin Is a Tumor Suppressor That Controls Cell Accumulation by Regulating the Localization and Activity of the Transcriptional Coactivator Yap1. *Sci. Signal.* **4**, ra33-ra33 (2011).

120. Qian, M. *et al.* Pharmacokinetics and Pharmacodynamics of DPC 333 ((2R)-2-((3R)-3-Amino-3{4-[2-methyl-4-quinolinyl] methoxy} phenyl)-2-oxopyrrolidiny)-N-hydroxy-4-methylpentanamide), a Potent and Selective Inhibitor of Tumor Necrosis Factor  $\alpha$ -Converting Enzyme in Rodent. *Drug Metab. Dispos.* **35**, 1916–1925 (2007).
121. Grünert, S., Jechlinger, M. & Beug, H. Opinion: Diverse cellular and molecular mechanisms contribute to epithelial plasticity and metastasis. *Nat. Rev. Mol. Cell Biol.* **4**, 657–665 (2003).
122. Shalem, O. *et al.* Genome-Scale CRISPR-Cas9 Knockout Screening in Human Cells. *Science* (80-. ). **343**, 84–87 (2014).
123. Jin, G. *et al.* A continuous fluorimetric assay for tumor necrosis factor- $\alpha$  converting enzyme. *Anal. Biochem.* **302**, 269–275 (2002).
124. Horiuchi, K. *et al.* Substrate Selectivity of Epidermal Growth Factor-Receptor Ligand Sheddases and their Regulation by Phorbol Esters and Calcium Influx. *Mol. Biol. Cell* **18**, 176–188 (2007).
125. Scott, A. J. *et al.* Reactive oxygen species and p38 mitogen-activated protein kinase mediate tumor necrosis factor  $\alpha$ -converting enzyme (TACE/ADAM-17) activation in primary human monocytes. *J. Biol. Chem.* **286**, 35466–76 (2011).